

Special Relativity and Quantum Theory

by Ruler and Compass

William G. Harter and Tyle C. Reimer*

University of Arkansas, Department of Physics, Fayetteville, AR 72701[†]

(Dated: May 23, 2015)

Abstract

A quantitatively precise and logically compelling Occam's Razor development for special relativity and quantum theory can be done with a few simple steps aided by ruler and compass. A number of concepts that students invariably find arbitrary, mysterious, or quasi-paradoxical are elegantly resolved. This geometric approach improves both conceptual visualization and the computational techniques for these subjects while showing they are really two sides of one subject. This unified approach could allow these pillars of modern physics to be introduced earlier and greater depth in a growing range of physics curricula. It also reveals heretofore hidden insight and provides new avenues for research. (*At current date above, this is an unfinished rough draft . WGH*)

I. INTRODUCTION: A CASE FOR GEOMETRY IN PHYSICS

Relativity and quantum theory are foundations of modern (20th century) physics, arguably the greatest renaissance of physical science that has occurred so far. Seminal work by Planck in 1900¹ and Einstein in 1905² lead to an explosion of new science and technology that already surpasses even the great classical renaissance of the 16th through 19th centuries. The latter was initiated most notably by Kepler, Galileo, Newton, Lagrange, Hamilton, Poincare, and Maxwell. Long before that were pre-classical renaissance movements including those in natural sciences by Aristotle, astronomy by Ptolemy and Copernicus, Middle Eastern algebra, and early geometry by Thales (600 BCE) and Euclid (300 BCE). There appears a 300 year gap wherein new mathematical science seems in no rush to advance.

In our post-modern rush toward ever more advanced theory, it is easy to regard ancient fundamental methods to be obsolete or irrelevant. In contrast, this article will describe a decade-long effort to improve modern STEM teaching using a combination of computer graphics with geometry of Thales and Euclid. Here modern silicon computers meet the most ancient computer, a ruler-and-compass. It is surprising to students and particularly to instructors that geometric development of both classical and modern physics can be such a powerfully elegant and creative pedagogy given a little help from the silicon.

One glance at tediously engraved plates of spider-web-like geometric constructions in Newton's *Principia* might convince one that such geometric tedium is quite obsolete. Nevertheless, it is geometry that allowed Newton to discover the algebraic shorthand of analytic geometry, calculus, and ultimately his classical mechanics. Nowadays, it is plate engraving that is obsolete. Modern students may easily produce fine coordinate grids to do 2 or 3-figure precision analytic geometry on paper or display nearly unlimited precision on a screen.

More important than numerical precision is the precision and clarity of logic. Newton's "spider-web" constructions would have been clearer if each logical step occupied a separate plate, an impracticality in 1687. But, starting in 1987 (another 300 year gap) we do many such mega-pixel "plates" in seconds. Now browsers do Giga-pixel color animation frames in milli-seconds so one can gray-out or re-color preceding steps to help clarify geometric logic. Still geometric logic always starts somewhere, that is, with certain axioms. To the extent that geometry or any mathematics underwrites physics, there must also be physical axioms.

A. Axiomatic hurdles

This geometric redevelopment first considers the axioms of modern physics and conceptual underpinnings. Modern physics axioms seem more mysterious or nebulous than rock-solid laws accepted in classical physics. Modern physics texts introduce a variety of rhetorical axiomatic restatements for relativity and, with even greater variety, for quantum mechanics. The plurality of modern physics axiom-sets is close to the number of textbook authors.

Relativity and quantum courses begin with axiomatic hurdles that increase difficulty to teach or learn, particularly if both teacher and learner espouse critical thinking. Students of these subjects comment (paraphrasing), “I don’t get this stuff, but then neither does the instructor!” The instructor may claim, (again paraphrasing), “OK, it seems crazy. But trust me! It’ll work out.” And, it usually does. Sort of.

But, are such hurdles and fundamental logical confusion really and forever necessary?

For over a century relativity has been introduced basically as Einstein presented it, and at least a half century of quantum mechanics texts are largely based on logical structure in the notes by Fermi, Oppenheimer, and earlier developers. There is a single exceptional QM restructuring in the Feynman Lectures Volume III of 1964. Full disclosure: Richard Feynman and William Wagner, one of Feynman’s co-authors of a general relativity text, were my graduate advisors from 1964 to 1967. Feynman and Wagner greatly influenced my theoretical pedagogy, but work to continue Feynman’s QM restructuring came much later.

B. Einstein Centennial redevelopment effort

In 2004 the Pirelli Relativity Challenge in honor of the 2005 Einstein Centennial stimulated a multimedia geometric redevelopment of upper division and graduate level modern physics pedagogy at the University of Arkansas. The goal was to significantly reduce conceptual confusion by effectively combining relativity and quantum theory using the geometry of optical wave interference.

The results as described below reduce several hurdles and improve the introduction to relativity and quantum theory for students of all ages. This gives one a way to derive, construct, relate, and explain a dozen (or so) fundamental variables of relativistic quantum mechanics by way of a half dozen (or so) ruler-and-compass steps on graph paper. Doing this

provides a visually compelling logic and derivation of algebraic formulas that are considerably simpler and more student-friendly than the old-fashioned Einstein-Lorentz formulation. Moreover, such a 6-step program represents a fairly radical curriculum unification of relativity and quantum theory into what is more nearly a single subject. This lets one see quantum mechanics as a relativistic effect while similarly, relativity is a quantum mechanical one.

The 6-step logic of Sec.III is preceded in Sec.II by historical context, philosophy, motivation, and most importantly, the improved axioms needed to build such a concise geometry of both classical and modern physics fundamentals. The underlying methodology is known generally as symmetry analysis, Lorentz symmetry in particular, but all this is presented simply as grown-up plane geometry and trigonometry. (And, as a bonus, students of all ages gain a clearer appreciation of those two ancient subjects, as well!)

II. HISTORICAL CONTEXT OF MODERN PHYSICAL AXIOMS

Most texts note the original historical axiomatic beginnings of modern physics. Here we view them as extraordinary prefaces to new chapters in a great story of light. First is Planck's 1900 axiom $E=hNv$ for his theory of low temperature light-in-a-box. This is the beginning of a subject we call quantum mechanics (QM) where cavity mode energy E is restricted to a discrete number $N=1,2,\dots$ of very tiny action quanta ($\hbar=1.05\cdot 10^{-34}$ Jsec.) in proportion to optical frequency $v(\text{Hz})$ or angular frequency $\omega=2\pi v\left(\frac{\text{radian}}{\text{second}}\right)$.

Shortly thereafter comes Einstein's 1905 theory based on the extraordinary lightspeed invariance axiom. This is now embodied in a 9-digit metrological super constant $c=299,792,458\text{m/sec}$ for speed of light. The c -axiom is an iconic beginning of the subject now called special relativity (SR). Also in 1905, Einstein's miracle year, he introduces the theory of the photoelectric effect. This begins the subject of quantum electrodynamics (QED) where quanta of light are emitted and absorbed in what we now know as the quantum field theory of modern molecular, atomic, nuclear, and subnuclear optical spectroscopy.

QED supports a century of exploration covering a spectral range of energy from nano-Kelvin to Tera-electron-volt, over 30 orders of magnitude, with some parts of the infrared and visible spectrum being studied with a precision of 15 to 18 decimal digits.

The degree to which the power and precision of modern physics has surpassed that of

classical physics might seem surprising given that the light-axioms of the modern science seem to lack the self-evident rock hard feel-of-steel logical precision of classical mechanics. A classicist (and our students) should be excused (even encouraged) to be skeptical of the modern SR and QM axioms and to become more aware of the mystery within them.

So it is that deeper evidence has shown we are fooled by the apparent classical hardness of rocks and steel. All this is now seen to be an illusion perpetrated by some extremely wavy and ethereal atomic or subatomic entities, indeed by light itself. Moreover the concept of mass in Newton's laws can no longer be taken for granted (or granite) and has always been at least as puzzling a mystery as any that the modern axioms are proposing.

Yet we become easily accustomed to undeniably wonderful technology such as global positioning systems (GPS) that achieve geographic ultra-precision more by modern physics of ethereal and wavy light and not so much by classical mechanics of steel frames. One may argue that modern physics deserves a natural philosophy and logical development that better reflects the ultra precision and elegance of the technology it is providing.

A. Mythos vs. Logos and Occam's Razor

This motivates us to reclaim intellectual tradition wherein technological success reinvigorates the perennial Mythos vs Logos battle to replace natural mysteries with simpler and more logical explanations. Ever since Thales of Miletus (600 BCE) explained and predicted a solar eclipse and Euclid (300 BCE) developed the geometry of Thales, inventors and artisans like Archimedes, Michaelangelo, Hypatia, daVinci and others have grown the Seven Liberal Arts into thousands of creative arts and sciences. Now relativity and quantum theory are among the latest of such intellectual success stories.

Philosophers generally agree that such explosive intellectual growth owes something to discovery of more concise and trustworthy axiom sets according to an ideal stated by William Ockham (also Occam 1386-1443 ACE). One ideal is known as Occam's Razor (*Pluralitas non est ponenda sine necessitate.*) and has many translations: literally (*A plurality of conjectures should not be made without necessity.*), logically (*Assume less to prove more.*), and practical programming advice (*Keeping it simple makes it powerful.*).

Mathematical development from the beginning of Euclidean geometry has repeatedly shown the value of finding deeper and sharper axioms. Doing so produces more powerful

theorems and thereby grows the discipline. To the extent that mathematics underwrites physics one might expect deeper and sharper physical axioms to similarly generate more powerful theoretical physics.

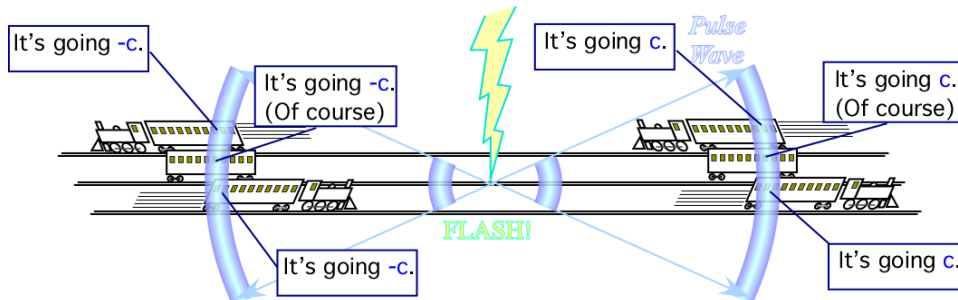


FIG. 1. Lightspeed c -Axiom

B. Lightspeed axiom meets Occam's Razor

The first modern physics axiom mentioned above is the SR lightspeed invariance axiom. In his famous monograph *The Meaning of Relativity*, Einstein envisions train passengers measuring train-relative velocity of a lightning flash-wave emanating from its strike point at a central railway station. Their measurements are sketched by cartoon comments in Fig. 1 for each of six trains on parallel tracks. Regardless of train speed or direction each passenger (if so equipped) records the *same* flash speed c relative to his or her respective train. (Henceforward we take a 4-figure approximation for light speed $c=3.000\cdot 10^8 m/s$.)

This version of the SR c -axiom is a pedagogical showstopper! Anyone being introduced to SR between the year 1905 and (We guess optimistically now.) a future year of 2050, is hard put to conceive of a finite velocity c that you cannot exceed, in fact that you cannot even *begin* to exceed, and that moreover, is the same speed for everyone in the universe no matter what train (or galaxy) they ride.

For years I introduced the c -axiom by calling it *The Coyote vs Roadrunner Axiom*. This is after the Chuck Jones cartoon characters so loved by students of all ages *circa* 1940-2012. In over 40 episodes a slow and frustrated Wile E. Coyote tries to run down a speedy Roadrunner by purchasing from the *Acme Co.* vehicles of dubious safety standards but enormous speed. (Most notable is a rocket powered unicycle.) No matter what Acme contraption Wile E. rides, the Roadrunner zooms by with identical 'meep-meep' passing speed. (This may be a

singular case where cartoon physics is inadvertently consistent with a real physical effect!)

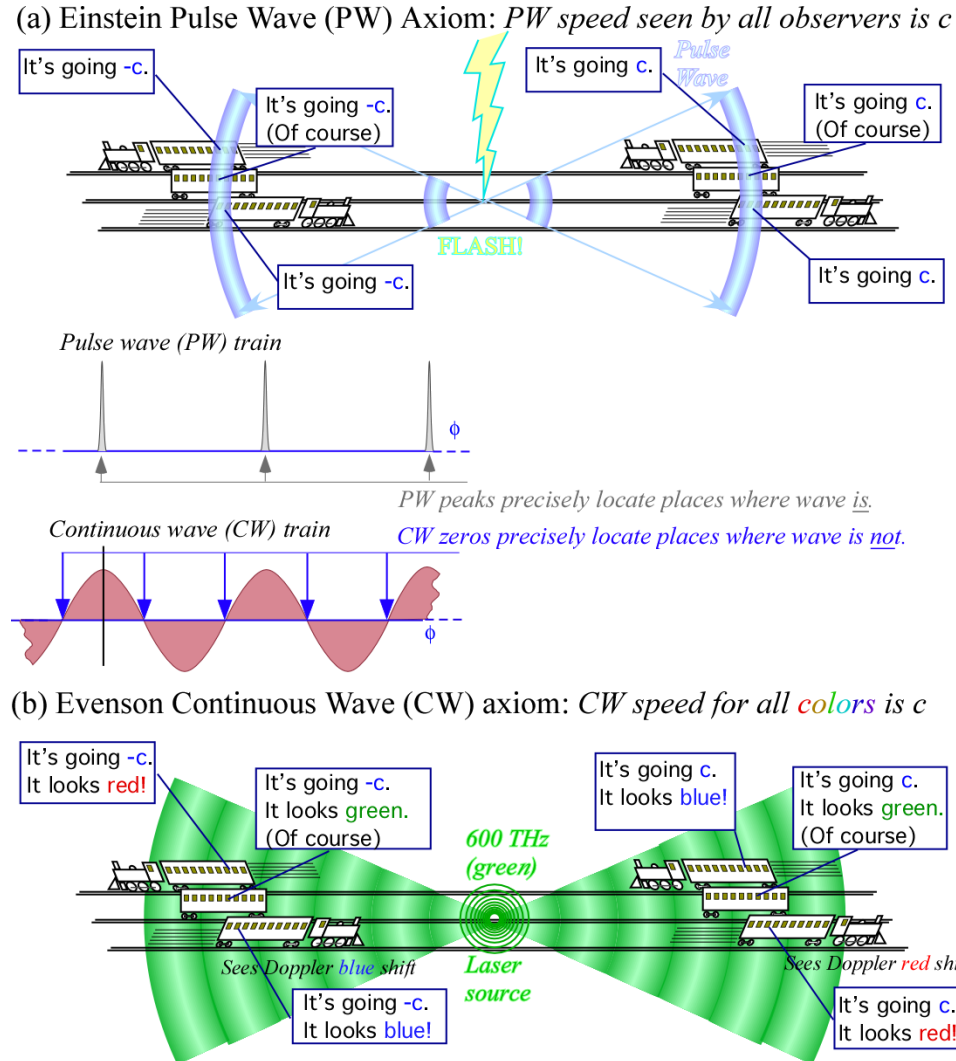


FIG. 2. Lightspeed c -Axioms for (a) Pulse Waves, (b) Continuous Waves (CW) f

C. Galileo loses one

Still it wears on one's credibility to base physics on a cartoon series, even one that is 20 years older than string theory or supersymmetry or other postmodern arts that, as of this writing, also seem equally unable to provide helpful new insight for modern physics students.

Instead, our students need a way to transcend the Galilean relativity that is programmed into our human limbic systems inherited from earlier animals (perhaps even coyotes). How then do we disabuse students of a Galilean notion that any velocity u_x added to your motion

causes you to see that same component u_x subtracted from the motion of all other things in the universe? One needs a way to show clearly how Galilean worldviews fail totally for passing light waves (or Roadrunners). Moreover, this primitive worldview cannot conceive of any speed that appears the same to all observers, except an undefinable infinite one.

To begin disabusing Galilean notions we apply Occam's razor to the Einstein c -axiom of Fig.1 involving a lightning flash wave shown again in Fig.2a. A flash is a complicated electromagnetic pulse wave (PW) composed of a multitude of Fourier components that are each a continuous wave (CW). With Occam's razor we cut the PW down to a single laser CW that has a more concise and eventually more comprehensible axiom.

The result will be called the Evenson CW axiom after Kenneth M. Evenson whose ultra-precise speed of light measurements led to a 1981 revision of international metrology that fixed $c=299,792,458m/sec$ as a definition of the meter in terms of the second. This paved the way for applications of greater metrological precision such as the GPS. A short retrospective of Ken's life and work is given in an Appendix.

The Einstein PW-axiom and the Evenson CW-axiom are compared in Fig.2. The latter Evenson CW axiom claims CW light in a vacuum travels the same speed c for all frequencies. While it is rare for an axiom to have a self-evident proof, the Evenson CW-axiom comes close to having just that. Moreover it becomes the main motivator for a compelling derivation of an analytic-geometric formulation of relativity and relativistic quantum mechanics. Indeed, we intend to show that all the mechanics that we experience every day is due pretty much to a simple fact: *All colors go c .*

Relativity is not just about high energy physics (or high-speed roadrunners). As we will see, it is about everything, slow or fast.

D. Doppler shifts add some color

It is important to see why Occam-razor surgery of the PW-axiom is a logical lifesaver that makes the Evenson CW axiom come alive for analysis. The acronym CW stands for *Continuous Wave* (This is standard laser jargon.) or *Coherent-state Wave*. (CW laser modes are described by quantum coherent oscillator states.) CW may also denote simply *Cosine Wave* (the real part of a classical plane wave), or finally and most important here, a *Colored Wave* (assuming optical frequency ν in the visible range of 450THz[red] to 700THz[blue])

The latter is in contrast to PW (*Pulse Wave, Particle-like Wave, or Packet Wave*) that is a colorless or “white” combination of CW that has much more complexity and variability.

Neither PW observers in Fig. 2a nor CW observers in Fig. 2b can see any shift in light wave speed away from the super-constant c . However moving CW observers of the blue-green 600 THz light could (in principle) see a shift in color, that is a shift in CW frequency ν or angular velocity $\omega=2\pi\cdot\nu$ of CW phase. This is the optical Doppler shift and is a primary relativistic variable. It is also a primary way for the highway patrol to very precisely measure your freeway velocity relative to a Doppler monitor. Doppler shift is *1st-order*, that is, linear in velocity if you travel at a freeway speed well below the ultimate speed limit of c .

Now most texts introduce relativity by way of *2nd-order* effects such as Einstein time dilation or Lorentz contraction that are quite mysterious and immeasurably tiny at freeway speeds. A first-things-first introduction uses CW Doppler, a *1st-order* effect that is far less mysterious. In 1626, Johannes Doppler showed how a descending frequency of a passing train whistle is a simple wave effect. One encounters more wave crests per second (a blue shift for light) when approaching a wave source and less (a red shift for light) when fleeing a source. But, how much more or less for *light* waves that have this strange c -limit? Also, why must there be such a limit?

Geometric construction of relativity in the following sections is based on thought experiments involving quite large Doppler shifts of a 600 THz blue-green CW light to ultraviolet 1200 THz and then a case of Doppler redshift of that 600 THz beam to infrared 300 THz. Here this kind of thought experiment is used first to clarify the Evenson CW axiom. Such extreme shifts require that pokey old trains of Einstein be replaced by relativistic spaceships. The thunderous old PW source of Thor is replaced by 600 THz CW laser sources as in Fig. 2b. Finally, high-resolution spectrometers managed by two laser physicists, Alice and Bob, will replace the old-fashioned Einstein train riders.

It has become traditional for quantum opticians to imagine optical channels between a point B and a point A to be manned (or woman-ed) by live characters named Bob and Alice, respectively. Alice’s tunable CW laser replaces Thor’s thunderbolts, and Bob’s high-resolution spectrometer on his faraway spaceship replaces train-riding observers in Fig. 2b.

E. Alice's tricks and Bob's surprises

This particular thought-vignette begins with Bob sitting stationary relative to Alice. Bob is located millions of kilometers to the East of Alice (far right of Fig. 2b.) with Alice's laser shining on Bob. Thus a precise 600 THz appears on both the digital readout of Alice's CW laser source and on a readout of Bob's frequency receiver. Unbeknownst to Bob, Alice is able to tune the laser on her spaceship and plans to do so as she accelerates toward Bob. Alice has cleverly programmed the laser to tune its frequency down with each increase of her velocity and do so just the right amount so Bob continues to see an unchanged 600 THz reading on his receiver-spectrometer.

Alice wants to fool Bob into thinking she has not moved and then surprise him by zooming by with a loud '*meep-meep.*' To really fool Bob into thinking that she is the dutiful stay-at-home he imagines, Alice must also detune wave *amplitude* using the same velocity formula that works for Doppler frequency. (This formula and its double duty nature will be derived later.) If Alice and Bob have a communication channel like a cell phone, Alice will also have to detune her end of that channel appropriately in order to not make Bob suspicious.

Now suppose Alice pauses her acceleration at a velocity corresponding to an octave Doppler blue factor of $b=2$, that is, while Bob thinks he is still receiving her steady blue-green 600 THz laser beam, she has actually down-tuned her laser to an infrared 300 THz. To receive Bob's calls Alice must tune her phone receiver up by factor of 2 and her phone transmitter down by a factor of 2, just like her laser, in order to call up Bob. (The tune-up-or-down by 2 is a result of time reversal symmetry as will be described shortly.)

Always the trickster, Alice asks Bob if he notices anything different about her laser beam. Bob replies, "It's still your beautiful blue-green and reads 600 THz to 18 digits." Alice says, "Okay, that checks your frequency, but what is your wavelength reading?"

Alice's leading question is a crucial one for relativity and quantum theory. She is asking if Bob is receiving some 'phony' kind of blue-green 600 THz, in this case, one that was produced by an infrared 300 THz laser moving very rapidly toward Bob. And, more generally, one may ask, "How many different kinds of 'phony' blue-green, or of any other color or frequency, are possible in the great vacuum of the universe?"

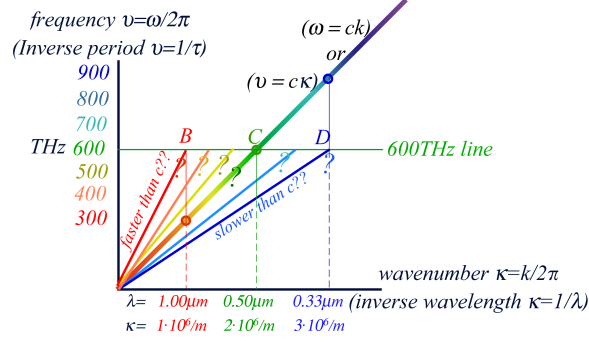


FIG. 3. Dispersion plot analysis of light speed v . color or frequency.

F. Dispersion plots: Keyboards of the gods

A (κ, v) graph in Fig.3 frames Alice’s question by plotting parameters that define Alice’s laser wave shape, frequency v of waves per second and wavenumber κ of waves per meter. Per-space-per-time (or per-space-time) plots are reciprocal to space-time (x, t) plots used by Minkowsky to represent Einstein-Lorenz frame relativity and are known as a *dispersion plots*. They help to clarify wave mechanics and, in turn, relativity and quantum mechanics. In a sense they are control panels for wave dynamics in space and time and one might prosaically name them *keyboards of the gods*. (The professional jargon is “Fourier-space.”)

Imagine a dispersion plot as an extraordinary keyboard that, like ordinary mortal keyboards, produces a wave of frequency v if pressed at point (κ, v) , but this ‘deity’ keyboard tunes *both* wave period τ (inverse $\tau=1/v$ of frequency $v=1/\tau$) *and* wavelength $\lambda=1/\kappa$. Ordinary mortal keyboards (and Alice’s laser control) cannot set v *and* κ independently. Instead, we will show CW frequency v must be locked to a particular wave number κ by a dispersion function $v(\kappa)$. For plane wave light this is a linear dispersion-less function $v=c\kappa$ plotted by the diagonal straight line also labeled $\omega=ck$ by angular parameters in Fig.3.

In Alice’s frame the v and κ values are well established. Her $v = 600$ THz laser puts out 600 trillion λ -wavelengths per second all going at speed $c=300$ million meters per second. Dividing a one-second travel distance by 600 trillion gives a half-micron wavelength ($\lambda = 300 \cdot 10^6 m / 600 \cdot 10^{12} = 0.5 \mu m$). Alice’s laser cavity length must be an integral multiple of wavelength λ for these waves to fit perfectly and resonantly amplify 600THz light.

But what wavelength does Bob see for the 600THz light beam coming from Alice’s spaceship laser that she has detuned to 300THz, a wavelength of $1 \mu m$ (300 million/300 trillion) as

she rapidly approaches Bob? Bob must see some $\lambda = 1/\kappa$ value on the horizontal 600THz line in Fig.3. Could it be point D with wavelength $\lambda = 1\mu m$ ($\kappa = 10^6$ waves per meter) that Alice set on her laser? Or could λ be some other value like point B with $\lambda = 1/4\mu m$ ($\kappa = 4 \cdot 10^6$). Or will Bob tally an in-between point C with $\lambda = 1/2\mu m$ ($\kappa = 2 \cdot 10^6$)?

G. Support for Evenson's Axiom

If the vacuum cannot support an infinite variety of blue green 600THz waves then Bob must find his λ at compromise point C on line $v=c\kappa$ in Fig.3. Point C has wavelength $\lambda = 0.5\mu m$ that Alice would have measured when she first turned on *her* blue-green 600 THz. If the vacuum treats all frequencies equivalently then they all lie on line $v=c\kappa$ with slope $v/\kappa=\omega/k=c$ and thus all travel at speed c .

This essentially proves Evenson's axiom: *All colors go c*. Any point like B to the left of C will have less κ , greater slope v/κ , and thus corresponds to a CW with a speed greater than c . Conversely, any point like D to the right of C corresponds to a CW slower than c .

One might speculate that a frequency- v oscillator produces all varieties of frequency v with a range of κ or λ but only the $\kappa = v/c$ variety survives resulting wave interference.

A key idea is that plane waves of different frequencies moving in a given direction must march in lock step. This is a powerful idea that will take us far into relativistic quantum mechanics. First of all, Einstein's mysterious PW axiom in Fig.1 is now a theorem since all Fourier components forming a PW must march in lock step and maintain a dispersion-free pulse going at speed c as agreed by *all* observers. (PW *shape* is quite another matter.)

Evenson's axiom demands a dispersion-less (linear) dispersion function $v = c\kappa$. This logical clarification jives with experimental observation of the night sky whether by eye or through Hubble and Spitzer telescopes. If speed of red light differed by even a small percentage from that of blue light coming from a billion light-year distant galaxy then their arrival times would differ by millions of years. That is plenty of time for a galaxy to move or change shape. The resulting image would be more like a psychedelic smear, not the crystal clear images of cataclysmic behavior Earthlings have recently come to enjoy.

In summary, Evenson's axiom shows that Bob cannot detect that Alice is tricking him. Bob sees 600THz light that has no birth certificate to tell it was actually created by Alice's 300THz laser advancing just fast enough to make him think she is using her 600Thz laser.

H. Rapidity: Doppler arithmetic and geometry

When Alice does her ‘*meep-meep*’ zoom-by passing of Bobs observatory, there are two surprises for him. First, that she has been moving all this time and second that he sees her 600 THz light suddenly redshift its frequency. (Assuming Alice maintains her speed and the 300 THz laser broadcasting from both ends of her spaceship, Bob hears ‘*MEEP-moop*’ if the wave optics could be vocalized like Doppler’s passing train whistle.)

To find Bob’s ‘*MEEP-moop*’ shift one re-examines the earlier shift of Alices $v_A=300\text{THz}$ source readout to Bob’s $v_B=600\text{THz}$ receiver readout. A question arises. Should one relate the Alice and Bob frequencies by an *arithmetic* Doppler decrement Δ (as in $v_B = v_A + \Delta$) or with a *geometric* Doppler blue-shift factor b (as in $v_B = b \cdot v_A$)?

Evenson’s axiom demands that waves of different frequencies such as Alice’s laser ($v_A=300\text{THz}$) and her cell phone ($v_a=3\text{THz}$) must march in lockstep and do so for any other observer such as Bob who sees $v_B=600\text{THz}=2v_A$ for her laser and therefore must see the same proportional increase $b=2$ in frequency ($v_b=6\text{THz}=2v_a$) for her cell phone.

Thus the Doppler factor $b_{BA}=2$ depends on the relative motion of Bob and Alice and not at all on the frequency of light waves that pass between them. Meanwhile an arithmetic decrement is $\Delta_{BA}=300\text{THz}$ for her laser but only 3THz for the cell phone. Doppler factor b is defined as received frequency divided by source frequency, and is greater than 1.0 if the spatial interval between source and receiver is decreasing and less than 1.0 if the interval is increasing, that is ($b<1$) for departing and ($b>1$) for arriving. (A Doppler factor b might be viewed has a be-happy-coefficient if Alice and Bob are simpatico.)

The Doppler factor flips in a time reversed situation. Suppose a detailed movie of Alice approaching Bob is played backwards. The digital readouts $v_A=300\text{THz}$ for Alice and $v_B=600\text{THz}$ for Bob remain the same, but Alice reverts to being a departing 300THz *receiver* and Bob becomes a 600THz *source*. (Output light becomes input light and vice-versa.) Then receiver-over-source ratio is $b=v_A/v_B=1/2$, inverse to what it is if source and receiver are approaching each other at the same speed.

This flip factor $b=1/2$ applies to Bob’s ‘*MEEP-moop*’ shift from 600THz to $(1/2)v_A=150\text{THz}$ that he receives from Alice’s departing $v_A=300\text{THz}$ source after passing. It is not a happy-feeling turn of events unless Alice reverses and returns to raise Bob’s frequency-reading.

Indeed, Alice must return to facilitate a wave-interference development of relativity and

quantum theory. Wave dynamics, like personal interactions, simply do not exist without having (at least) two-to-tango. Feynman's approach to quantum processes is based on $\langle A|B \rangle$ amplitudes that tell to what extent a condition A arises after B and vice versa. Pairwise Doppler relativity underlies the wave mechanics that precisely governs quantum processes.

The Evenson CW axiom depicted in Fig.2 and Fig.3 claims that CW laser light goes c (*en vacuo*) regardless of color (frequency). Alternatives to this lead to logically untenable behavior of optical Doppler shifts. Instead, lock-step marching of frequencies favors Doppler blue-shift factors b_{BA} that relate frequency v_A of approaching source-A (Alice returns!) to frequency v_B seen by receiver-B (Bob awaits!) in a *linear* transfer equation.

$$(B/A) = b_{BA} = \frac{v_B}{v_A} \text{ or: } v_B = b_{BA}v_A = (B/A)v_A \quad (1)$$

(Transform coefficient b_{BA} is the same for *all* frequency values it transforms.)

Each *arrival* case has a time-reversed *departure* case with *inverse* red-shift factor r_{AB} .

$$(A/B) = r_{AB} = \frac{v_A}{v_B} \text{ or: } v_A = r_{AB}v_B = (A/B)v_B \quad (2)$$

Then Bob (source) says goodbye to departing Alice (receiver). Colorful mnemonic of b for *blue* (or “be-happy”) and r for *red* (or “remorse”) is replaced by transform (R/S) that is *source-to-receiver* ratio with right-index source frequency v_S in *denominator*.

$$(R/S) = \frac{v_R}{v_S} = \frac{1}{(S/R)} \quad (3)$$

Usual quantum Hebrew-like right-to-left index order applies to Doppler arithmetic of Lorentz transforms of motion in one-dimension of space. Then (R/S) is blue ($(R/S) = b_{RS} > 1$) if R -to- S space is decreasing (or deflating) and red ($(R/S) = r_{RS} < 1$) if it is increasing or inflating. A third receiver C (Carla, a slightly evil twin sister to Alice) can come online and see Alice's laser beam at frequency $v_C = (C/A)v_A$. If Carla can see Bob passing on v_B light he got from Alice, then Carla also sees $v_C = (C/B)v_B$. Then (1) implies a product rule.

$$v_C = (C/A)v_A \text{ and } v_C = (C/B)v_B = (C/B)(B/A)v_A \text{ imply: } (C/A) = (C/B)(B/A) \quad (4)$$

Defining relative *rapidity* $\rho_{AB} = \ln(A/B)$ turns the product rule (4) into a ρ -sum rule (5).

$$\rho_{CA} = \rho_{CB} + \rho_{BA} \text{ where: } e^{\rho_{CA}} = (C/A) = e^{-\rho_{AC}} = 1/(A/C) \quad (5)$$

A 1TeV proton has velocity $u = .9999956c$, Doppler ratio $b = (C/A) = 2132$, rapidity $\rho_{CA} = 7.665$ so ρ -arithmetic is simpler. Sum rule (5) makes ρ a Galilean-like parameter for adding speeds easily in Lorentz symmetry. (ρ , b , u , and energy are all related later by (18) and (49).)

III. LASER PHASOR CLOCKS IN SPACE AND TIME

A single laser CW moving in time t and space x is denoted by a complex exponential in Eq.(6) and shown by *phasor* clocks lined up above a related space-time plot in Fig.4.

$$\psi(x, t) = Ae^{i(kx - \omega t)} = A(\cos(kx - \omega t) + i\sin(kx - \omega t)) \quad (6)$$

Real angular wavenumber (wavevector) $k = 2\pi\kappa$ and frequency $\omega = 2\pi\nu$ are per-space-time quantities discussed after Fig.3. Together they determine the *phase* $\phi = kx - \omega t$ at each point x in space and time t . The phase is a dimensionless quantity giving a reading in ϕ -radians of a clock hand on a *phasor*-clock at space-time point (x, t) . (ϕ is also called *gauge* as in a gas-gauge or a sweep-second-hand. It is a polar coordinate of wave function $\psi(x, t)$.)

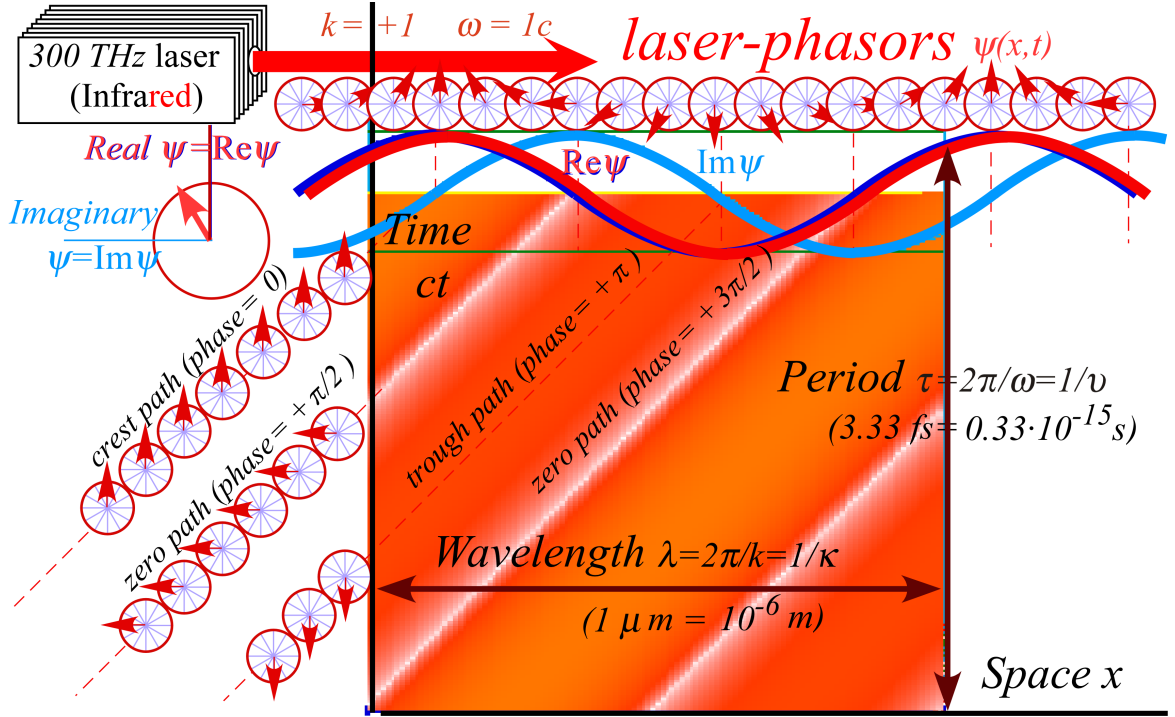


FIG. 4. Plane wave phasors drawn above their space-time (x, ct) -plot for single 300Thz CW.

A phasor is analogous to Hamilton-Poincare oscillator phase space with abscissa q and ordinate p giving clockwise elliptical orbits. A physicist's complex phasor has a real axis ($Re(\psi)$ in Fig.4 top left) for plotting oscillating variables such as electric field.

$$Re \psi(0, t) = E(t) = A\cos(\omega t) \quad (7)$$

An imaginary axis ($Im(\psi)$) tracks field time rate of change. The latter is scaled to units of angular frequency ω . Then orbits are clockwise circles sketched by clock hands in Fig.4.

$$Im \psi(0, t) = \dot{E}(t)/\omega = -A \sin(\omega t) \quad (8)$$

At $x=0$ amplitude A is real ($A=1$). Elsewhere, A is a complex factor like Ae^{ikx} , however amplitude A may also be complex $|A|e^{i\phi_0}$ so as to set initial phase lag ϕ_0 at origin $(0,0)$.

$$\psi(x, t) = Ae^{ikx}e^{-i\omega t} = |A|e^{i\phi_0}e^{ikx}e^{-i\omega t} = |A|e^{i(kx-\omega t+\phi_0)} \quad (9)$$

For $\omega > 0$, phasors turn *clockwise* at rate ω as time t advances but each is set *anti-clockwise* (back in time) by $k \cdot \Delta x$ relative to neighbors Δx to its right. Thus, phase-leading phasors feed phase-lagging ones, and the positive- k wave shown in upper Fig.4 moves left to right.

Just below the phasor clock wave in the top row of Fig.4 is a cosine-wave real part (7) and a sine-wave imaginary part (8). Both move left-to-right at phase velocity ω/k with the latter exactly a quarter wave ahead. (It mirrors a U.S. corporate mantra, “*Imagination precedes Reality by exactly one Quarter!*”) As phasor clock hands rotate clockwise at angular velocity ω any phase value ϕ translates at $c = \omega/k$ while clock bodies remain fixed to x axis.

$$\phi = kx - \omega t = const. \implies x = \frac{\omega}{k}t + const. \quad (10)$$

The space-time (x,ct) -plot centered in Fig.4 tracks the left-to-right motion of just the real part (7) of the wave represented by Eq.(6) or Eq.(9). There clock bodies move at or very near the phase velocity of light with hands virtually frozen! It will be shown that clock trains for all moving frames adjust their local ω and k to phase-match each clock in Fig.4.

One gains insight from wave-optical-relativity or *relawavity* of laser waves that now *are* our most precise clocks and meter-sticks. Old Swiss cuckoo-clocks lack 18-figure precision of CW or PW laser oscillators and do not reveal the relativistic logic of wave mechanics.

In Fig.4, white lines track real-part zero-paths with phase $\phi = (2n+1)\pi/2$ lying between crest paths ($\phi = 2n\pi$) in light shaded regions and trough paths ($\phi = (2n+1)\pi$) in dark-red regions. Real CW zero-paths become precise space-time grids in Fig.5 below. Much insight is gained by letting Nature provide its own coordinate grids and “frames.”

IV. LASER-PHASOR LORENTZ-MINKOWSKI FRAME GEOMETRY

If two green $600THz$ waves in Fig.5a-b collide they make a space-time grid as in Fig.5c where they interfere to create a standing wave with real-zero-paths making a square grid in

(ct)-time *vs.* (x)-space. Zeros of wave real parts of the wave-sum factored into a product of a complex exponential (*phase* factor $e^{-i\omega t}$) and amplitude (*group* or *envelope* factor $2\cos kx$). Zeros of the latter are vertical white lines parallel to time axes ($kx=(n+1/2)\pi$ grid lines). Zeros of real part of phase factor $\text{Re } e^{-i\omega t}=\cos(\omega t)$ are horizontal lines parallel to the space axis ($\omega ct=(n+1/2)\pi$ grid lines). Plots of vertical time axes and horizontal space axes are *Minkowski* plots, complementary to *Newtonian* plots of space versus horizontal t -axes.

Fig.6 shows how Fig.5 appears in a left-moving frame facing a right-beaming laser blue-shifted by $b_{BA}=2$ to 1200THz and a receding left-beaming laser red-shifted to 300THz . A Doppler factor of $b_{BA}=2$ represents enormous relative velocity u between Alice and Bob. To meet at such speed would end their relationship in a blinding flash. Derivation is needed of their u and related quantities including cost of slowing them. This will be done in the original scenario wherein Alice travels at positive velocity (left-to-right) toward Bob fast enough that he experiences Doppler $b_{BA}=2$ and sees a searing UV-beam of 1200THz going left to right. Add to this sister Carla who is far to the right and co-moving with Alice while shining 600THz back at Bob. He sees Carla's light red-shifted ($r_{BC}=\frac{1}{2}$) to a gentler infra-red beam of 300THz going right to left. If Alice and Carla have identical velocity and 600THz frequency set for their counter-propagating laser beams then they make for themselves a standing wave like Fig.5 with a 2-CW Cartesian time-space (x, t) grid.

Now what does Bob see if Alice and Carla's beams interfere to form their shared (x, t) grid? A related question: What grid does Bob make by beaming his own 300THz lab laser leftward (like Carla's beam) and his own 1200THz laser rightward (like Alice's beam)?

The answer must be: He makes the (x', ct') grid in Fig.6. And, (with ideal coherence discussed later) so do Alice and Carla's beams. Both Minkowski (x', ct') grids display *Einstein-Lorentz transformation* (ELT) to Bob's lab frame from that of Alice or Carla. This gives a quick derivation of ELT matrices by factoring Doppler-shifted wave-sums to get real-zeros giving (x', ct') and (ω', ck') plots. This is done easily by algebra as follows and then even more easily by geometry in Fig.7 that reveals underlying physics of ELT.

A sum Ψ of right-moving wave $\psi_R=e^{iR}$ and left-moving wave $\psi_L=e^{iL}$ factors as follows.

$$\Psi(x, t)=e^{iR}+e^{iL}=e^{i\frac{R+L}{2}}(e^{i\frac{R-L}{2}}+e^{-i\frac{R-L}{2}})=e^{i\frac{R+L}{2}}2\cos\frac{R-L}{2}=\psi_{\text{phase}}\psi_{\text{group}} \quad (11)$$

Right wave phase $R=k_Rx-\omega_Rt$ is a blue-shift $e^\rho(k_Ax-\omega_At)$ of Alice's phase ($k_Ax-\omega_At$). Left wave phase $L=k_Lx-\omega_Lt$ is a red-shift $e^{-\rho}(-k_Ax-\omega_At)$ of Carla's phase ($-k_Ax-\omega_At$).

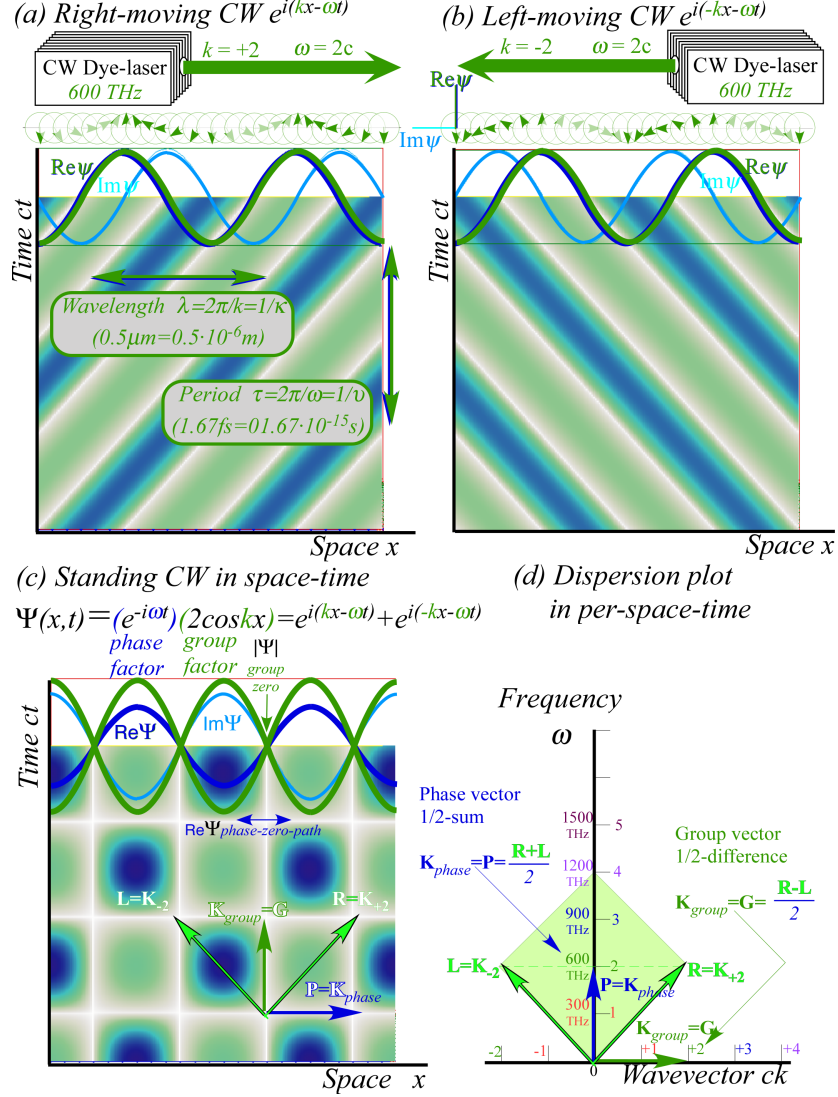


FIG. 5. Colliding pair of 600THz CW. Real wave zeros trace square coordinate grid.

Phase of factor ψ_{phase} is a half-sum $\frac{R+L}{2}$ and that of factor ψ_{group} is a half-difference $\frac{R-L}{2}$.

$$\frac{R+L}{2} = \frac{k_R+k_L}{2}x - \frac{\omega_R+\omega_L}{2}t = \frac{e^\rho - e^{-\rho}}{2}k_A x - \frac{e^\rho + e^{-\rho}}{2}\omega_A t \quad (12)$$

$$\frac{R-L}{2} = \frac{k_R-k_L}{2}x - \frac{\omega_R-\omega_L}{2}t = \frac{e^\rho + e^{-\rho}}{2}k_A x - \frac{e^\rho - e^{-\rho}}{2}\omega_A t \quad (13)$$

The CW geometry begins in Fig 5d with a baseball diamond. Its 1st-baseline is an (ω, ck) vector $\mathbf{R} = (\omega_A, ck_A) = \omega_A(1,+1)$ of Alice's right-moving laser beam. Its 3rd-baseline is a vector $\mathbf{L} = (\omega_C, ck_C) = \omega_A(1,-1)$ of Carla's left-moving laser beam having same frequency but opposite wave vector. Then half-sum phase vector $\mathbf{P} = (\mathbf{R} + \mathbf{L})/2 = \omega_A(1,0)$ is drawn to

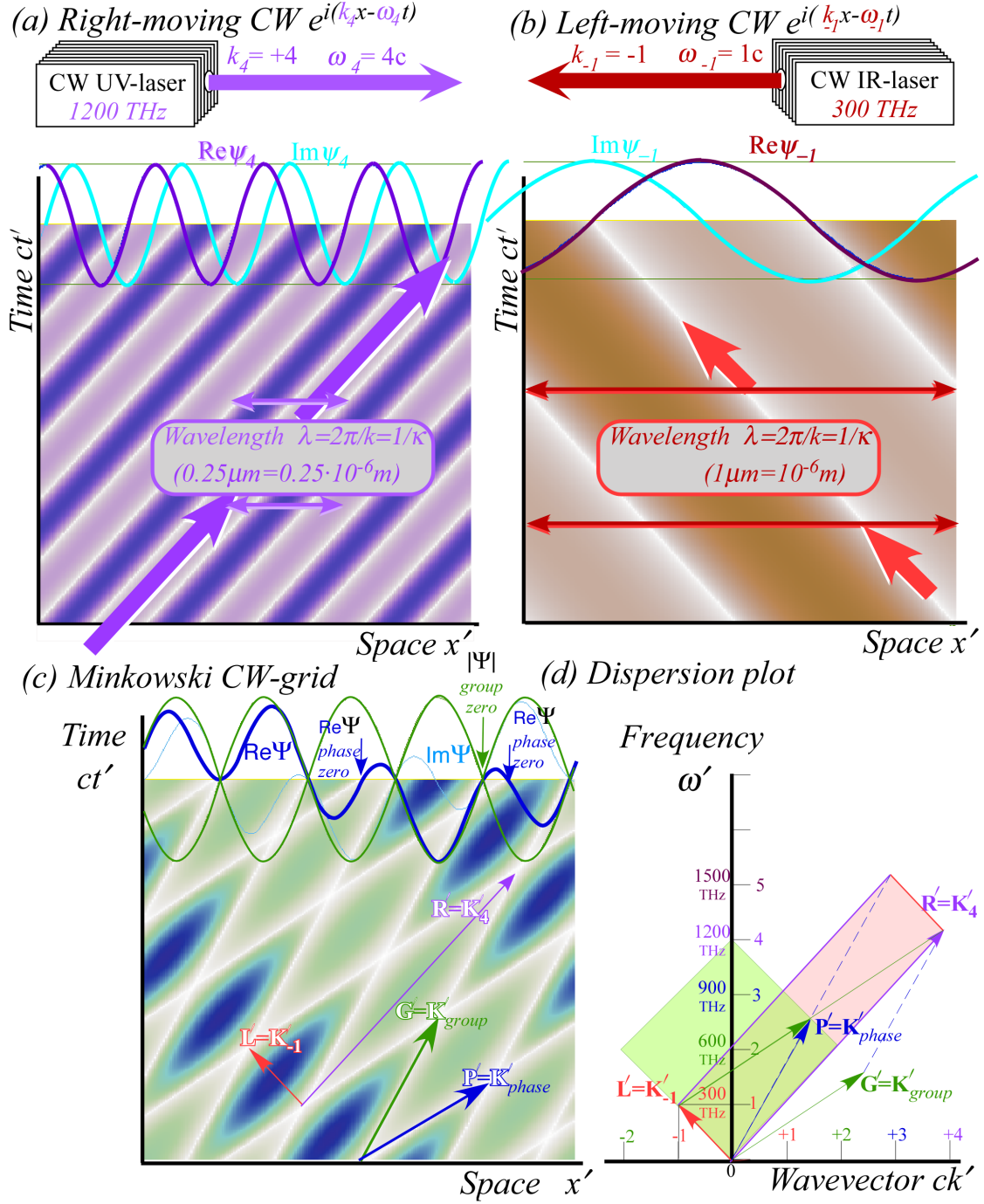


FIG. 6. (a-b) 1200THz collides 300THz CW (c) (x', ct') -zero-paths (d) $(\mathbf{P}', \mathbf{G}')$ -lattice vectors.

diamond center (Pitcher's mound!). Half-difference group vector $\mathbf{G} = (\mathbf{R} - \mathbf{L})/2 = \omega_A(0, 1)$ is to below 1st baseline (Grandstand!) along ck -axis in Fig.5d. Alice and Carla's reciprocal-space (ω, ck) vectors \mathbf{P} and \mathbf{G} switch positions to be their space-time (ct, x) axes with \mathbf{G} along group-zero path defining x -axis and \mathbf{P} along phase-zero path that defines their ct -axis

in Fig.5c. Bob's view of zero-paths in Fig.6 is plotted in detail in Fig.7 for wave-crest paths.

According to Bob, Alice's right-moving $600THz$ laser beam is blue-shifted by $b_{BA}=e^\rho=2$ as she approaches him. So vector \mathbf{R}' that Bob ascribes to Alice is her vector \mathbf{R} doubled in length to $\mathbf{R}'=\omega_A b_{BA}(1,+1)$. (It must stay on the 1st-baseline to obey Evenson's axiom.) Meanwhile, Bob sees Carla's left-moving $600THz$ laser beam red-shifted by $b_{BC}=e^{-\rho}=\frac{1}{2}$ as she recedes and her vector \mathbf{L} halved in length to $\mathbf{L}'=\omega_A b_{BC}(1,-1)$ along the 3rd baseline. Bob's phase $\mathbf{P}'=(\mathbf{R}'+\mathbf{L}')/2$ and group $\mathbf{G}'=(\mathbf{R}'-\mathbf{L}')/2$ vectors define his warped view of Alice's baseball diamond (Fig.5c-d) using his (x',ct') and (ω',ck') coordinates in Fig.7c-d.

$$\begin{pmatrix} \omega'_{phase} \\ ck'_{phase} \end{pmatrix} = \mathbf{P}' = \frac{\mathbf{R}'+\mathbf{L}'}{2} = \omega_A \begin{pmatrix} \frac{e^\rho+e^{-\rho}}{2} \\ \frac{e^\rho-e^{-\rho}}{2} \end{pmatrix} = \omega_A \begin{pmatrix} \cosh \rho \\ \sinh \rho \end{pmatrix} = \omega_A \begin{pmatrix} \frac{5}{4} \\ \frac{3}{4} \end{pmatrix} \quad (14)$$

$$\begin{pmatrix} \omega'_{group} \\ ck'_{group} \end{pmatrix} = \mathbf{G}' = \frac{\mathbf{R}'-\mathbf{L}'}{2} = \omega_A \begin{pmatrix} \frac{e^\rho-e^{-\rho}}{2} \\ \frac{e^\rho+e^{-\rho}}{2} \end{pmatrix} = \omega_A \begin{pmatrix} \sinh \rho \\ \cosh \rho \end{pmatrix} = \omega_A \begin{pmatrix} \frac{3}{4} \\ \frac{5}{4} \end{pmatrix} \quad (15)$$

Ratio $\frac{V'_{phase}}{c} = \frac{\omega'_{phase}}{ck'_{phase}}$ is slope of phase vector \mathbf{P}' in Fig.7d (ω', ck') -plot. Note $V'_{phase} > c$.

$$\frac{V'_{phase}}{c} = \frac{\omega'_{phase}}{ck'_{phase}} = \frac{\cosh \rho}{\sinh \rho} = \coth \rho = \frac{5}{3} \quad (16)$$

Ratio $\frac{V'_{group}}{c} = \frac{\omega'_{group}}{ck'_{group}}$ is slope of group vector \mathbf{G}' in Fig.7d (ω', ck') -plot. Note $V'_{group} < c$.

$$\frac{V'_{group}}{c} = \frac{\omega'_{group}}{ck'_{group}} = \frac{\sinh \rho}{\cosh \rho} = \tanh \rho = \frac{3}{5} \quad (17)$$

Alice and Carla see a $600THz$ standing wave between them. So velocity u of Alice, Carla, and standing wave is precisely group velocity $V'_{group}=u=\frac{3}{5}c$ in Bob's (x', ct') frame. This relates conventional *relativity parameter* $\beta \equiv \frac{u}{c}$, rapidity $\rho = \rho_{BA}$, and blue-shift $b = b_{BA} = e^\rho$.

$$\frac{V'_{group}}{c} = \frac{u}{c} = \tanh \rho = \frac{e^\rho - e^{-\rho}}{e^\rho + e^{-\rho}} = \frac{b - b^{-1}}{b + b^{-1}} = \frac{b^2 - 1}{b^2 + 1} \equiv \beta \quad (18)$$

Inverse Doppler-blue includes a conventional *Lorentz coefficient* $\lambda = \sqrt{1-\beta^2}$ in denominator.

$$b = \sqrt{\frac{1+\beta}{1-\beta}} = \sqrt{\frac{1+u/c}{1-u/c}} = \frac{1+u/c}{\sqrt{1-u^2/c^2}} \equiv \frac{1+\beta}{\lambda} \quad (19)$$

Period $\tau=2\pi/\omega$ (*seconds per wave*) and wavelength $\lambda=2\pi/k$ (*meters per wave*) are plotted in Fig.7a based on frequency $\nu=\omega/2\pi$ (*waves per second*) and wave-number $\kappa=k/2\pi$ (*waves per meter*) values plotted in Fig.7b. Alice's wavelength unit $\lambda_A=\frac{1}{2}\cdot 10^{-6}$ meter (or

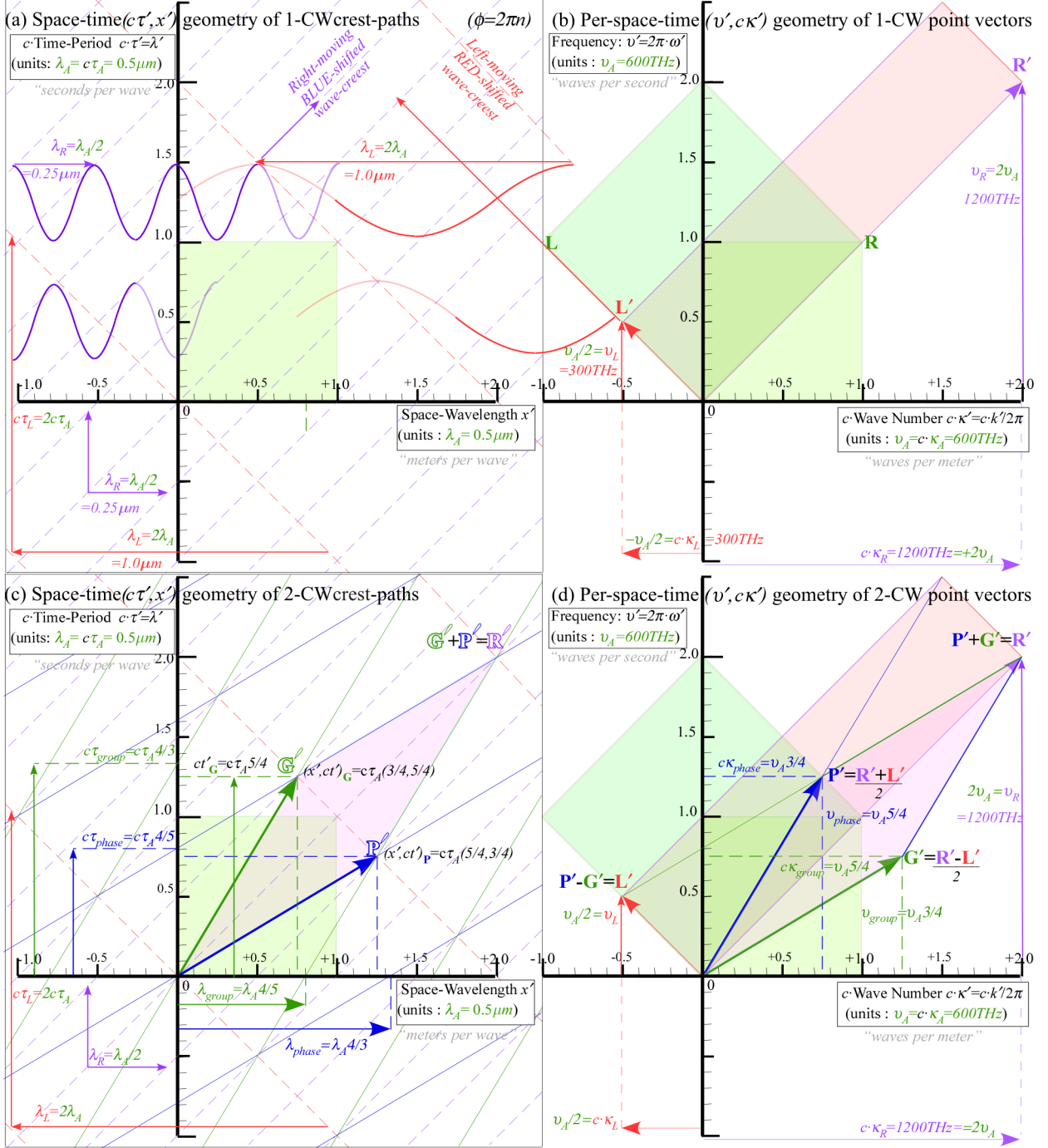


FIG. 7. Plot of Fig. 6 so point $(c\kappa', v')$ in (b) or (d) maps to paths in (a) or (c) of slope $\frac{v'}{c\kappa'} = \frac{\lambda'}{c\tau'}$.

period $= \tau_A = \lambda_A/c = \frac{5}{3} \cdot 10^{-15}$ seconds per wave) scales Fig. 7a while her laser frequency unit, $\nu_A = 600 \text{ THz} = c \cdot \kappa_A$ (or wave-number $= \kappa_A = 2 \cdot 10^6$ waves per meter) scales Fig. 7b. Alice's right-moving laser vector \mathbf{R} is seen by Bob to blue-shift by factor $b_{BA} = e^{\rho} = 2$ to $\mathbf{R}' = 2\mathbf{R}$, while Carla's left-moving \mathbf{L} vector red-shifts to $\mathbf{L}' = \frac{1}{2}\mathbf{L}$. Vector components $(c\kappa', v')$ get inverted to

give wavelength $\lambda' = \frac{1}{\kappa'}$ or period $\tau' = \frac{1}{\nu'}$ intervals between dash-line crest-paths intercepting space or time axes as right-moving short- λ_R waves hit left-moving long- λ_L waves in Fig. 7b. In Fig. 7c dash-line 1-CW paths vanish due to interference and solid-line 2-CW paths appear as derived from components $(c\kappa_{phase}, \nu_{phase})$ of phase vector $\mathbf{P}' = \frac{\mathbf{R}' + \mathbf{L}'}{2}$ and $(c\kappa_{group}, \nu_{group})$ of group vector $\mathbf{G}' = \frac{\mathbf{R}' - \mathbf{L}'}{2}$ in Fig. 7d. Recall (14) and (15).

Inverses of \mathbf{P}' -point coordinates $(c\kappa_{phase}, \nu_{phase}) = (\frac{3}{4}, \frac{5}{4})\nu_A$ in Fig. 7d are space-time axial intercepts of phase-wave period $\frac{1}{\nu_{phase}} \equiv \tau_{phase} = \frac{5}{4}\tau_A$ and wavelength $\frac{1}{\kappa_{phase}} \equiv \lambda_{phase} = \frac{4}{3}c\tau_A$ shown in Fig. 7c where phase-wave crests move at their velocity $V_{phase} = \frac{\lambda_{phase}}{\tau_{phase}} = \frac{5}{3}c$ along lines parallel to \mathbb{P}' -vector. Similarly, \mathbf{G}' -point coordinates $(c\kappa_{group}, \nu_{group}) = (\frac{5}{4}, \frac{3}{4})\nu_A$ invert to group wave period $\tau_{group} = \frac{4}{3}\tau_A$ and wavelength $\lambda_{group} = \frac{5}{4}c\tau_A$ moving at $V_{group} = \frac{\lambda_{group}}{\tau_{group}} = \frac{3}{5}c$ parallel to \mathbb{G}' .

Vectors $(\mathbf{P}', \mathbf{G}')$ in (ν, κ) -space of Fig. 7d map to vectors $(\mathbb{P}', \mathbb{G}')$ in (t, x) -space of Fig. 7c. Slopes trade since velocity is $\frac{\text{frequency}}{\text{wave-number}} = \frac{\nu}{\kappa}$ in (ν, κ) and $\frac{\text{space}}{\text{time}} = \frac{\lambda}{\tau}$ in (t, x) . The $(\mathbf{P}', \mathbf{G}')$ rhombus in Fig. 7d spawns a rhombic lattice of crest-paths in Fig. 7c that are extensions of \mathbb{P}' and \mathbb{G}' . \mathbb{P}' -lines have constant $\phi'_{phase} = k'_{phase}x' - \omega'_{phase}t' = 2\pi N_p$ while \mathbb{G}' -lines have constant $\phi'_{group} = k'_{group}x' - \omega'_{group}t' = 2\pi N_g$. Integer $N_k = \{.. -1, 0, 1, 2..\}$ give crest-paths in Fig. 7c. Odd $\frac{1}{4}$ -integer $N_k = \frac{1}{2}\{.. -\frac{1}{2}, \frac{1}{2}, \frac{3}{2}, \frac{5}{2}..\}$ give two zero-paths for each crest-path as shown in Fig. 6c.

A. Transformations and phase invariance

A laser phasor sketched in Fig. 4 should be taken seriously as a gauge of time (clock) and of space (metric ruler) by giving time (wave period τ) and distance (wavelength λ) in Fig. 7c. A reading of phase ϕ by Alice at a space-time point must equal reading ϕ' by Bob in spite of their unequal readings (x, t) and (x', t') for that point and unequal frequency-wavevector readings (ω, k) and (ω', k') for a laser group-wave or its phase-wave.

$$\begin{aligned}\phi'_{phase} &\equiv k'_{phase}x' - \omega'_{phase}t' = k_{phase}x - \omega_{phase}t \equiv \phi_{phase} \\ \phi'_{group} &\equiv k'_{group}x' - \omega'_{group}t' = k_{group}x - \omega_{group}t \equiv \phi_{group}\end{aligned}\tag{20}$$

Bob's (ω', k') components are in (14) and (15). Alice's (ω, k) are the same with $\rho = 0$. An Einstein-Lorentz Transformation (ELT) of Bob's (x', t') to Alice's (x, t) follows.

$$\begin{aligned}\phi_{phase} &\equiv x' \frac{\omega_A}{c} \cosh \rho - t' \omega_A \sinh \rho = 0 \cdot x - \omega_A t \Rightarrow ct = ct' \cosh \rho - x' \sinh \rho \\ \phi_{group} &\equiv x' \frac{\omega_A}{c} \cosh \rho - t' \omega_A \sinh \rho = \frac{\omega_A}{c} x - 0 \cdot t \Rightarrow x = -ct' \sinh \rho + x' \cosh \rho\end{aligned}\tag{21}$$

The ELT matrix form and its inverse resolve Bob-Alice space-time for Fig. 7c.

$$\begin{pmatrix} ct \\ x \end{pmatrix} = \begin{pmatrix} \cosh \rho & -\sinh \rho \\ -\sinh \rho & \cosh \rho \end{pmatrix} \begin{pmatrix} ct' \\ x' \end{pmatrix} \Rightarrow \begin{pmatrix} ct' \\ x' \end{pmatrix} = \begin{pmatrix} \cosh \rho & +\sinh \rho \\ +\sinh \rho & \cosh \rho \end{pmatrix} \begin{pmatrix} ct \\ x \end{pmatrix} \quad (22)$$

Direct derivation of ELT uses base vectors \mathbb{P}' and \mathbb{G}' or \mathbf{P}' and \mathbf{G}' in (14) and (15).

$$\mathbf{P}' = \begin{pmatrix} \omega'_{phase} \\ ck'_{phase} \end{pmatrix} = \omega_A \begin{pmatrix} \cosh \rho \\ \sinh \rho \end{pmatrix} = \begin{pmatrix} \omega_A \\ 0 \end{pmatrix} \cosh \rho + \begin{pmatrix} 0 \\ \omega_A \end{pmatrix} \sinh \rho = \mathbf{P} \cosh \rho + \mathbf{G} \sinh \rho \quad (23)$$

$$\mathbf{G}' = \begin{pmatrix} \omega'_{group} \\ ck'_{group} \end{pmatrix} = \omega_A \begin{pmatrix} \sinh \rho \\ \cosh \rho \end{pmatrix} = \begin{pmatrix} \omega_A \\ 0 \end{pmatrix} \sinh \rho + \begin{pmatrix} 0 \\ \omega_A \end{pmatrix} \cosh \rho = \mathbf{P} \sinh \rho + \mathbf{G} \cosh \rho \quad (24)$$

Thus ELT matrices (25) identical to (22) resolve Bob-Alice per-space-time for Fig. 7d.

$$\begin{pmatrix} \omega \\ ck \end{pmatrix} = \begin{pmatrix} \cosh \rho & -\sinh \rho \\ -\sinh \rho & \cosh \rho \end{pmatrix} \begin{pmatrix} \omega' \\ ck' \end{pmatrix} \Rightarrow \begin{pmatrix} \omega' \\ ck' \end{pmatrix} = \begin{pmatrix} \cosh \rho & +\sinh \rho \\ +\sinh \rho & \cosh \rho \end{pmatrix} \begin{pmatrix} \omega \\ ck \end{pmatrix} \quad (25)$$

The effects of ELT on time, frequency, wave-number, and wavelength is most easily seen by examining contraction and dilation of wave variables involving both sides of Fig. 7 or Fig. 8.

B. Hyperbolic contraction and dilation functions of wave quantities

Lorentz *length contraction* is a 2nd-order relativistic effect. Alice's group wavelength λ_A in Fig. 5c contracts in Fig. 8a by $\frac{4}{5}$ to λ_{group} , the interval between group crests crossing x' -axis.

$$\lambda_{group} = \lambda_A \operatorname{sech} \rho = \lambda_A \sqrt{1 - \tanh^2 \rho} = \lambda_A \sqrt{1 - u^2/c^2} = \frac{4}{5} \lambda_A \quad (26)$$

Two group zeros exist for each crest so zero-path intervals in Fig. 6a are $\frac{1}{2} \lambda_{group}$. Inverse to λ_{group} in Fig. 8a is wave-number $\kappa_{group} = \frac{1}{\lambda_A}$ in Fig. 8b. Alice's κ_A dilates by $\frac{5}{4}$ to κ_{group} .

$$\kappa_{group} = \kappa_A \cosh \rho = \frac{\kappa_A}{\sqrt{1 - \tanh^2 \rho}} = \frac{\kappa_A}{\sqrt{1 - u^2/c^2}} = \frac{5}{4} \kappa_A \quad (27)$$

Einstein *time dilation* or "clock-slowness" is perhaps the most famous 2nd-order effect. Alice's group period τ_A in Fig. 5c expands in Fig. 8a by $\frac{5}{4}$ to \mathbb{G}' time component $\tau_A \cosh \rho$.

$$t' = \tau_A \cosh \rho = \frac{\tau_A}{\sqrt{1 - \tanh^2 \rho}} = \frac{\tau_A}{\sqrt{1 - u^2/c^2}} = \frac{5}{4} \tau_A \quad (28)$$

SR treatments focus on Einstein dilation and Lorentz contraction formulas and leave stu-

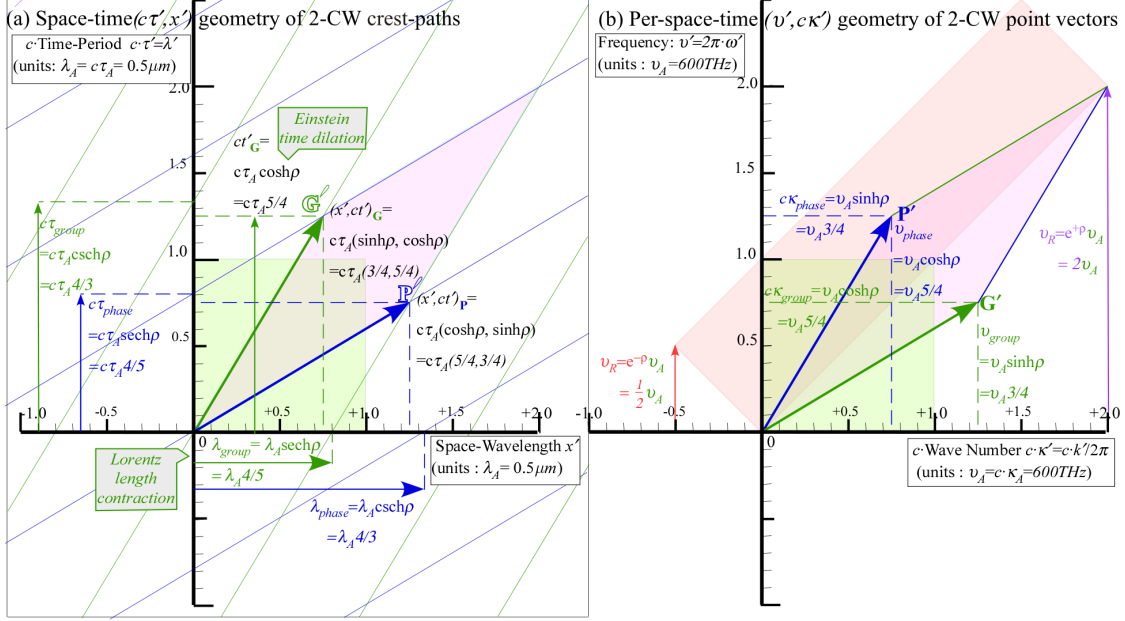


FIG. 8. Hyperbolic functions for relativistic shifts (a) Space-time (x, ct) (b) Per-space-time $(c\kappa, v)$

dents more mystified than enlightened. More enlightened wave geometry in Fig.8 reveals dual pairs of contraction-dilation effects, most with no famous name attached. Alice's group-wave κ_{group} number-dilation (27) or Bob's phase-period τ_{period} contraction, use even 2^{nd} -order hyperbolic function $\cosh \rho$ or its inverse $\text{sech} \rho$. Others, like Alice's group-period τ_{group} contraction or Bob's phase-wavelength λ_{phase} dilation, use odd 1^{st} -order hyperbolic function $\sinh \rho$ or its inverse $\text{csch} \rho$ with range $\pm\infty$. Each is a fraction of Alice's wave unit $(\lambda_A = c\tau_A)(\frac{1}{2}, \frac{3}{4}, \frac{4}{5}, \frac{5}{4}, \frac{4}{3}, 2)$ listed in Table I. They repeat along Bob's x' or ct' axes in Fig.8a.

Equations (14-15) or geometric pairs in Fig.5c-d, Fig.6c-d, and Fig.8a-b allow more comprehensive coverage of SR effects. The Evenson axiom lets one *first* use CW Doppler light to find per-space-time ELT of (ω, ck) . Then space-time ELT of $(c\tau, \lambda)$ follows.

$phase$	$b_{RED}^{Doppler}$	$\frac{c}{V_{phase}}$	$\frac{\kappa_{phase}}{\kappa_A}$	$\frac{\tau_{phase}}{\tau_A}$	$\frac{v_{phase}}{v_A}$	$\frac{\lambda_{phase}}{\lambda_A}$	$\frac{V_{phase}}{c}$	$b_{BLUE}^{Doppler}$
$group$	$\frac{1}{b_{BLUE}^{Doppler}}$	$\frac{V_{group}}{c}$	$\frac{v_{group}}{v_A}$	$\frac{\lambda_{group}}{\lambda_A}$	$\frac{\kappa_{group}}{\kappa_A}$	$\frac{\tau_{group}}{\tau_A}$	$\frac{c}{V_{group}}$	$\frac{1}{b_{RED}^{Doppler}}$
$rapidity$ ρ	$e^{-\rho}$	$\tanh \rho$	$\sinh \rho$	$\text{sech} \rho$	$\cosh \rho$	$\text{csch} \rho$	$\coth \rho$	$e^{+\rho}$
$value\ for$ $\beta=3/5$	$\frac{1}{2} = 0.5$	$\frac{3}{5} = 0.6$	$\frac{3}{4} = 0.75$	$\frac{4}{5} = 0.80$	$\frac{5}{4} = 1.25$	$\frac{4}{3} = 1.33$	$\frac{5}{3} = 1.67$	$\frac{2}{1} = 2.0\text{height}$

TABLE I. Hyperbolic rapidity functions. Final row lists numerical values for Doppler $b=2$.

Space-time metrology begins with the famous Einstein-Lorentz pair. They correspond to the Lorentz $\text{sech}\rho$ -column $(\tau_{phase}, \lambda_{group})$ and the Einstein $\text{cosh}\rho$ -column $(v_{phase}, \kappa_{group})$ of Table I that describe Alice’s $\nu_A=600$ THz or $\tau_A=\frac{5}{3}fs$ or $\lambda_A=\frac{1}{2}\mu\text{m}$ standing CW cavity mode in Fig.5 that is a model for a laser clock. Its “ticker” or time standard is the time $t_{phase}=\tau_A$ between mid-cavity phase-wave crests. It is also a laser meter stick, or at least half of a *micro-meter* stick where its length standard is $\lambda_{group}=\lambda_A$ group-wave. (To upgrade it to a *1m* standard, one would lengthen it to hold *exactly* two-million half-micron waves.)

Bob sees quite warped standards coming from Alice including a mid-cavity “tick” time $t'_{phase}=\tau_A \cosh\rho=\frac{5}{3}\frac{5}{4}fs$ dilated by $\frac{5}{4}$ from $1.67fs$ to $2.083fs$ and a group-wave length contracted from $\lambda_A=\frac{1}{2}\mu\text{m}$ by $\frac{4}{5}$ to $\lambda'_{group}=\lambda_A \text{sech}\rho=\frac{1}{2}\frac{4}{5}\mu\text{m}=\frac{2}{5}\mu\text{m}$. So Bob sees Alice’s time 25% late and her laser group wave 20% short. Now, Bob can build his own 600THz laser CW-standing wave. (Just to show Alice and Carla how it’s done!). But, then after doing her own Fig.8 sorting, Alice must conclude that it is *Bob* who is 25% late and 20% short.

This begins a most pernicious kind of lovers-quarrel where each contestant is both right and wrong. Here it is labeled the *Heighway Paradox* after John E. Heighway, a talented NASA electric rocket engineer and author of several novel relativistic viewpoints. Sketched below the 1st paradox (Fig.9a) is a 2nd paradox (Fig.9b) involving larger 1st-order Doppler shifts. (Recall that these are responsible for the smaller 2nd-order shifts in the 1st paradox.)

In the 2nd paradox (Fig.9b) Bob complains that Alice’s $\frac{1}{2}\mu\text{m}$ laser appears at $\frac{1}{4}\mu\text{m}$ and thus 50% short on wavelength. (Now Carla has left in disgust.) Alice replies, “No Bob, you’re the short one giving me a lousy $\frac{1}{4}\mu\text{m}$. Who sold you that so-called $\frac{1}{2}\mu\text{m}$ laser?”

Since the mutuality of a ($b=2$)-Doppler blue-shift is well understood, the 2nd paradox evaporates, and with it, so should the 1st paradox. One might still argue that light waves just give flaky metrology. (*Quick! Sell the GPS!*) Do the steel mirror cavities actually maintain their rigidly assigned $\lambda_A=\frac{1}{2}\mu\text{m}$ while only the light wave shrinks to $\lambda'_{group}=\frac{2}{5}\mu\text{m}$?

If so, then laser resonance would fail! Anyone who has tuned a laser or Etalon plates feels how precisely sensitive laser waves are to cavity length. Optical interference is our most precise measure of *relative* differences in position, time, frequency, and velocity.

Steel cavities (along with Alice and Bob) are made of waves and do what waves do! They undergo relative space-time shift ratios drawn in Fig.8 and listed in Table I. As will be shown later, these eight shift ratios *are* the underlying variables of relativistic quantum mechanics. Their precise shiftiness precisely gives mechanics, both quantum and classical.

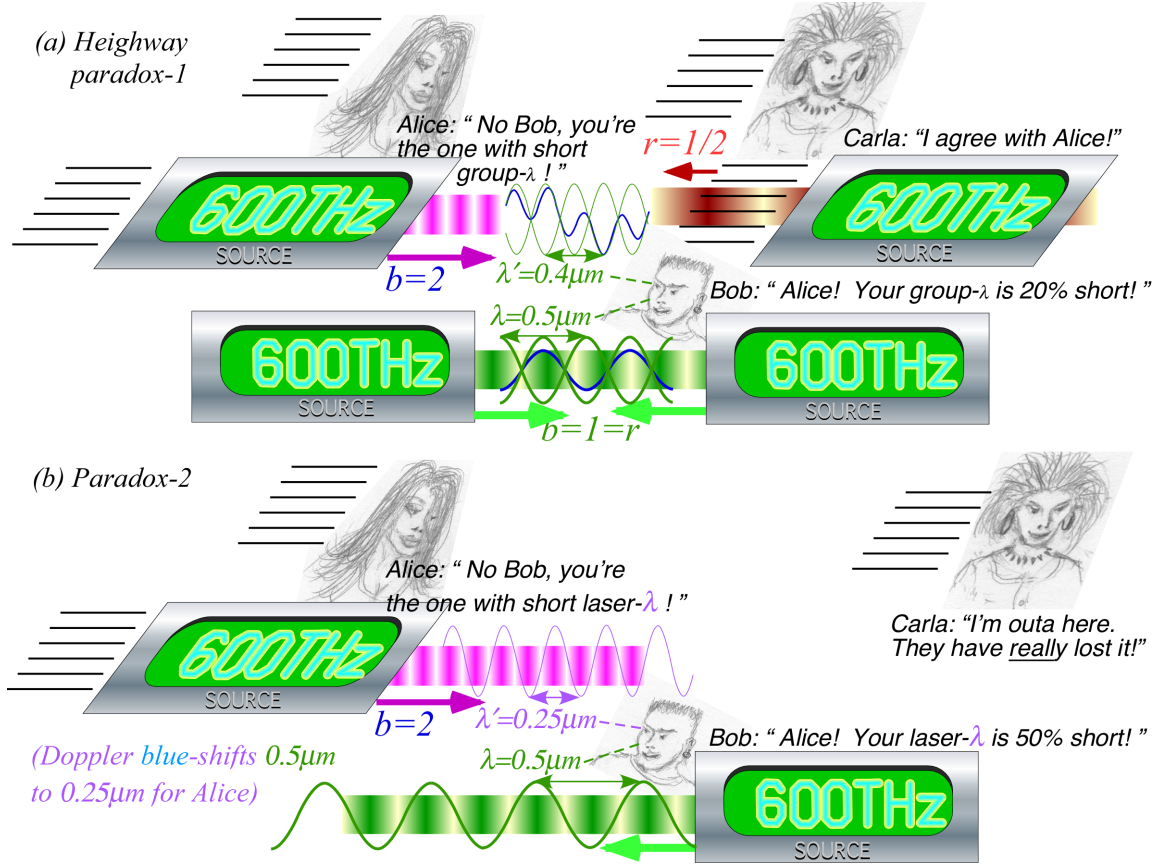


FIG. 9. Highway paradox for (a) 2-CW laser frame shifts (b) 1-CW laser Doppler shifts

C. Thales-Euclid means and geometry of hyperbolic invariants

A reverse analysis of the Alice, Bob, and Carla laser thought experiment is instructive. Imagine as before, that Bob detects counter-propagating laser beams of frequency ω_R going left-to-right (previously Alice's laser) and ω_L going right-to-left (Carla's laser). We ask two questions: (1.) To what velocity u_E must Bob accelerate so he sees beams with equal frequency ω_E ? And, (2.) What is that frequency ω_E ?

Query (1.) has a Jeopardy-style answer-by-question: What is beam group velocity?

$$u_E = V_{group} = \frac{\omega_{group}}{k_{group}} = \frac{\omega_R - \omega_L}{k_R - k_L} = c \frac{\omega_R - \omega_L}{\omega_R + \omega_L} \quad (29)$$

Query (2.) similarly: What ω_E is blue-shift $b\omega_L$ of ω_L and red-shift ω_R/b of ω_R ?

$$\omega_E = b\omega_L = \omega_R/b \Rightarrow b = \sqrt{\omega_R/\omega_L} \Rightarrow \omega_E = \sqrt{\omega_R \cdot \omega_L} \quad (30)$$

V'_{group}/c is ratio of difference mean $\omega'_{group} = \frac{\omega_R - \omega_L}{2}$ to arithmetic mean $\omega'_{phase} = \frac{\omega_R + \omega_L}{2}$.

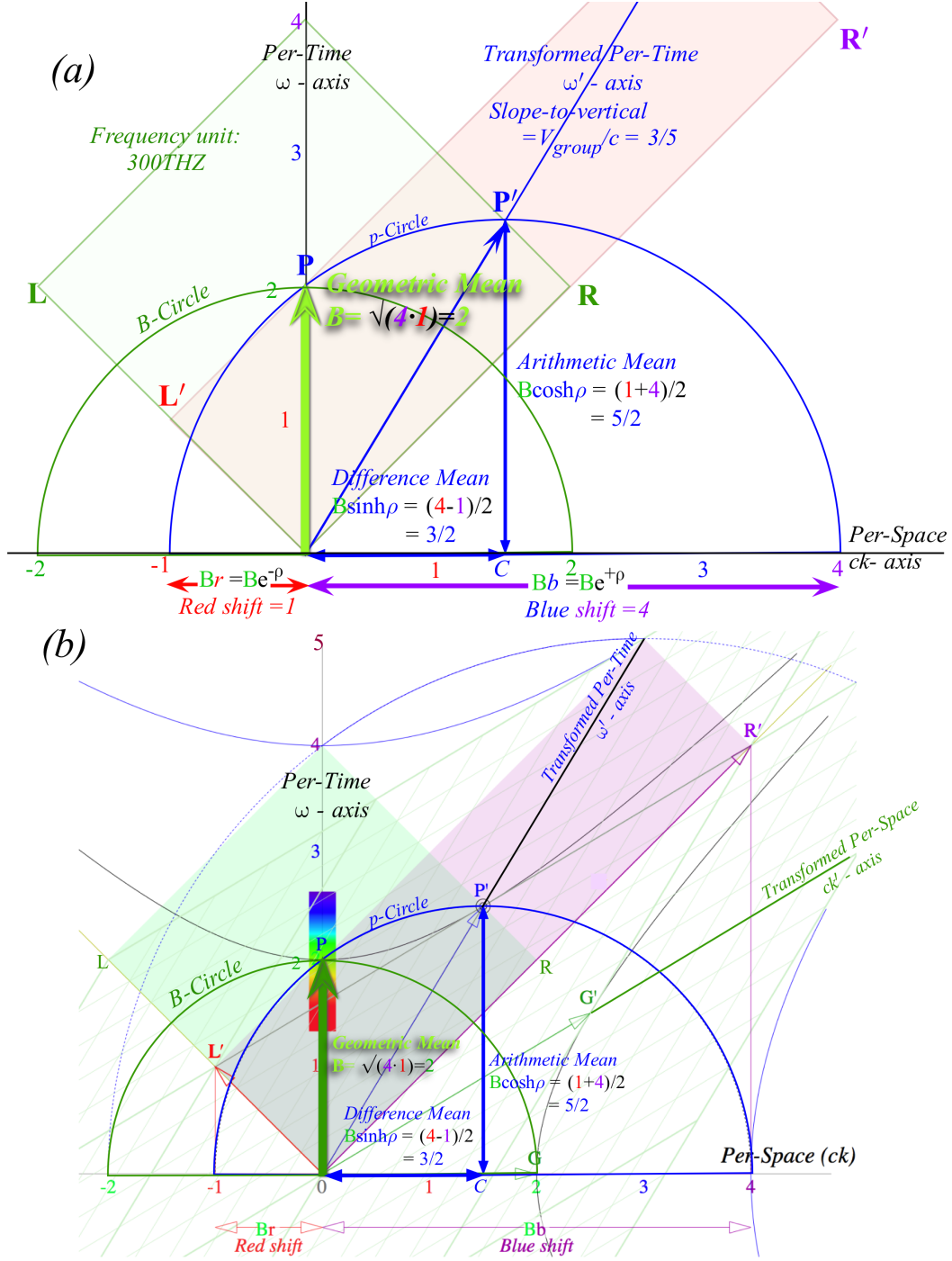


FIG. 10. (a) Thales-Euclid geometric and arithmetic means (b) Hyperbola construction step

Frequency $\omega_E = B$ is geometric mean $\sqrt{\omega_L \cdot \omega_R}$ of left and right-moving frequencies defining the geometry in Fig. 7 as detailed in Fig. 10a. Line sum of $\omega_L = \omega_E e^{-\rho}$ and $\omega_R = \omega_E e^{+\rho}$ is bisected at center C of a circle connecting shifted phase vector \mathbf{P}' to its original \mathbf{P} .

Original **P** (**P**itcher's mound) is the geometric mean point $\sqrt{1 \cdot 4}=2$ at Alice's base frequency $B=v_A=600$ THz (Fig.10 units are 300 THz.) that lets you construct points **P'**,**P''**,... on a hyperbola that other frames claim to be 600 THz. Simply prick any point ck' with compass needle, set its pencil to point-**P**, and draw arc **PP'** to the hyperbola point $\omega'(k')$ on vertical above ck' . (Whole arc is optional if graph paper gives verticals.) Time-flip axiom $e^{-\rho}e^{+\rho}=r \cdot b=1$ implies phase points **P'**,**P''**,... form hyperbolas $\omega'_R\omega'_L=\omega_A^2$ whose asymptotes hold Doppler-shifted rectangles with area $2\omega_A^2$ of initial ($\rho=0$) "baseball diamond." Cartesian (ω', ck') hyperbola equations for $\omega_A=2$ and $\omega_A=4$ in Fig.10b are also ρ -invariant to ELT.

$$\omega_A^2 = (\omega')^2 - (ck')^2 = (\omega'')^2 - (ck'')^2 = \dots \quad (31)$$

Similar equation sets with signs reversed apply to points **G'**,**G''**,... for group-vector hyperbola plots on the right of Fig.10b. Negative- k_A hyperbolas would lie to the left.

$$(ck_A)^2 = (ck')^2 - (\omega')^2 = (ck'')^2 - (\omega'')^2 = \dots \quad (32)$$

Negative- ω_A hyperbolas lie below Fig.10b. Alice's invariant or *proper frequency* ω_A in per-space-time relations (31) is matched by a space-time ρ -invariant τ_A known as *proper time*.

$$(c\tau_A)^2 = (ct')^2 - (x')^2 = (ct'')^2 - (x'')^2 = \dots \quad (33)$$

A common name for τ_A is *age*, Alice's in this case. If Alice's laser clock and cycle counter is attached at birth and remains *always with her* then counter reading τ_A is a precise reading of her age. The key words '*always with her*' mean *no* separation. If she leaves her clock downstairs and sleeps upstairs (in a higher gravitational energy) then the clock understates her age! Proper separation x_A is defined similarly to proper time τ_A by an x_A -hyperbola.

$$x_A^2 = (x')^2 - (ct')^2 = (x'')^2 - (ct'')^2 = \dots \quad (34)$$

D. Space-proper-time plots and the stellar-aberration angle

Lewis C. Epstein developed a novel approach to space-time relativity that uses the transverse stellar aberration angle σ to define relative velocity by $u=c \sin \sigma$ as sketched in Fig.11 in place of longitudinal Doppler definition $u=c \tanh \rho$ by rapidity ρ given in (17). This alternative to Minkowski- (x, ct) -plots involves flipping proper-time definition (33) as follows.

$$(c\tau)^2 + (x')^2 = (ct')^2 \quad (35)$$

E. Unifying circular-hyperbolic relativistic geometry

Fig.13 begins to relate hyperbolic and circular geometry using Thales structure in Fig. 10. Elementary sine (slope of *incline*), tangent, and secant geometry of $(\sin \sigma, \tan \sigma, \sec \sigma)$ in Fig.13a for a $\frac{3}{5}:\frac{4}{5}:\frac{5}{5}$ triangle shows $\tan \sigma$ is length of tangents subtending secants $\sec \sigma$. It is useful to define angle $\sigma=37^\circ=0.6435 \text{radian}$ by total sector area $\sigma=0.6435 \text{m}^2$ as well as arc length of unit circle. Angle σ is relative to horizontal x -axis with vertical sine y -component.

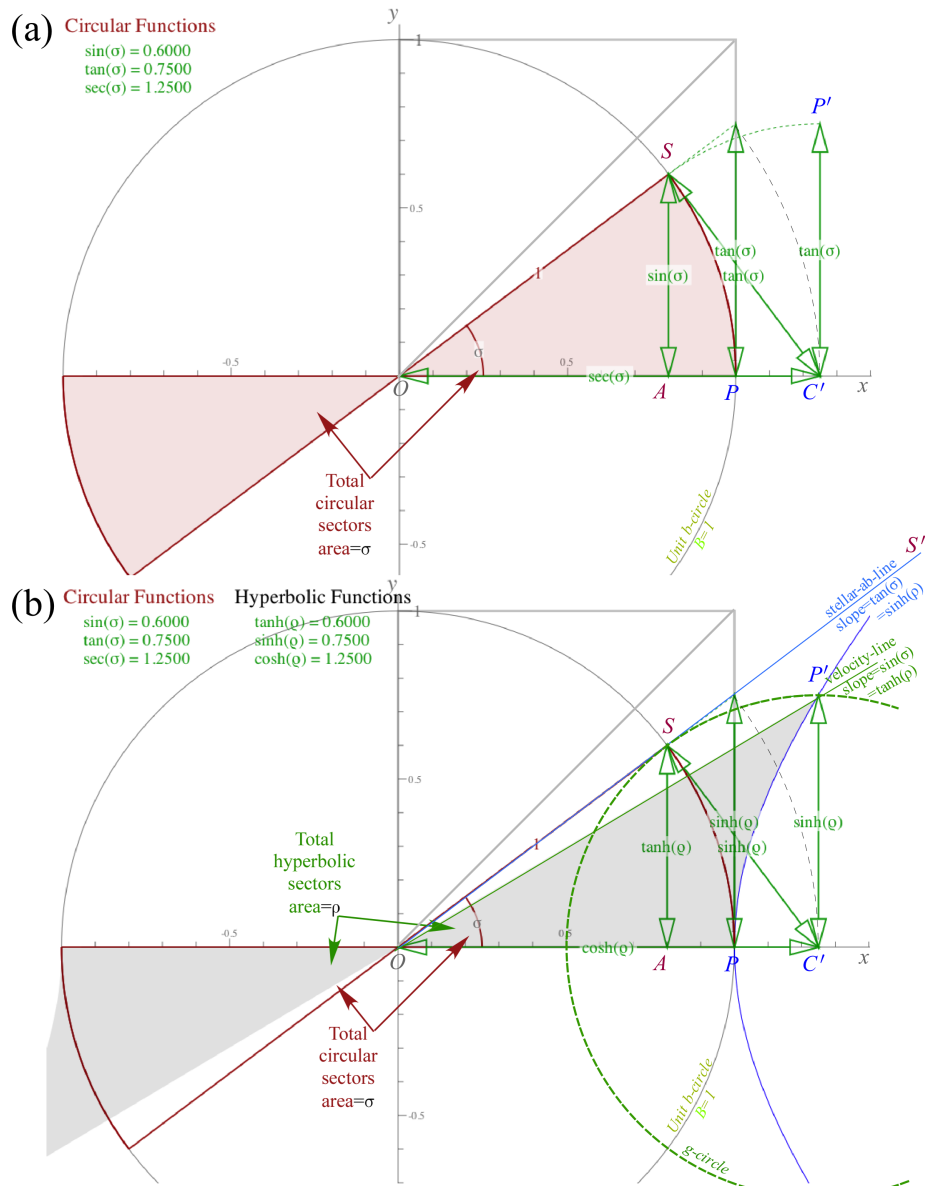


FIG. 13. (a) Elementary sine, tangent, and secant geometry (b) Hyperbolic equivalents are equal.

Hyperbolic functions in Fig.13b use a sector area ρ defined to make $\sinh \rho = \tan \sigma$ and $\tanh \rho = \sin \sigma$. A unit-hyperbola subtends area $\rho/2$ so its branch-pair subtends ρ .

$$\rho/2 = \frac{1}{2} \cosh \rho \sinh \rho - \int d(\cosh \rho) \sinh \rho \quad (36)$$

Each circular function $f_c(\sigma)$ of angle σ has a ‘country-cousin’ hyper-function $g_h(\rho) = f_c(\sigma)$ of rapidity ρ in adjacent column of Fig.14 (upper left). Its ‘cousin-pair’ $f_h(\rho) = g_c(\sigma)$ lies in an adjacent row. The 1st ($\sin \Rightarrow \tan$)-pair $\tan \sigma = \sinh \rho$ and $\sin \sigma = \tanh \rho$ of lines $P'C'$ and SA in Fig.13 is listed first in Fig.14. The 2nd ($\sec \Rightarrow \cosh$)-pair is line CP' (Einstein t -dilation $\sec \sigma = \cosh \rho$) and line $A'S$ (Lorentz x -contraction $\cos \sigma = \operatorname{sech} \rho$.) (Recall Fig.12.) Slope of hyperbola tangent-line- QAP' is $\csc \sigma = \coth \rho$ and its y -intercept $OQ = \cot \sigma = \operatorname{csch} \rho$ is the 3rd ($\cot \Rightarrow \csc$)-pair type listed. Fig.14 shows other objects described by $g_h(\rho) = f_c(\sigma)$ functions.

Fig.13a-b sets up ruler-compass construction of $g_h(\rho) = f_c(\sigma)$. First, a compass-swing about center point C' at ($x = \sec \sigma = \cosh \rho$) of vertical ($\tan \sigma = \sinh \rho$)-radius $C'S$ thru $C'P'$ starts the g -circle companion to Thales p -circle. Arc SP' is one of three arcs in Fig.14 that

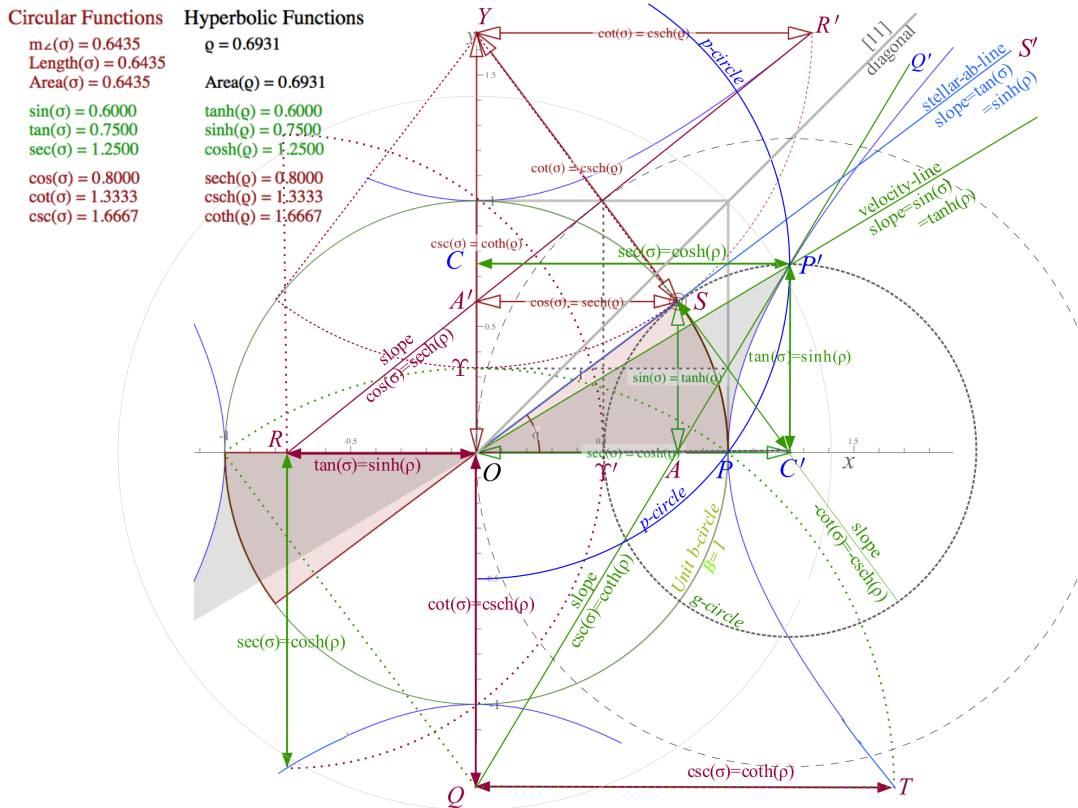


FIG. 14. Hyperbolic functions of rapidity ρ related to circular stellar-aberration σ -functions

subtend stellar angle σ . Arc PS of b -circle (radius $B=1$) about origin O has arc length σ . p -circle arc PP' has radius $\sec \sigma = \cosh \rho$ around center point C at $(y = \tan \sigma = \sinh \rho)$, and g -circle arc SP' has radius $\tan \sigma = \sinh \rho$ around center point C' at $(x = \sec \sigma = \cosh \rho)$. The intersection S of b -and- g -circles defines tangent-normal lines $C'SY$ and OSS' inclined by stellar-aberration angle σ to the main axis OC' . This is also shown in Fig. 15. There Fig. 14 has been reflected through its [11]-diagonal so x -axial PP' hyperbola and p -circle are on y -or- v -axes as in conventional $v(\kappa)$ dispersion plots such as Fig. 10b.

Prime phase point P' in Fig. 15 at $(v, c\kappa) = B(\sinh \rho, \cosh \rho)$ is on Alice's v_A -axis OP' of slope $\coth \rho$. P' is a hyperbolic tangent point for line $LP'R$ of slope $\tanh \rho = \frac{LL'}{L'R}$ with axis intercepts $QO = Bcsch \rho$ and $AO = Bsech \rho$. ($P'Q$ parallels G' line of group $c\kappa_A$ -axis.) Prime stellar point S at $(v, c\kappa) = B(\sech \rho, \tanh \rho)$ defines stellar ray OSk of slope $c\sech \rho$. S is b -circle tangent point for line $C'SY$ having slope $-\sinh \rho = -\frac{A'S}{AS}$ with axis intercepts of $C'O = B \cosh \rho$ and $OY = B \coth \rho$. All ρ -functions are related to σ -functions in Table II.

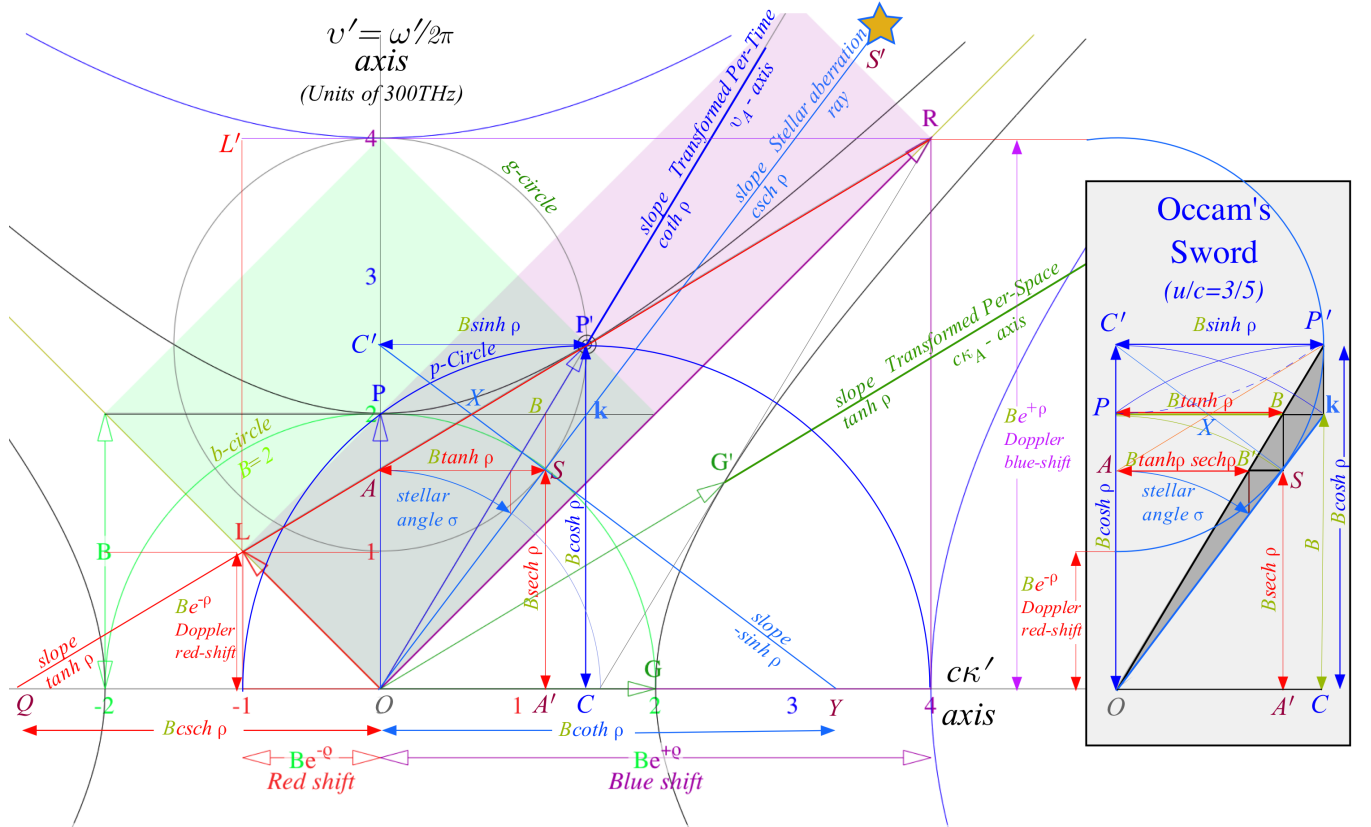


FIG. 15. Bob- $(v', c\kappa')$ -view of Alice- $(v_A, c\kappa_A)$ tangent geometry and (inset) Occam-Sword pattern.

<i>time</i>	$b_{RED}^{Doppler}$	$\frac{c}{V_{phase}}$	$\frac{\kappa_{phase}}{\kappa_A}$	$\frac{\tau_{phase}}{\tau_A}$	$\frac{v_{phase}}{v_A}$	$\frac{\lambda_{phase}}{\lambda_A}$	$\frac{V_{phase}}{c}$	$b_{BLUE}^{Doppler}$
<i>space</i>	$\frac{1}{b_{BLUE}^{Doppler}}$	$\frac{V_{group}}{c}$	$\frac{v_{group}}{v_A}$	$\frac{\lambda_{group}}{\lambda_A}$	$\frac{\kappa_{group}}{\kappa_A}$	$\frac{\tau_{group}}{\tau_A}$	$\frac{c}{V_{group}}$	$\frac{1}{b_{RED}^{Doppler}}$
<i>rapidity</i> ρ	$e^{-\rho}$	$\tanh \rho$	$\sinh \rho$	$\operatorname{sech} \rho$	$\cosh \rho$	$\operatorname{csch} \rho$	$\operatorname{coth} \rho$	$e^{+\rho}$
<i>stellar</i> \forall <i>angle</i> σ	$1/e^{+\rho}$	$\sin \sigma$	$\tan \sigma$	$\cos \sigma$	$\sec \sigma$	$\cot \sigma$	$\operatorname{csc} \sigma$	$1/e^{-\rho}$
$\beta \equiv \frac{u}{c}$	$\sqrt{\frac{1-\beta}{1+\beta}}$	$\frac{\beta}{1}$	$\frac{1}{\sqrt{\beta^2-1}}$	$\frac{\sqrt{1-\beta^2}}{1}$	$\frac{1}{\sqrt{1-\beta^2}}$	$\frac{\sqrt{\beta^2-1}}{1}$	$\frac{1}{\beta}$	$\sqrt{\frac{1+\beta}{1-\beta}}$
<i>value for</i> $\beta=3/5$	$\frac{1}{2}=0.5$	$\frac{3}{5}=0.6$	$\frac{3}{4}=0.75$	$\frac{4}{5}=0.80$	$\frac{5}{4}=1.25$	$\frac{4}{3}=1.33$	$\frac{5}{3}=1.67$	$\frac{2}{1}=2.0$

TABLE II. Hyperbolic and circular function pairing. Final row has values for $\frac{u}{c} = \frac{3}{5}$.

Table II relates ‘cousin-pairs’ of functions $f_h(\rho)$ based on p -hyperbola and $f_c(\sigma)$ based on b -circle. b -circle tangent intercept $B \operatorname{coth} \rho = B \operatorname{csc} \sigma$ at bottom of Fig. 15 is paired with p -hyperbola tangent intercept $B \operatorname{csch} \rho = B \cot \sigma$ in 3rd-column-pair of Table II relating, respectively, phase velocity V_{phase} and wavelength λ_{phase} . Just above that in Fig. 15 is b -circle tangent slope $-B \sinh \rho = -B \tan \sigma$ paired with p -hyperbola tangent slope $B \tanh \rho = B \sin \sigma$ in 1st-column-pair relating, respectively, group velocity V_{group} and frequency v_{group} (1st ‘cousin-pair’ of Fig. 13). Mid-Fig. 15 has coordinate pair $B \operatorname{sech} \rho = B \cos \sigma$ and $B \cosh \rho = B \sec \sigma$ of tangent intercepts OA and OC' related to $\tau_{phase} = \lambda_{group}$ and $v_{phase} = \kappa_{group}$, respectively, by 2nd-column-pair of Table II. These are the Lorentz-contraction and Einstein dilation factors and the only ‘cousin-pair’ to be mutually reciprocal. (The value of each Table II column is reciprocal to the value of its mirror-image column.) Values rise left-to-right for $\frac{u}{c} = \frac{3}{5}$, but trade on the way to high-speed limits $\frac{u}{c} \rightarrow \pm 1$, $\sigma \rightarrow \pm \frac{\pi}{2}$, or $\rho \rightarrow \pm \infty$. (See Fig. 21 ahead.) Applications that follow use a pattern-recognition aid labeled *Occam’s Sword* in Fig. 15 (inset). It focuses mostly on geometry of $(\sin \rightleftharpoons \tan)$ and $(\cos \rightleftharpoons \sec)$ columns of Table II. (The $(\cot \rightleftharpoons \operatorname{csc})$ intercepts are outliers for low to moderate $\frac{u}{c}$ values.) The sword has a staircase whose steps belong to a $(\cosh \rho)^n$ -geometric series: $(B \cosh \rho, B, B \operatorname{sech} \rho, \dots)$. Multiplying that series by $\tanh \rho$ gives line $(C'P' = B \sinh \rho)$, then $(PB = B \tanh \rho)$, and lowest step $(AB' = B \tanh \rho \operatorname{sech} \rho)$. Steps subtend a triple-cross- X -point of tangents $C'XS$, AXP' , and b -baseline PXB . Extensions of the tangents have κ -axis $(\cot \rightleftharpoons \operatorname{csc})$ -intercepts on either side of the sword in Fig. 15. The sword’s leading \mathbf{k} -edge defines wavevectors for waveguides and for free-electron lasers that make them easier to analyze and visualise.

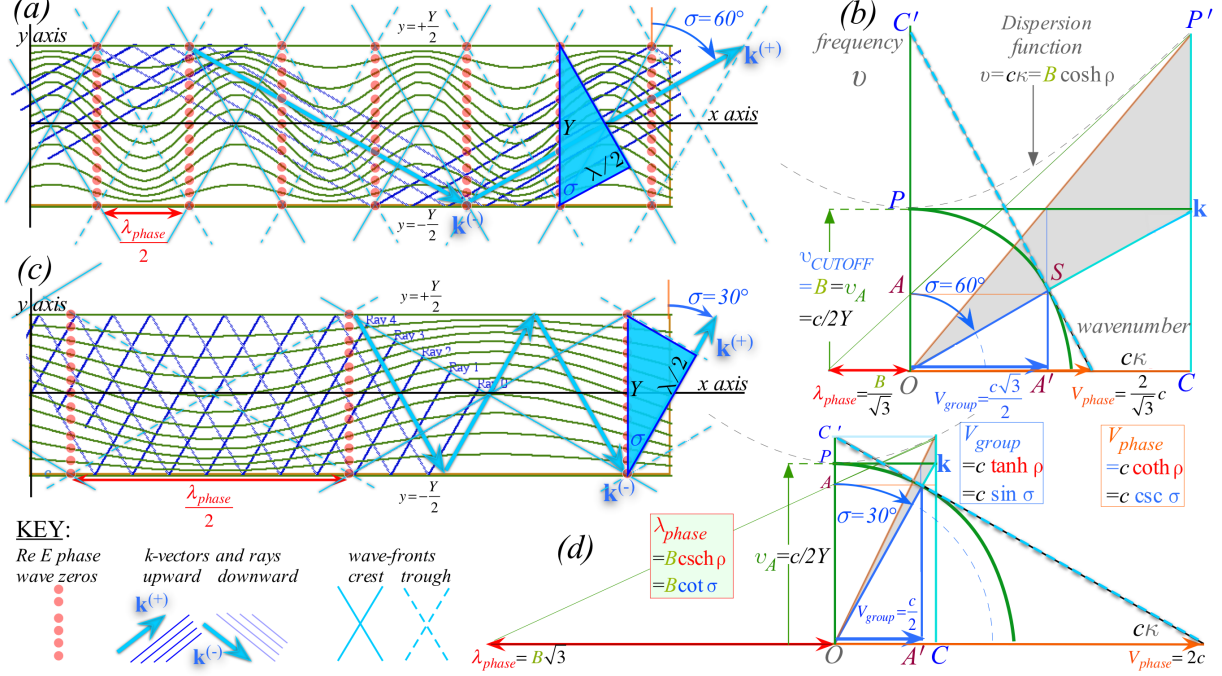


FIG. 16. TE-Waveguide and Occam sword geometry for stellar angle $\sigma=30^\circ$ and $\sigma=60^\circ$.

1. TE-Waveguide geometry

Consider a sum of plane waves with wave-vectors $\mathbf{k}^{(+)}=(k \sin \sigma,+k \cos \sigma)=(k_x, k_y)$ and $\mathbf{k}^{(-)}=(k \sin \sigma,-k \cos \sigma)=(k_x,-k_y)$ at declination angles $\pm \sigma$ relative to the y -axis in Fig.16.

$$E_z(\mathbf{r}, t)=e^{i(\mathbf{k}^{(+)} \cdot \mathbf{r}-\omega \cdot t)}+e^{i(\mathbf{k}^{(-)} \cdot \mathbf{r}-\omega \cdot t)}=e^{i(k_x \cdot x-\omega \cdot t)}\left[e^{ik_y \cdot y}+e^{-ik_y \cdot y}\right] \quad (37)$$

The result in xy -plane is a Transverse-Electric-(TE)-mode \mathbf{E} -field with plane-normal z -component E_z that vanishes on metallic floor and ceiling ($y=\pm \frac{Y}{2}$) of the waveguide.

$$E_z(\mathbf{r}, t)=e^{i(k \cdot x \sin \sigma-\omega \cdot t)} 2 \cos(k y \cos \sigma)|_{y=\frac{Y}{2}}=0 \quad \text{implies: } k \frac{Y}{2} \cos \sigma=n \frac{\pi}{2} \quad (38)$$

Fig.16 shows two examples of lowest ($n=1$) guide modes with Occam-sword geometry. Projection $Y \cos \sigma$ of floor-to-ceiling Y onto $\mathbf{k}^{(\pm)}$ -vectors is shown by right triangles at guide ends (or Eq.38) to be $\frac{\pi}{k}=\frac{\lambda}{2}$, that is $\frac{1}{2}$ -wave $\frac{\lambda}{2}$. Waveguide angle σ and dispersion function follows.

$$v=c \kappa=c \sqrt{\kappa_x^2+\kappa_y^2}=c \sqrt{\kappa_x^2+\kappa^2 \cos ^2 \sigma}=\sqrt{c^2 \kappa_x^2+\left(\frac{c}{2 Y}\right)^2}=\sqrt{c^2 \kappa_x^2+v_A^2} \quad (39)$$

Surprising insight into Fig.16 waves results if we note it is what Bob sees if Alice and Carla beam their $v_A=600$ THz 2-CW across Bob's x -line of motion and not along it as in Fig.6. Bob can Doppler shift his wave-number κ_x to zero and reduce frequency v in (39) to $v=v_A$.

Then Bob will be co-moving with Alice and Carla and see Alice's $\mathbf{k}^{(+)}$ -vector at zero aberration angle ($\sigma=0$) if she is below Fig.16 beaming straight up the y -axis. Meanwhile, Carla's $\mathbf{k}^{(-)}$ -vector points straight down. For $\sigma=0$, the wave given by (38) is a y -standing wave of wavelength $\lambda_A=2Y$ between Alice and Carla and not just a half-wave section ($Y=\frac{\lambda_A}{2}$) modeling this xy -wave guide. Ideally Alice and Carla's laser mode viewed along y looks like their x -standing wave in Fig.5 and appears the same over its x -beam-width by having zero x -wave number ($\kappa_x=\kappa_A \sin \sigma=0$). Zero- κ_x or infinite x -wavelength ($\lambda_x=\lambda_A \csc \sigma=\infty$) is a flat-line wave parallel to the x -axis oscillating at Alice's (or Carla's) frequency v_A .

This x -flat wave is better known in wave guide theory as a *cut-off-frequency* mode where the cut-off-frequency $v_{CUTOFF}=\frac{c}{2Y}=v_A$ is the lower bound to frequency that can enter a waveguide of width Y . In Fig.16b it corresponds to dispersion function bottom point B (or P) that is well separated from its phase point P' in the upper left of the figure. That separation $OC=B \sinh \rho=B \tan \sigma$ gives a mode in Fig.16a that is more robust than the near-cutoff mode in Fig.16c having less OC and more nearly vertical \mathbf{k} -vector in Fig.16d.

The $\tan \sigma$ -column of Table II represents the phase wave-number ratio $\frac{\kappa_{phase}}{\kappa_A}$ of Bob's κ_{phase} to κ_A that Alice and Carla claim is their output. Later it is shown that $OC=\kappa_x$ is mode wave *momentum* while vertical interval $CP'=B \cosh \rho=B \sec \sigma=v_{phase}$ or phase frequency ratio $\frac{v_{phase}}{v_A}$ in Table II correspond to mode carrier wave *energy*. These determine wave robustness and their ratio $\frac{v_{phase}}{\kappa_{phase}}=\frac{\lambda_{phase}}{T_{phase}}$ is the phase velocity V_{phase} .

The importance of waveguide phase or carrier behavior is matched by that of group or signal wave dynamics. Each has six of twelve variables listed in Table II. Matching phase velocity $V_{phase}/c=\coth \rho=\csc \sigma$ is reciprocal to $V_{group}/c=\tanh \rho=\sin \sigma$. Both are indicated by arrow lengths at the base of Occam Sword plots in Fig.16b or Fig.16d. The latter has V_{group} much lower than V_{phase} while the former has both closer to light speed c .

Group velocity V_{group} equals projection $c \sin \sigma$ of $\widehat{c\mathbf{k}}$ -vector onto the waveguide x -axis. One may imagine a signal bouncing off guide floor or ceiling riding on the \mathbf{k} -vectors normal to phase wavefronts moving at speed c along $\mathbf{k}^{(+)}$ or $\mathbf{k}^{(-)}$ in Fig.16a or Fig.16c. So a signal wastes time bouncing around the guide x -axis while the phase crests proceed via a greater $c \csc \sigma$. A signal may be imagined as an extra wrinkle in symmetry of identical wave crests due to lately added Fourier components that are limited to the envelope's group velocity while the established underlying phase maintains Evenson's c -lockstep. $(v, c\kappa_x)$ per-space-time geometry of Fig.16b or d determines that of space-space (x, y) in Fig.16a or c.

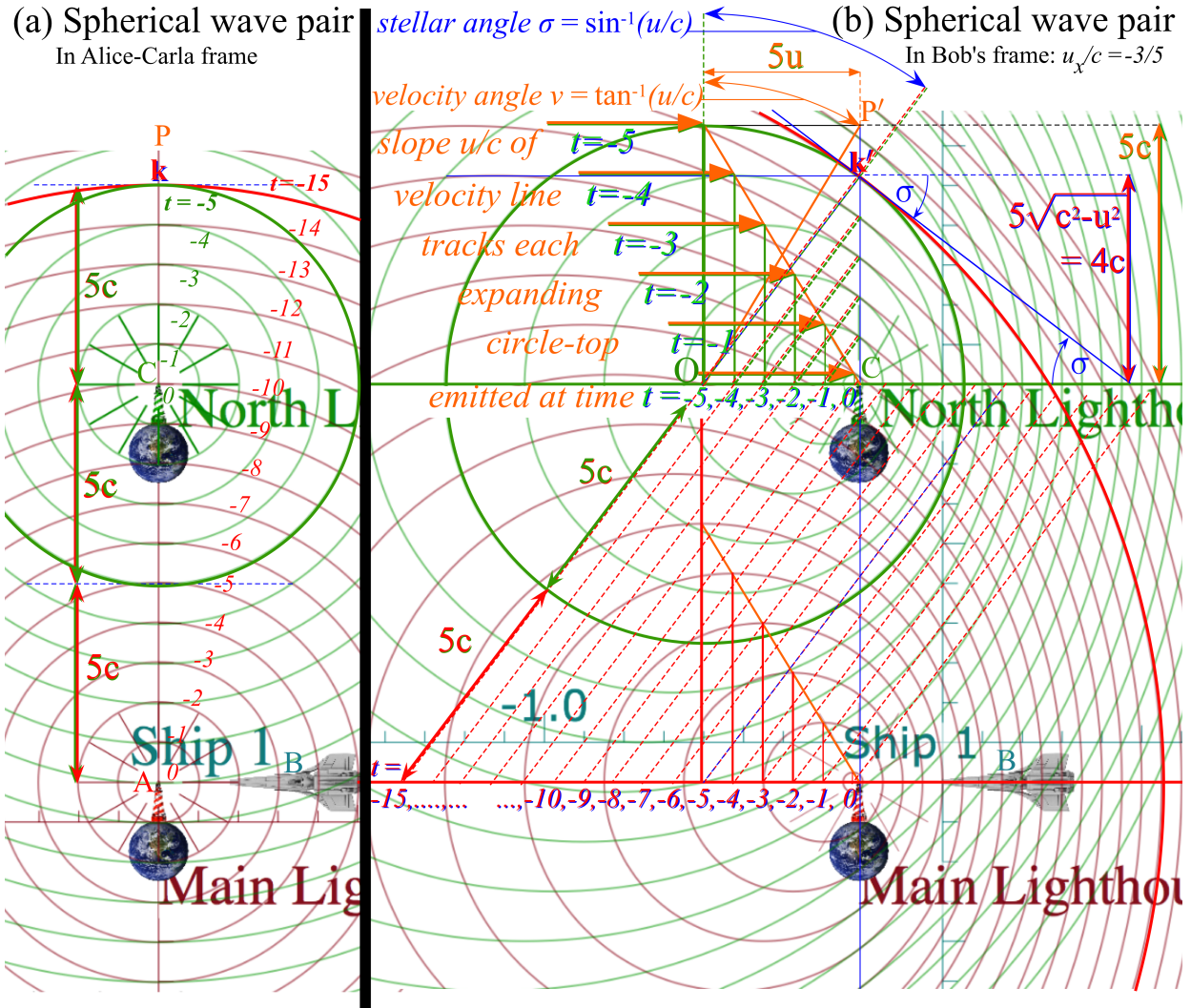


FIG. 17. Spherical wave pair. (a) Alice-Carla source frame. (b) Bob-frame (dilated by $\frac{5}{4}$)

2. Spherical wave geometry

A pair of synchronized spherical waves are shown in Fig. 17a being emitted by laser lighthouses separated by 10 light-seconds. The upper lighthouse C belonging to Carla emits a green blink every second in response to each red blink wave arriving from the lower lighthouse A occupied by Alice and *vice versa* so A and C blink together with a 10 second delay between each stimulus-response pair. The waves along line AC collide head-on and would form a standing wave if they were CW (Continuous Waves) like previous examples in Fig. 5 through Fig. 8. Here red and green PW (Pulse Waves) are imagined merging and marching lock-step along line CP just above line AC . Fig. 17a shows green PW of radius $5c$

that is 5 seconds old at $t=0$. It is moving upward through its tangent point \mathbf{k} shared with its stimulus wave, a red PW of radius $15c$ that is 15 seconds old.

Fig.17b shows Bob's view of the Alice-Carla waves from his frame that is approaching theirs along the x -axis at velocity $u = -3c/5$. Bob must see each blink wave expand at rate c as a perfect circle around each point of emission as the emitting laser moves on at velocity $u' = +3c/5$ toward Bob. Bob sees top and bottom points on each circular wave move vertically at rate $\pm c$, but each successive emission point advances to position $x' = u't'$ where Alice-Carla time interval Δt is seen dilated to $\Delta t' = \Delta t \cosh \rho = \frac{5}{4} \Delta t$ by Bob. Six such emission points are labeled by Alice-Carla emission times $t = (-5, -4, -3, -2, -1, 0)$ along the upper (green) laser path and $t = (-15, \dots, -6, -5, -4, -3, -2, -1, 0)$ along the lower (red) laser path. Dilation factor $\frac{5}{4}$ increases the size of the light circles (spheres) by exactly that factor in Bob's frame.

Light wave circles do not translate in any frame. Their centers are fixed as radii vary at a uniform c -rate only. Blink circle geometry dilates by Einstein time factor $\cosh \rho$ of (28). However, transverse-to-motion y -distance between Alice and Carla's lighthouses for Bob does not vary with x -rapidity $\rho_x = \rho$. Placing dilated circles in y -fixed space involves 1st-order asimultaneity effects including stellar σ -rotation of their \mathbf{k}' -vectors.

Top points of wave circles in Fig.17b move to the left by $5u$ -units as they rise by $5c$ -units. Meanwhile, the \mathbf{k}' -point corresponding to top tangent point \mathbf{k} in Fig.17a follows a stellar angle path in Bob's view of Fig.17b by moving to the right by $5u$ -units but rising by only $4c$ -units. \mathbf{k}' -points lie on a line tilting into source direction of travel by angle $\sigma = \sin^{-1} \frac{u}{c}$. Bob's circle-top points lie on a line tilting away from normal to source velocity by slightly smaller angle $\nu = \tan^{-1} \frac{u}{c}$. Difference $\sigma - \nu$ between these angles (angular Occam sword-width) decreases with $\frac{u}{c}$ as all three parameters σ , ν , and ρ approach $\frac{u}{c}$.

The rectangle $O C \mathbf{k}' P'$ in Fig.17b has the geometry of the Occam Sword rectangle in Fig.15(inset) and Fig.16d. The \mathbf{k} -line defines the \mathbf{k} -vector normal to the red and green wavefronts at each mutual tangent point and that direction tilts by stellar angle σ .

3. Doppler geometry of spectral ellipse in (x,y) space

Space-space geometry of two circular PW sources in Fig.17 is developed further in Fig.18 for a single CW source. The wave crests are bounded by a circular crest of radius c that supports an Occam sword pattern with the same proportions as the one drawn in the upper

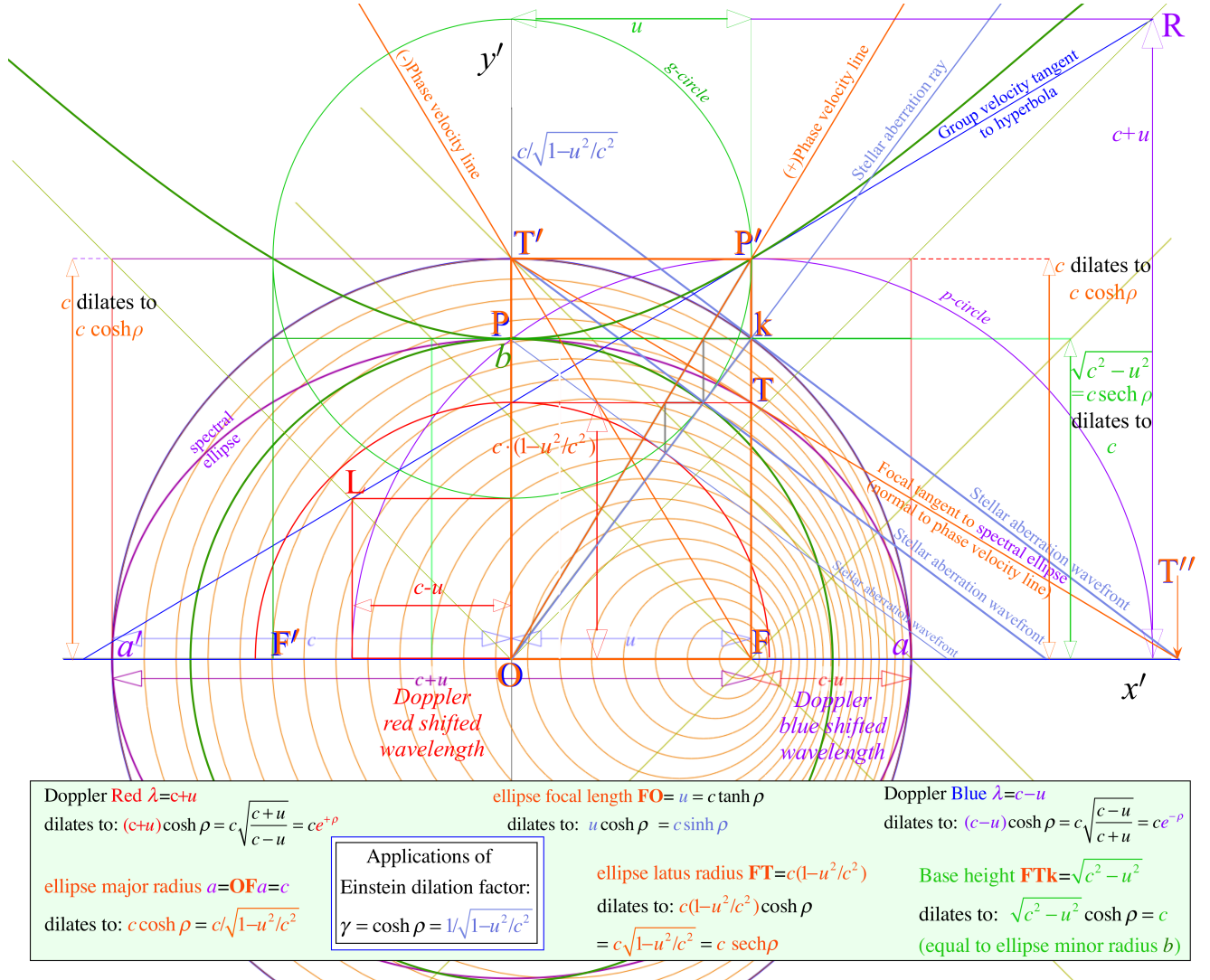


FIG. 18. Geometry of spectral ellipse in Bob's space-space (x', y') view of Alice source at $\frac{u}{c} = \frac{3}{5}$.

half of Fig. 17b with an added hyperbola and ellipse. The hyperbola is a proportional copy of the dispersion hyperbola seen in previous Fig. 15 and Fig. 16d. The ellipse will serve to quantify Doppler wavelength as a function of wave direction around its focal point F . Dimensions in Fig. 18 are velocities multiplied by an Alice-Carla time unit as in Fig. 17b. Here a unit Alice time interval $\Delta t=1$ is dilated to $\Delta t' = \cosh \rho = \frac{1}{\sqrt{1-\beta^2}} = \frac{5}{4}$ for Bob assuming $\beta \equiv \frac{u}{c} = \frac{3}{5}$. Key dimensions are labeled by functions of u and c that are to be dilated by $\cosh \rho$ in the box at the base of Fig. 18 and thereby converted to (x', y') -distance in Bob's light-second units. This shows a remarkable connection of space-space geometry and algebra to that of the frequency-wavenumber $(\nu, c\kappa)$ -per-time-per-space diagrams in Fig. 15.

Doppler frequency blue-shift doubling $e^{+\rho}=2$ of frequency in Fig.15 is connected to halving $e^{-\rho}=\frac{1}{2}$ of wavelength in Fig.18 corresponding to the segment $\mathbf{Fa}=c-u$ whose $\cosh\rho$ dilation is exactly $ce^{-\rho}$. A small square with diagonal \mathbf{OL} has side $ce^{-\rho}$ that is a lower bound for the g -circle and the p -circle in either figure. Opposite to that is a large square with diagonal \mathbf{OR} and side dimension $ce^{+\rho}$ serving as upper bound for p and g circles. In Fig.18, dimension $ce^{+\rho}$ corresponds to a $\cosh\rho$ dilation of segment $\mathbf{a'F'F}=c+u$.

The spectral ellipse aba' and its tangent-line $\mathbf{T'TT''}$ in Fig.18 are two features not present in Fig.15. Ellipse major radius $\mathbf{OFa}=c$ dilates to $c \cosh\rho$, that equals the radius $\mathbf{FTkP'}$ of the p -circle. Ellipse minor radius $b=\mathbf{OP}=\mathbf{FTk}=\sqrt{c^2-u^2}$ dilates to $b \cosh\rho=c$ and is equal to the major radius of the dispersion hyperbola that is its bottom (Base= B) in Fig.15.

Focal length $\mathbf{OF}=u=c \tanh\rho$ of the ellipse dilates to $u \cosh\rho=c \sinh\rho$. This corresponds to the hyperbola wavenumber $c\kappa=B \sinh\rho$ in Fig.15 and segment $\mathbf{Pk}=u$ in Fig.18. It connects to ellipse tangent point \mathbf{T} and vertical latus-radius $\mathbf{TF}=c\sqrt{1-\frac{u^2}{c^2}}$ that dilates to $c \operatorname{sech}\rho$. Ellipse tangent-line $\mathbf{T'TT''}$ has slope $-\frac{u}{c}$ normal to the positive phase velocity line having slope $\frac{c}{u}$, quite like the stellar \mathbf{k} -ray that is normal to its wave front tangents. (Slope values are invariant to uniform dilation.) As noted before, sword pattern steps form geometric series in $\cosh^n\rho$. In Fig.18 the 4th (top) y -intercept step $\frac{c}{\sqrt{1-\frac{u^2}{c^2}}}=c \cosh\rho$ dilates to $c \cosh^2\rho$.

4. Doppler geometry of spectral ellipse in wavenumber per-space (κ_x, κ_y)

Fig.19 returns to frequency and wavenumber description of Alice's lasers now assuming each may be aimed at an arbitrary angle θ relative to the y -axis normal to the x -axial line of relative Alice-Bob motion as they approach each other. In Fig.19a four \mathbf{k} -vectors in $\pm y$ and $\pm x$ directions are labeled \mathbf{k}_0 , \mathbf{k}_{180} , \mathbf{k}_{+90} and \mathbf{k}_{-90} , respectively. Fig.19b diagrams extreme Doppler effects seen by Bob for a rapid approach $\frac{u}{c}=\frac{\sqrt{3}}{2}$ previously treated in the waveguide example of Fig16a whose geometry in Fig16b has a similar "sword" ($P'\mathbf{k}O$ matches $P'\mathbf{k}'_0F'$) and the same stellar aberration angle $\sigma=60^\circ$. Fig.19b shows a complete tangent line going between upper right hand corner R of blue-Doppler square (with side \mathbf{Rk}'_{-90}) and upper left hand corner L of the tiny red-Doppler square (with side \mathbf{Lk}'_{+90}). This line is tangent to the dispersion hyperbola at P' and to the Doppler ellipse just above its prime focus F' . The Doppler blue-shift for $\sigma=60^\circ$ is $e^\rho=\cosh\rho+\sinh\rho=\sec\sigma+\tan\sigma=2+\sqrt{3}$ and reciprocal red-shift is $e^{-\rho}=2-\sqrt{3}$. The rapidity is a quite rapid $\rho=\rho_x=1.317$.

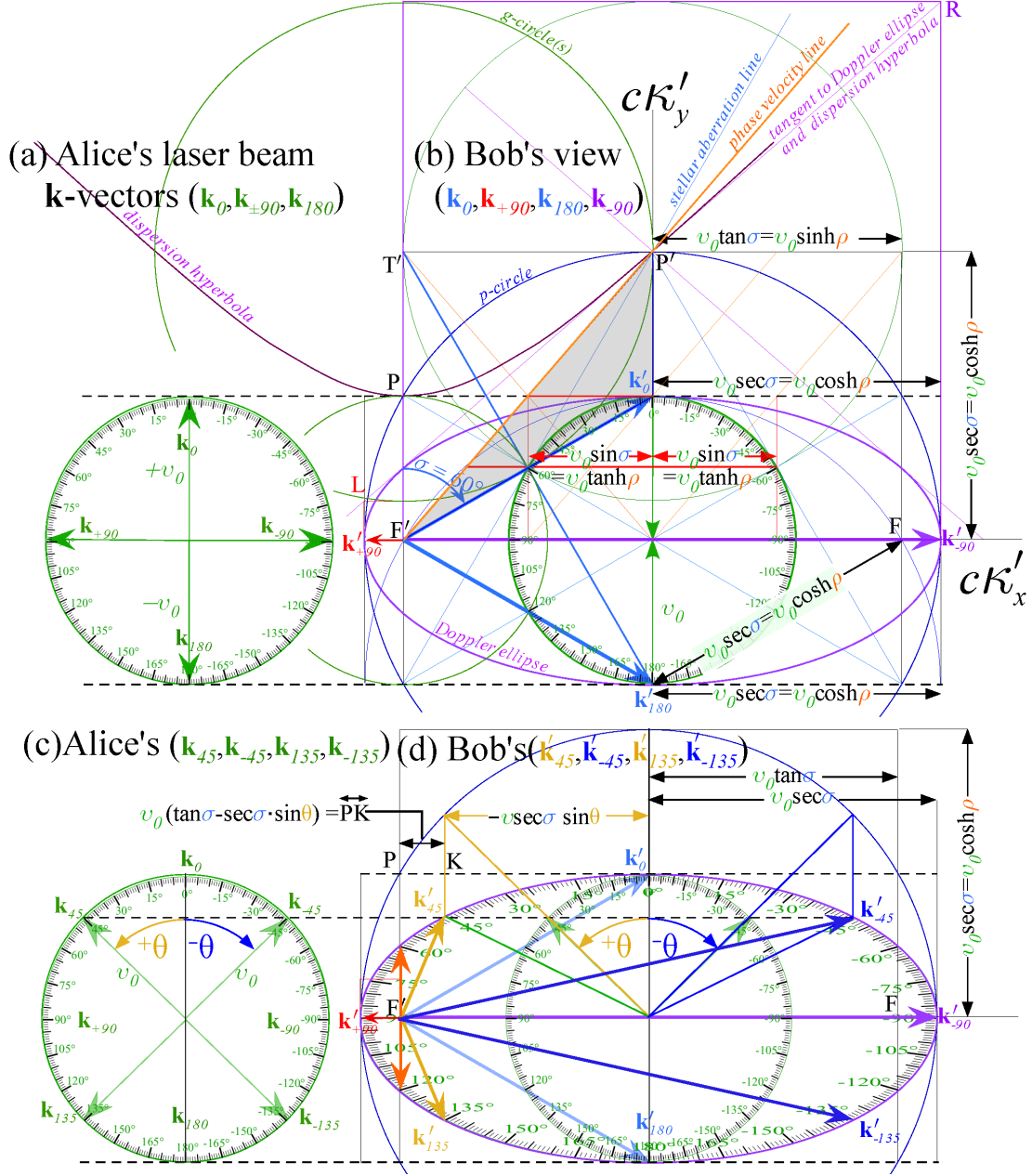


FIG. 19. Doppler spectral ellipse geometry in wavenumber (κ_x, κ_y) -per-space

It is helpful to return to the original algebraic ELT formulas of (14) or (25) for comparison.

$$\begin{pmatrix} v'(\theta) \\ c\kappa'_x(\theta) \\ c\kappa'_y(\theta) \\ c\kappa'_z(\theta) \end{pmatrix} = \begin{pmatrix} \cosh \rho & \sinh \rho & \cdot & \cdot \\ \sinh \rho & \cosh \rho & \cdot & \cdot \\ \cdot & \cdot & 1 & \cdot \\ \cdot & \cdot & \cdot & 1 \end{pmatrix} \begin{pmatrix} v_0 \\ -v_0 \sin \theta \\ v_0 \cos \theta \\ 0 \end{pmatrix} = v_0 \begin{pmatrix} \cosh \rho - \sinh \rho \sin \theta \\ \sinh \rho - \cosh \rho \sin \theta \\ \cos \theta \\ 0 \end{pmatrix} \quad (40)$$

This extension of (25) has a unit sub-matrix for (y, z) -components normal to x -boost axis.

If Alice points her laser at Bob ($\theta = -\frac{\pi}{2}$) the ELT reduces to a blue-Doppler e^ρ shift for him.

$$\begin{pmatrix} v'(-\pi/2) \\ c\kappa'_x(-\pi/2) \\ c\kappa'_y(-\pi/2) \\ c\kappa'_z(-\pi/2) \end{pmatrix} = \begin{pmatrix} \cosh \rho & \sinh \rho & \cdot & \cdot \\ \sinh \rho & \cosh \rho & \cdot & \cdot \\ \cdot & \cdot & 1 & \cdot \\ \cdot & \cdot & \cdot & 1 \end{pmatrix} \begin{pmatrix} v_0 \\ v_0 \\ 0 \\ 0 \end{pmatrix} = v_0 \begin{pmatrix} \cosh \rho + \sinh \rho \\ \sinh \rho + \cosh \rho \\ 0 \\ 0 \end{pmatrix} = v_0 \begin{pmatrix} e^\rho \\ e^\rho \\ 0 \\ 0 \end{pmatrix} \quad (41)$$

He sees the monster \mathbf{k}'_{-90} -vector along positive x -axis in Fig.19b. For ($\theta = +\frac{\pi}{2}$) there is a tiny \mathbf{k}'_{+90} -vector pointing the other way. Given this we ask: Can Bob *see* a minus- \mathbf{k} beam?

$$\begin{pmatrix} v'(\pi/2) \\ c\kappa'_x(\pi/2) \\ c\kappa'_y(\pi/2) \\ c\kappa'_z(\pi/2) \end{pmatrix} = \begin{pmatrix} \cosh \rho & \sinh \rho & \cdot & \cdot \\ \sinh \rho & \cosh \rho & \cdot & \cdot \\ \cdot & \cdot & 1 & \cdot \\ \cdot & \cdot & \cdot & 1 \end{pmatrix} \begin{pmatrix} v_0 \\ v_0 \\ 0 \\ 0 \end{pmatrix} = v_0 \begin{pmatrix} \cosh \rho - \sinh \rho \\ \sinh \rho - \cosh \rho \\ 0 \\ 0 \end{pmatrix} = v_0 \begin{pmatrix} e^{-\rho} \\ -e^{-\rho} \\ 0 \\ 0 \end{pmatrix} \quad (42)$$

This question hi-lights differences between (\mathbf{k}, ω) -space and space-time that exist despite the remarkable geometric similarity shared, for example, between Fig.18 and Fig.19. A pure optical \mathbf{k} -wave imagined in Fig.19 would fill the entire universe uniformly and thus might be seen by Bob no matter where he is located or going. More practical wave states such as spherical waves in Fig.17 and Fig.18 are quite complicated combinations of \mathbf{k} -waves that have singularities or other features to pin down space-time geography. They also have non-uniform amplitudes varying with time and location and this limits their range and duration.

Another difference between Fig.18 and Fig.19 is that the latter does not involve t -dilation so critical to the former. Instead, the (y, z) -components of any \mathbf{k} transverse to the x -boost axis are identical for Alice and Bob while the k'_x -component and \mathbf{k}' -length or frequency v' vary with rapidity ρ or aberration angle σ and Alice-angle θ according to ELT (40).

$$v'(\theta) = v_0(\cosh \rho_x - \sinh \rho_x \sin \theta) = v_0(\sec \sigma - \tan \sigma \sin \theta) \quad (43)$$

$$c\kappa'_x(\theta) = v_0(\sinh \rho_x - \cosh \rho_x \sin \theta) = v_0(\tan \sigma - \sec \sigma \sin \theta) \quad (44)$$

Alice and Bob agree on y -component $c\kappa_y(\theta) = c\kappa'_y(\theta) = \cos \theta$ of each \mathbf{k} -vector and interval PK in Fig.19b is an example of (44) bending $c\kappa_x$ from leaning backwards by $\theta=45^\circ$ to $c\kappa'_x$ pointing toward positive x -axis. Any \mathbf{k} not on x -axis follows the ellipse toward $+x$ -direction.

The \mathbf{k} -vector starting way back at $\theta = 60^\circ$ is made vertical by this relativistic aberration. The elliptic protractor \mathbf{k} solves Alice-Bob stellar aberration relations forwards or backwards.

Each wavevector \mathbf{k} or $\vec{\kappa}=\mathbf{k}/2\pi$ has hypotenuse length $|\kappa|$ that is related to frequency $\nu=c|\kappa|$ as given by (43). The \mathbf{k} -vector false-coloring sketched in Fig.19 shades longer \mathbf{k} -vectors toward the blue or violet for the longest \mathbf{k}'_{-90} and shorter ones toward the red color of the shortest case \mathbf{k}'_{+90} . At larger values of Alice-Bob relative velocity most of the Doppler shifted frequencies must fall outside of the visible spectrum and are plotted as black (or invisible) outside of that narrower visible rainbow. This is done in Fig.20 for examples that begin with Alice using only her favorite color $\nu_0=600\text{THz}$ green for a uniform array of \mathbf{k} -directions that Bob sees Doppler-shortened or lengthened while being rotated into “headlight” directions according to (40). This provides a revealing lab-based picture of radiation of atoms accelerated in free-electron lasers and related experiments in high energy spectroscopy at SLAC.

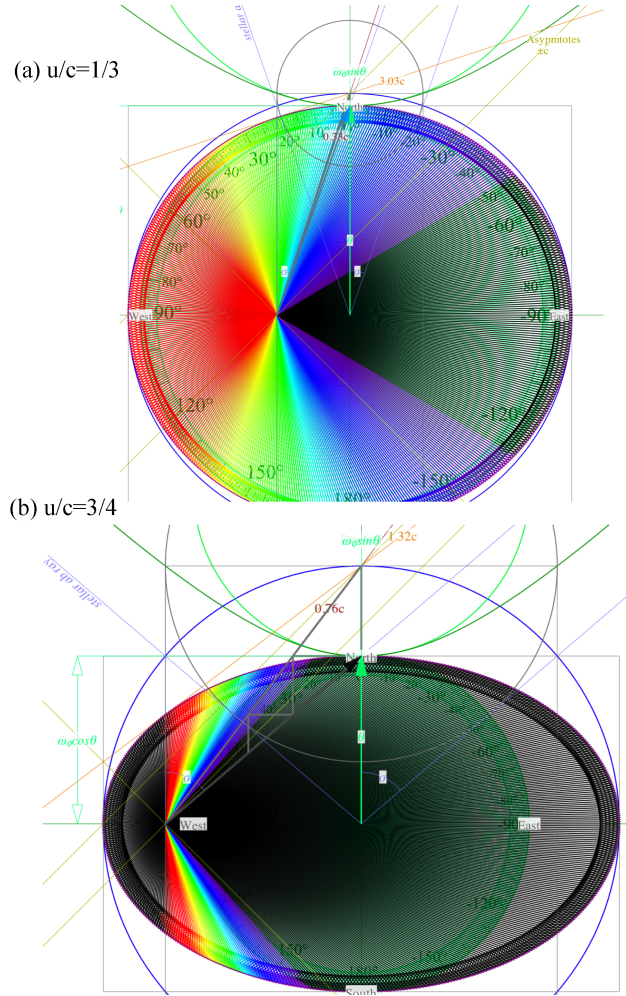


FIG. 20. Doppler aberration (a) $\frac{u}{c} = \frac{1}{3}$. (b) $\frac{u}{c} = \frac{3}{4}$.

V. BASIC RELATIVISTIC QUANTUM MECHANICS

In Sec.IV paired Continuous Wave (2-CW) properties are derived by optical interference of a left-right pair of single Continuous plane Waves (1-CW) each labeled by frequency-wavevector $2\pi(v_L, c\kappa_L)=(\omega_L, c\mathbf{k}_L)$ and $2\pi(v_R, c\kappa_R)=(\omega_R, c\mathbf{k}_R)$, respectively. 2-CW properties such as group velocity $\frac{v_R-v_L}{v_R+v_L}c$, (29), invariant frequency $\sqrt{v_L v_R}$, (30), a Minkowski coordinate frame (Fig.5c or Fig.6c) are things that lie beyond the reach of a single 1-CW. A 1-CW by itself just obeys Evenson's axiom that fixes its phase velocity to exactly $c=2.99792458 \cdot 10^8 m/s \cong 3 \cdot 10^8 m/s$. This pins its internal phasor clocks to a standstill as noted in discussion of 300THz CW example in Fig.4 following equation (10).

Real world occupants such as humans must regard c as mortally unattainable velocity. An intrepid photon chaser (Wile E. Coyote?) going at ever increasing rate ρ in pursuit of a 1-CW will not see light's speed reduce at all but will observe its frequency and amplitude dying exponentially according to Doppler-red factor $e^{-\rho}$. Thus a 1-CW disappears without revealing any sign of a 1-CW rest-frame. Neither will this same chaser see a c change by attempting to pursue a 1-CW *upstream*. Again, rest frame search is futile. (But, this time it may be the chaser who dies exponentially, burned by the $e^{+\rho}$ blue-shift factor.)

All this leaves the 1-CW, a mythical lone Fourier component $\psi_1 = a_{\mathbf{k}_1, \omega_1} e^{i(\mathbf{k}_1 \bullet \mathbf{r} - \omega_1 t)}$, outside our mortal world where real things have locations that change with more-or-less well defined velocities. One might ask, "What is the least that might lend mortality to a 1CW or give it a frame of reference in the classical world?"

The answer is a *second* 1-CW $\psi_2 = a_{\mathbf{k}_2, \omega_2} e^{i(\mathbf{k}_2 \bullet \mathbf{r} - \omega_2 t)}$! But, ψ_2 must *differ* from ψ_1 in at least one way: wave vector direction $\hat{k}_2 = \frac{\mathbf{k}_2}{|\mathbf{k}_2|}$ of ψ_2 cannot equal $\hat{k}_1 = \frac{\mathbf{k}_1}{|\mathbf{k}_1|}$ of ψ_1 and preferably should be *opposite*. ($\hat{k}_2 = -\hat{k}_1$) To acquire solid mortal credentials requires head-on interference to make the 2-CW described first by equation (11) that leads directly to Minkowski wave coordinates in Fig.6c, phase \mathbf{P}' and group \mathbf{G}' base vector transformations (14-15), Doppler- V_{group} relations (18), and shows Einstein-Lorentz transformation (ELT) matrices for (x, ct) -space-time (22) are equal to those for Fourier (ck, ω) -per-space-time in (25). It turns out that 2-CW interference endows other mortal properties such as classical mass and relativistic mechanics of energy-momentum that characterize a quantum matter wave. Such endowment uses phase coordinates of frequency $\omega_{phase} = 2\pi v_{phase}$ and wave-vector or wave-number $k_{phase} = 2\pi \kappa_{phase}$ of the P-hyperbola listed in Table II, Fig.10, and Fig.15.

A. Basic wave mechanics of matter

Since the last century, fundamental developments of quantum mechanics have relied on concepts from advanced classical mechanics of Lagrange, Hamilton, Legendre, Jacobi, and Poincare that were developed mostly in the preceding (19th) century. The latter contains a formidable web of formalism using ecclesiastical terms such as *canonical* that once implied higher levels of truth, but for modern physics students, they mean not so much.

Below is a simpler approach that connects wave geometry of Sec.IV to 16th through 18th century mechanics of Galileo, Kepler, and Newton and then derives mechanics fundamentals for the 20th and 21st centuries. It also clarifies some 19th century concepts that are often explained poorly or not at all, including Legendre contact transformations, canonical momentum, Poincare invariant action, and Hamilton-Jacobi equations. Understanding of these difficult classical ideas and connections is helped by wave geometry.

2-CW geometry of Fig.15 has hyperbolic coordinates of phase frequency $v_{phase} = B \cosh \rho$ and wave number $c\kappa_{phase} = B \sinh \rho$ with slope equal to group velocity $\frac{V_{group}}{c} = \frac{u}{c} = \tanh \rho$. Each depends on rapidity ρ that approaches $\frac{u}{c}$ for Galilean-Newtonian speeds ($u \ll c$).

$$\begin{aligned} v_{phase} &= B \cosh \rho \approx B + \frac{1}{2}B\rho^2 & (\text{for } u \ll c) \\ c\kappa_{phase} &= B \sinh \rho \approx B\rho & (\text{for } u \ll c) \\ \frac{u}{c} &= \tanh \rho \approx \rho & (\text{for } u \ll c) \end{aligned} \quad (45)$$

At low speeds v_{phase} and κ_{phase} are simple functions u^2 and u of group velocity u .

$$v_{phase} \approx B + \frac{1}{2}[B/c^2]u^2 \quad \Leftarrow \text{for } (u \ll c) \Rightarrow \quad \kappa_{phase} \approx [B/c^2]u \quad (46)$$

Recall Newtonian energy $E = const. + \frac{1}{2}Mu^2$ and Galilean momentum $p = Mu$. A single scale factor $h = Mc^2/B$, relates both $(v, c\kappa)$ wave coordinates to classical E and p formulas.

$$hv_{phase} \approx Mc^2 + \frac{1}{2}Mu^2 \quad \Leftarrow \text{for } (u \ll c) \Rightarrow \quad h\kappa_{phase} \approx Mu \quad (47)$$

One may ask, “Is this just a coincidence?” Also, “What is that constant ($const. = hB = Mc^2$)?”

The answer to the second question involves the base or bottom value $B = v_A$ of Alice’s frequency hyperbola. It is also Bob’s bottom due to hyperbola invariance. The constant

$$const. = hB = hv_A = Mc^2 \quad (48)$$

may be the most famous formula in physics. Here it is Einstein's rest-mass-energy equation. It is an add-on to Newton's kinetic energy $\frac{1}{2}Mu^2$ that is perhaps the *second* most famous physics formula. This add-on does not contradict Newton's result. Physical effects depend only on *difference* or *change* of energy so any *constant* add-on has no observable effect.

The question of false coincidence criticizes (47) for Galilean-Newtonian formulas valid only at low velocity ($u \ll c$) and low ρ . The approximate v_{phase} and κ_{phase} in (47) need to be replaced by Table II formulas $v_{phase}=B \cosh \rho$ and $c\kappa_{phase}=B \sinh \rho$ that hold for all ρ .

$$\begin{aligned} E = hv_{phase} = Mc^2 \cosh \rho & \quad \Leftarrow \text{for all } \rho \Rightarrow & \quad p = h\kappa_{phase} = Mc \sinh \rho \\ & = \frac{Mc^2}{\sqrt{1 - \frac{u^2}{c^2}}} & \quad \Leftarrow \text{for } -c < u < c \Rightarrow & \quad = \frac{Mu}{\sqrt{1 - \frac{u^2}{c^2}}} \end{aligned} \quad (49)$$

Here the old-fashioned $\frac{u}{c}$ -form for $\cosh \rho$ in Table II gives Einstein's 1905 form for exact total energy $E=hv_{phase}$. Sixteen years later, DeBroglie's 1921 formula $p=h\kappa_{phase}$ for wave momentum appears. The $\frac{u}{c}$ -form for $Mc \sinh \rho$ derives relativistic momentum p similarly.

Underlying (49) is physics of "scale factor" h or the Planck constant $h=6.62607 \cdot 10^{-34} J \cdot s$ that appears in his cavity energy axiom $E_N=hNv$. Thus (49) gives just the lowest quantum level ($N=1$) of Planck's axiom. (Modern form $E_N=\hbar N\omega$ in Sec.II has angular frequency $\omega=2\pi v$ and angular $\hbar=1.05 \cdot 10^{-34} J \cdot s$.) A quick-fix replaces h with hN , but underlying quantum oscillator theory of electromagnetic cavity waves still needs to be discussed.

So far, the axioms behind (49) are just Evenson's (*All colors go c.*) discussed after Fig.2 and a time reversal axiom or Doppler inversion symmetry ($r=\frac{1}{b}$) following Fig.3. These involve space, time, frequency and *phase* factors of plane light waves that are sufficient to develop the special relativity theory. But this phase approach has so far ignored *amplitude* factor A of a light wave $\psi=Ae^{i(\mathbf{k}\cdot\mathbf{r}-\omega t)}$. While phase factor $e^{i(kr-\omega t)}$ describes the *quality* aspects of the light, the amplitude factor A describes the *quantity* of light, or more to the point, an average number N of *quanta* or *photons* in the wave that is related to the N factor of Planck's axiom. Raising N raises overall phase frequency Nv_{phase} and in proportion, both total energy hNv_{phase} and total wave mass $M_N=hNv_{phase}/c^2$.

The logical efficiency of optical axioms leading to (49) sheds some light on the three of the most logically opaque concepts of physics, namely energy, momentum and mass by expressing them as frequency v (inverse time τ) and wavenumber κ (inverse length λ). Perhaps, the terms *energy* and *momentum* will someday go the way of *phlogiston*!

1. *What is energy?*

Once I asked a professor lecturing on energy, “What is *Energy*?” He replied, “It measures ability to do *Work*.” So, I asked, “What is *Work*?” He replied, “Well, it’s *Energy*, of course!”

Probably, he would give the same circular logic if asked about *momentum*, another *sine qua non* of basic physics. A favorite flippant response to E and p questions is that momentum is the “Bang” and energy is the \$Buck\$ that pays for it. (\$1.00=10kWhr is close to national average.) This satisfies many who know the (unfortunate) American expression “Get more bang for your buck!” particularly if it is around the 4th of July.

Wave energy and momentum results (49) defeat such circular logic by showing how energy E is proportional to temporal frequency (v_{phase} waves per second) and momentum \mathbf{p}_α is proportional spatial frequency (κ_{phase} waves per meter in direction α). One should note the ratio of momentum \mathbf{p} and energy E in (49) is $\frac{\mathbf{p}}{E} = \frac{c\mathbf{k}}{\omega} = \frac{\mathbf{u}}{c}$ for any scale-factor h (or hN).

The answer in (49) for wave energy inside Alice’s laser cavity is a product of her tick-rate $v_{phase} = v_A = 600\text{THz}$ with scale factor h (actually hN) and Einstein dilation factor $\cosh\rho$ that is $\cosh 0 = 1$ for her and $\cosh\rho = \frac{5}{4}$ for Bob in Fig.9a. There Bob is complaining about her $1 - \frac{4}{5} = 20\%$ less wavelength $\lambda_{group} = (\frac{1}{2}\mu m)\text{sech}\rho = (\frac{1}{2}\frac{4}{5}\mu m)$ instead of complimenting her for $\frac{5}{4} - 1 = 25\%$ more wave energy. (When you can’t say something nice...) Also, Bob fails to note her considerable increase of momentum from zero ($\sinh 0 = 0$) to $p = hN\kappa_{phase} = hN\kappa_A \sinh\rho = hN\frac{v_A}{c}\frac{3}{4}$. (He could be excused for overlooking such a tiny momentum. It is over $\frac{1}{c}$ -times smaller than the energy value $E = hNv_A \cosh\rho = hNv_A\frac{5}{4}$ that he records for her wave.)

A most remarkable thing about (energy-momentum) $\propto (v_{phase}, \kappa_{phase})$ relations (49) (now with hN in for h) and the Alice-Bob story is that (49) applies not just to Alice’s light wave but also to its laser cavity frame. (Recall discussion around Fig.9.) In fact *any* mass M including Alice and Bob themselves is subject to the claim that it has an internal “heartbeat” frequency $v_{phase} = Mc^2/Nh$ that is *incredibly fast* due to the c^2 -factor and tiny Planck- h divisor. Also, Alice’s light wave with $v_{phase} = v_A$ actually has a mass $M_A = Nhv_A/c^2$ that is *incredibly tiny* in this case due to the tiny Planck- h factor with the huge c^2 -divisor. Such relations in (49) of mass, energy, momentum, and frequency need further clarification.

2. What's the matter with energy?

Evenson axioms of optical dispersion and time symmetry imply a 2-CW light geometry that leads directly to exact mass-energy-momentum and frequency relations (49) with low-speed approximations (47). A light wave with rest mass and rest energy proportional to a proper invariant phase frequency $v_{phase}=v_A=v'_A$ is effectively a quantum matter wave that acquires intrinsic rest mass $M_{A_N}=Nhv_A/c^2$ due to its phase frequency.

In so doing, concepts of mass or matter lose classical permanence and become fungible. We define three types of mass M_{rest} , M_{mom} , and M_{eff} distinguished by their dependence on rapidity ρ or velocity u . The first is $M_{rest}=M_{A_N}$. The other two approach M_{rest} at low u .

Einstein rest mass M_{A_N} is invariant to ρ . It labels a hyperbola with bottom base level $E_N(\rho=0)=M_{A_N}c^2$ respected by all observers including Alice and Bob. Each mode A of Alice's cavity has a stack of $N=1,2,3,\dots$ hyperbolas, one for each quantum number N .

$$\begin{aligned} E_N^2 &= (hNv_A)^2 = (M_{A_N}c^2)^2 \cosh^2 \rho = (M_{A_N}c^2)^2 (1 + \sinh^2 \rho) \\ &= (M_{A_N}c^2)^2 + (cp_N)^2 \end{aligned} \quad (50)$$

(E,cp) -space hyperbola $E^2=(Mc^2)^2+(cp)^2$ in Fig.22 is a plot of an exact Einstein-Planck matter wave dispersion(49). The inset is a plot of approximation (47) for low p and $u \ll c$. Properties and pitfalls of this Bohr-Schrodinger approximation are discussed later.

The second type of mass M_{mom} is *momentum-mass* defined by ratio $\frac{p}{u}$ of relativistic momentum $p=Mc \sinh \rho$ from (49) with group velocity $u=c \tanh \rho$. M_{mom} satisfies Galileo's old definition $p=M_{mom}u$ using the newly defined relativistic wave quantities.

$$\begin{aligned} \frac{p}{u} &\equiv M_{mom} = \frac{M_{rest}c}{u} \sinh \rho = M_{rest} \cosh \rho \xrightarrow{u \rightarrow c} M_{rest}e^\rho / 2 \\ &= \frac{M_{rest}}{\sqrt{1 - u^2/c^2}} \xrightarrow{u \ll c} M_{rest} \end{aligned} \quad (51)$$

The third type of mass M_{eff} is *effective-mass* defined by ratio $\frac{dp}{du}$ of *change* of momentum $p=Mc \sinh \rho$ from (49) with *change* of group velocity $du=c \operatorname{sech}^2 \rho d\rho$. M_{eff} satisfies Newton's old definition $F=M_{eff}a$ using relativistic wave quantities.

$$\frac{F}{a} \equiv M_{eff} \equiv \frac{dp}{du} = \frac{dp}{d\rho} \bigg/ \frac{du}{d\rho} = M_{rest}c \cosh \rho / c \operatorname{sech}^2 \rho = M_{rest} \cosh^3 \rho \quad (52)$$

A standard derivation of M_{eff} uses group velocity $V_{group} = \frac{dv}{d\kappa} = u$ as the independent variable.

$$\begin{aligned} \frac{F}{a} &\equiv M_{eff} \equiv \frac{dp}{du} = \frac{h d\kappa}{dV_{group}} = h \left/ \frac{d}{d\kappa} \frac{dv}{d\kappa} \right. = h \left/ \frac{d^2v}{d\kappa^2} \right. \\ &= M_{rest} \left/ (1 - u^2/c^2)^{3/2} \right. \xrightarrow{u \ll c} M_{rest} \end{aligned} \quad (53)$$

Group velocity and its tangent geometry is a crucial but hidden part of the matter wave theory. Physicists tend to commit to memory the derivative formula $\frac{dv}{d\kappa} = \frac{d\omega}{dk}$ for group velocity and forget the finite-difference formula $\frac{\Delta v}{\Delta \kappa} = \frac{\Delta \omega}{\Delta k}$ from which it is derived. This is mistaken since the latter is exact for discrete frequency spectra while the former is ill-defined and may give wrong results. The wave Minkowski coordinate geometry starts out with half-difference V'_{group} in (17) and (18) in Sec.IV. What follows in Fig.6 through Fig.15 is based entirely upon the more reliable finite-difference definition $\frac{\Delta v}{\Delta \kappa} = \frac{\Delta \omega}{\Delta k}$.

Nevertheless, Nature is kind to derivative definition $\frac{dv}{d\kappa}$ as seen in Fig.15. There hyperbolic tangent slope of line RL with altitude $\Delta v = v_R - v_L$ and base $\Delta \kappa = \kappa_R - \kappa_L$ has a finite-difference slope $\frac{\Delta v}{\Delta \kappa} = \tanh \rho$ exactly equal to the derivative $\frac{dv}{d\kappa} = \tanh \rho$ of the hyperbola at tangent point P' on phase velocity line OP'. Geometry of Doppler $v_{BLUE} = v_R$ and $v_{RED} = v_L$ is at play.

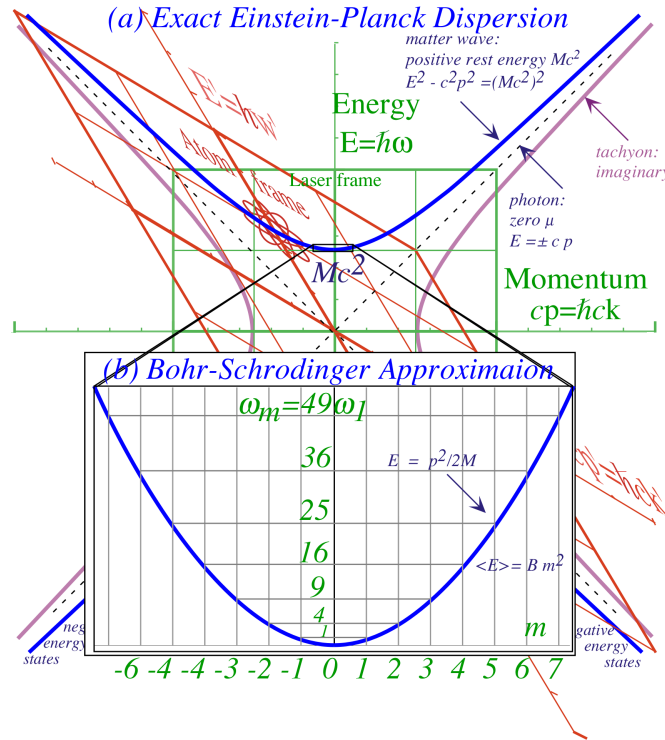


FIG. 22. (a) Einstein-Planck energy-momentum dispersion (b) Bohr-Schrodinger approximation

That slope $\frac{dv}{d\kappa}$ equals $V_{group}=u$ and is the velocity of Alice relative to Bob. It is also related to the momentum/energy ratio $\frac{c\mathbf{p}}{E}=\frac{\mathbf{u}}{c}$ as noted before.

$$V_{group} = u = \frac{\Delta v}{\Delta \kappa} = \frac{dv}{d\kappa} = \frac{d\omega}{dk} = \frac{dE}{dp} = \frac{c^2 p}{E} \quad (54)$$

As slope $\frac{dv}{d\kappa}=u$ of dispersion hyperbola $v(\kappa)$ affects velocity u and relations with momentum p , so does curvature $\frac{d^2v}{d\kappa^2}$ affect acceleration a and its relation to force F or momentum time rate of change $\frac{dp}{dt}$ in the effective-mass M_{eff} equations (52) and (53). One is inclined to regard M_{eff} as a quantum mechanical result since it is a product of Planck constant h with inverse $\frac{d^2v}{d\kappa^2}$, the approximate *Radius of Curvature* ($RoC=1/\frac{d^2v}{d\kappa^2}$) of dispersion function $v(\kappa)$. Geometry of a dispersion hyperbola $v=v_A \cosh \rho$ is such that its bottom ($\rho=0=u$) radius of curvature RoC equals the rest frequency $v_A=M_{rest}c^2/h$ that is labeled as the b -circle radius B in Fig.15. Hyperbola curvature decreases as ρ increases, and so its RoC and M_{eff} grow according to (52) in proportion to exponential $e^{3\rho}$ as velocity u approaches c , three times faster than the e^ρ for high- ρ growth of momentum mass M_{mom} in (51).

Since 1-CW dispersion ($v=\pm c\kappa$) is flat, its RoC and photon effective mass are infinite ($M_{eff}^\gamma=\infty$). This is consistent with the Evenson's axiom prohibiting c -acceleration. (All colors *always* go c .) The other extreme is photon rest mass which is zero ($M_{rest}^\gamma=0$). Between these extremes, photon momentum-mass M_{mom}^γ depends on CW color or frequency v .

$$\begin{aligned} (a) \gamma - \text{rest mass: } & M_{rest}^\gamma = 0, \\ (b) \gamma - \text{momentum mass: } & M_{mom}^\gamma = \frac{p}{c} = \frac{h\kappa}{c} = \frac{hv}{c^2}, \\ (c) \gamma - \text{effective mass: } & M_{eff}^\gamma = \infty. \end{aligned} \quad (55)$$

Newton's *Optics* text is famous for his rejection of wave nature of light in favor of a corpuscular one. He described interference effects as light's "fits." Perhaps, light having three mass values in (55) would, for Newton, verify its schizophrenic insanity. Also 2-CW 600THz cavity momentum \mathbf{p} averages zero, but each photon adds a tiny mass M_{mom}^γ .

$$M_{mom}^\gamma = \frac{hv}{c^2} = v(7.4 \cdot 10^{-51})kg \cdot s = 4.4 \cdot 10^{-36}kg \quad (\text{for: } v = 600\text{THz})$$

A 1-CW state has zero M_{rest}^γ , but 1-photon momentum (49) is a non-zero $p^\gamma=M_{mom}^\gamma c$.

$$p^\gamma = h\kappa = \frac{hv}{c} = v(2.2 \cdot 10^{-42})kg \cdot m = 1.3 \cdot 10^{-27}kg \cdot m \cdot s^{-1} \quad (\text{for: } v = 600\text{THz})$$

These numbers are so tiny that relativistic or quantum effects go unnoticed for so long. Note Galileo's $p=MV$ is exact for light in the form $p^\gamma=M_{mom}^\gamma c$. It seems like "Galileo's Revenge" and includes exact Galilean addition (5) of rapidity and of phase angular velocity (11).

B. Field quantization

The continuous *classical* mechanical world is revealing an underlying ethereal wave-like *quantum* mechanical world. There classical quantities such as energy and momentum become “quantized” as they get restricted to discrete values or “spectra” like key-notes of a piano or Fraunhofer lines in solar spectra. Quantization occurs when waves bounce around a trap of some kind where they self-interfere. There results a natural selection of survival-by-the-fittest waves that fit in the trap with discrete quantum wave-numbers n of undulations.

For light (em fields $\sum A_{\mathbf{k},\omega} e^{i(\mathbf{k}\cdot\mathbf{r}-\omega t)}$) there are two kinds of quantization. 1st-quantization is of phase- $(\mathbf{k}\cdot\mathbf{r}-\omega t)$ variables \mathbf{k} and ω . 2nd-quantization is of field amplitudes $A_{\mathbf{k},\omega}$. Modes for 1st-quanta $n=1,2,3$ are sketched above photon energy levels for 2nd-quanta $N=1,2,\dots$ in Fig.23. Each photon level- N_n is drawn as a relativistic hyperbola in a stack for mode- n . Cavity boundary conditions 1st-quantize classical wave mode variables (ω_n, ck_n) that have

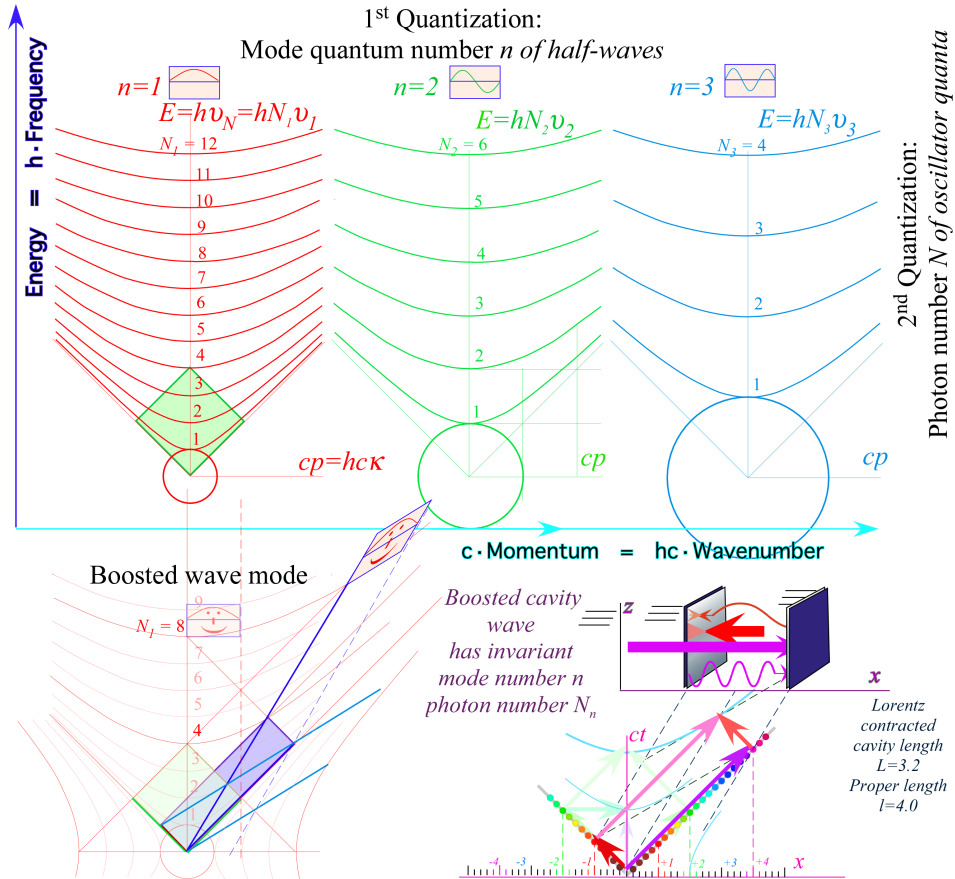


FIG. 23. 1st quantized cavity wave modes $n=1,2,3$ and their quantized photon levels $N_n=1,2,3..$

discrete numbers $n=1,2,3,..$ of half-wave anti-nodes fitting a model cavity of length- ℓ as sketched at the top of Fig.23 with nodes dividing interval ℓ into exactly n equal sections.

$$(a) \text{ wave vector : } k_n = \frac{\pi}{\lambda_n} = n \frac{\pi}{\ell} \quad (b) \text{ } \angle\text{-frequency : } \omega_n = ck_n = cn \frac{\pi}{\ell} \quad (56)$$

2^{nd} -quantization of cavity mode k_n (or \mathbf{k} in 3D cavity) uses normal coordinates $A_{k_n}=A_{\mathbf{k}}$ satisfying Maxwell equations that behave as harmonic oscillators. A 2-CW-standing-wave vector potential amplitude $A_{\mathbf{k}} \equiv \mathbf{A} = \mathbf{e}_1 |A| \sin(\mathbf{k} \cdot \mathbf{r} - \omega t + \phi)$ has Maxwell \mathbf{E} -and- \mathbf{B} -fields.

$$\begin{aligned} \mathbf{E} &= -\frac{\partial \mathbf{A}}{\partial t} & \mathbf{B} &= \nabla \times \mathbf{A} \\ \mathbf{E} &= \mathbf{e}_1 E_0 \cos(\mathbf{k} \cdot \mathbf{r} - \omega t + \phi) & \mathbf{B} &= (\mathbf{k} \times \mathbf{e}_1) B_0 \cos(\mathbf{k} \cdot \mathbf{r} - \omega t + \phi) \end{aligned} \quad (57)$$

Two unit polarization directions \mathbf{e}_1 of \mathbf{E} and $\mathbf{e}_2 = \mathbf{k} \times \mathbf{e}_1 \frac{1}{k}$ of \mathbf{B} share equal energy. (Let: $k = \frac{\omega}{c}$)

$$(a) E_0 \mathbf{e}_1 = |A| \omega \mathbf{e}_1 \quad (b) B_0 (\mathbf{k} \times \mathbf{e}_1) = |A| k \mathbf{e}_2 \quad (58)$$

Maxwell equations gives orthonormal unit vectors $\{\mathbf{e}_1, \mathbf{e}_2, \mathbf{e}_k\}$ and average field energy $\langle U \rangle V$ in a volume V containing the 2-CW vector potential amplitude: $\mathbf{A} = \mathbf{e}_1 |A| \sin(\mathbf{k} \cdot \mathbf{r} - \omega t + \phi)$.

$$\begin{aligned} \langle U \rangle V &= \left\langle \frac{\epsilon_0}{2} \mathbf{E} \cdot \mathbf{E} + \frac{1}{2\mu_0} \mathbf{B} \cdot \mathbf{B} \right\rangle V = V \left(\frac{\epsilon_0}{2} |A|^2 \omega^2 + \frac{|A|^2}{2\mu_0} k^2 \right) \langle \cos^2(\mathbf{k} \cdot \mathbf{r} - \omega t + \phi) \rangle \\ &= \frac{\epsilon_0}{2} \omega^2 |A|^2 V = \frac{1}{2\mu_0} k^2 |A|^2 V \text{ given average: } \langle \cos^2(\mathbf{k} \cdot \mathbf{r} - \omega t + \phi) \rangle = \frac{1}{2} \end{aligned} \quad (59)$$

Constants $\epsilon_0 = 8.854 \cdot 10^{-7} \frac{Nm^2}{C^2}$ and $\mu_0 = 4\pi 10^{-7} \frac{N}{A^2}$ have geometric mean $c^{-1} = \sqrt{\epsilon_0 \mu_0}$, an old and still awe inspiring expression for the speed of light.

Feynman's approach to field quantization (using Occam's razor) favors Fourier combinations of 1-CW moving waves $e^{i(kr - \omega t)}$ rather the 2-CW standing waves in (57).

$$\mathbf{A} = \sum_{\mathbf{k}} [(a_{\mathbf{k}1} \mathbf{e}_1 + a_{\mathbf{k}2} \mathbf{e}_2) e^{i(\mathbf{k} \cdot \mathbf{r} - \omega t)} + \text{c.c.}] = \sum_{\mathbf{k}} \sum_{\alpha=1}^2 [a_{\mathbf{k}\alpha} \mathbf{e}_\alpha e^{i(\mathbf{k} \cdot \mathbf{r} - \omega t)} + a_{\mathbf{k}\alpha}^* \mathbf{e}_\alpha e^{-i(\mathbf{k} \cdot \mathbf{r} - \omega t)}] \quad (60)$$

The \mathbf{k} -sum $k_\alpha = N_\alpha \frac{2\pi}{\ell}$ ($N_\alpha = 1, 2, \dots \infty$; $\alpha = x, y, z$) separates the the 2D polarization base vectors of (58) belonging to its \mathbf{E} and \mathbf{B} oscillator dimensions. Fourier amplitudes $a_{\mathbf{k}\alpha}$ of 1-CW modes in (60) are complex and half the magnitude of the 2-CW amplitude $A_{\mathbf{k}\alpha}$ in (59) since $A \cos \phi = \frac{A}{2} e^{i\phi} + \frac{A}{2} e^{-i\phi}$. Setting $\langle U \rangle V$ in (59) to Planck $E = \hbar N \omega$ relates A to N .

$$\langle U \rangle V = \hbar N \omega = \frac{\epsilon_0}{2} \omega^2 |A|^2 V \quad \Rightarrow \quad |A| = \sqrt{\frac{2\hbar N}{\epsilon_0 \omega V}} \quad \Rightarrow \quad |\mathbf{E}| = \omega |A| = \sqrt{\frac{2\hbar N \omega}{\epsilon_0 V}} \quad (61)$$

This would presume all energy to be concentrated into a single quantum level $N_{\mathbf{k}\alpha}$ of a single cavity mode \mathbf{k} and polarization- α . Lasers and coordinate frames in Fig.5 and Fig.6 require coherent state N -distribution in a single 2-CW mode, and do not work with pure N -states.

1. *Quantum numbering of photons and modes*

Building 1-CW Fourier expansions of fields \mathbf{E} and \mathbf{B} to construct their energies $U_E V$ and $U_B V$ from vector potential \mathbf{A} in (60) is detailed in Appendix B.

$$\begin{aligned} U_E V &= \sum_{\mathbf{k}\alpha} \frac{\varepsilon_0 V}{2} [2|a_{\mathbf{k}\alpha}|^2 \omega^2 - a_{-\mathbf{k}\alpha}^* a_{\mathbf{k}\alpha}^* \omega^2 e^{-2i\omega t} - a_{-\mathbf{k}\alpha} a_{\mathbf{k}\alpha} \omega^2 e^{-2i\omega t}] \\ U_B V &= \sum_{\mathbf{k}\alpha} \frac{\varepsilon_0 V}{2} [2|a_{\mathbf{k}\alpha}|^2 \omega^2 + a_{-\mathbf{k}\alpha}^* a_{\mathbf{k}\alpha}^* \omega^2 e^{-2i\omega t} + a_{-\mathbf{k}\alpha} a_{\mathbf{k}\alpha} \omega^2 e^{-2i\omega t}] \end{aligned} \quad (62)$$

Cancellation of cross-terms simplifies total energy sum.

$$UV = (U_E + U_B) V = \sum_{\mathbf{k}\alpha} 2\varepsilon_0 \omega^2 |a_{\mathbf{k}\alpha}|^2 V = \sum_{\mathbf{k}\alpha} 2\varepsilon_0 V \omega^2 a_{\mathbf{k}\alpha}^* a_{\mathbf{k}\alpha} \quad (63)$$

This may be factored and relabeled into a harmonic oscillator Hamiltonian.

$$\begin{aligned} UV &= \sum_{\mathbf{k}\alpha} \frac{1}{2} \left[2\omega \sqrt{\varepsilon_0 V} (a_{\mathbf{k}\alpha}^{\text{Re}} - i a_{\mathbf{k}\alpha}^{\text{Im}}) \right] \left[2\omega \sqrt{\varepsilon_0 V} (a_{\mathbf{k}\alpha}^{\text{Re}} - i a_{\mathbf{k}\alpha}^{\text{Im}}) \right] \\ &= \sum_{\mathbf{k}\alpha} \frac{1}{2} [\omega Q_{\mathbf{k}\alpha} + i P_{\mathbf{k}\alpha}] [\omega Q_{\mathbf{k}\alpha} + i P_{\mathbf{k}\alpha}] \\ &= \sum_{\mathbf{k}\alpha} \frac{1}{2} (P_{\mathbf{k}\alpha}^2 + \omega^2 Q_{\mathbf{k}\alpha}^2) \end{aligned} \quad (64)$$

Real and imaginary parts of phasor amplitudes $a_{\mathbf{k}\alpha}$ are coordinates $Q_{\mathbf{k}\alpha}$ and momenta $P_{\mathbf{k}\alpha}$.

$$\begin{aligned} Q_{\mathbf{k}\alpha} &= 2\sqrt{\varepsilon_0 V} a_{\mathbf{k}\alpha}^{\text{Re}} = \sqrt{\varepsilon_0 V} (a_{\mathbf{k}\alpha} + a_{\mathbf{k}\alpha}^*) \quad \text{where: } a_{\mathbf{k}\alpha} = a_{\mathbf{k}\alpha}^{\text{Re}} + i a_{\mathbf{k}\alpha}^{\text{Im}} = \frac{1}{2\sqrt{\varepsilon_0 V}} \left(Q_{\mathbf{k}\alpha} + \frac{i P_{\mathbf{k}\alpha}}{\omega} \right) \\ P_{\mathbf{k}\alpha} &= 2\omega \sqrt{\varepsilon_0 V} a_{\mathbf{k}\alpha}^{\text{Im}} = \omega \sqrt{\varepsilon_0 V} (a_{\mathbf{k}\alpha} - a_{\mathbf{k}\alpha}^*) / i \quad \text{and: } a_{\mathbf{k}\alpha}^* = a_{\mathbf{k}\alpha}^{\text{Re}} - i a_{\mathbf{k}\alpha}^{\text{Im}} = \frac{1}{2\sqrt{\varepsilon_0 V}} \left(Q_{\mathbf{k}\alpha} - \frac{i P_{\mathbf{k}\alpha}}{\omega} \right) \end{aligned} \quad (65)$$

Amplitudes $a_{\mathbf{k}\alpha}$ and $a_{\mathbf{k}\alpha}^*$ become operators of photon destruction $\mathbf{a}_{\mathbf{k}\alpha}$ and creation $\mathbf{a}_{\mathbf{k}\alpha}^\dagger$ that find 2D oscillator waves and energy spectrum for each \mathbf{k} -mode and each polarization $\alpha=x, y$.

$$E_{\mathbf{k}} = \hbar \Omega_{\mathbf{k}} = \hbar (N_{\mathbf{k}} + 1) \omega_{\mathbf{k}} = \hbar (N_{x,\mathbf{k}} + N_{y,\mathbf{k}} + 1) \omega_{\mathbf{k}} \quad (66)$$

The ground quantum state has zero ($N_{\mathbf{k}}=0$) photons with zero-point energy $\hbar \omega_{\mathbf{k}}$. (Zero point energy is $\frac{1}{2} \hbar \omega_{\mathbf{k}}$ for each polarization dimension.) There are two energy-degenerate states having one photon ($N_{\mathbf{k}}=1$) each with energy $E_{\mathbf{k}} = \hbar 2 \omega_{\mathbf{k}}$, that is, one photon with x -polarization or else one photon with y -polarization. Similarly, there are three states of two photons ($N_{\mathbf{k}}=2$) with energy $E_{\mathbf{k}} = \hbar 3 \omega_{\mathbf{k}}$, that is, $(N_{x,\mathbf{k}}, N_{y,\mathbf{k}}) = (2,0)$, $(1,1)$, or $(0,2)$. A general $N_{\mathbf{k}}$ -photon energy level $E_{\mathbf{k}} = \hbar (N_{\mathbf{k}} + 1) \omega_{\mathbf{k}}$ has polarization degeneracy of $N_{\mathbf{k}} + 1$.

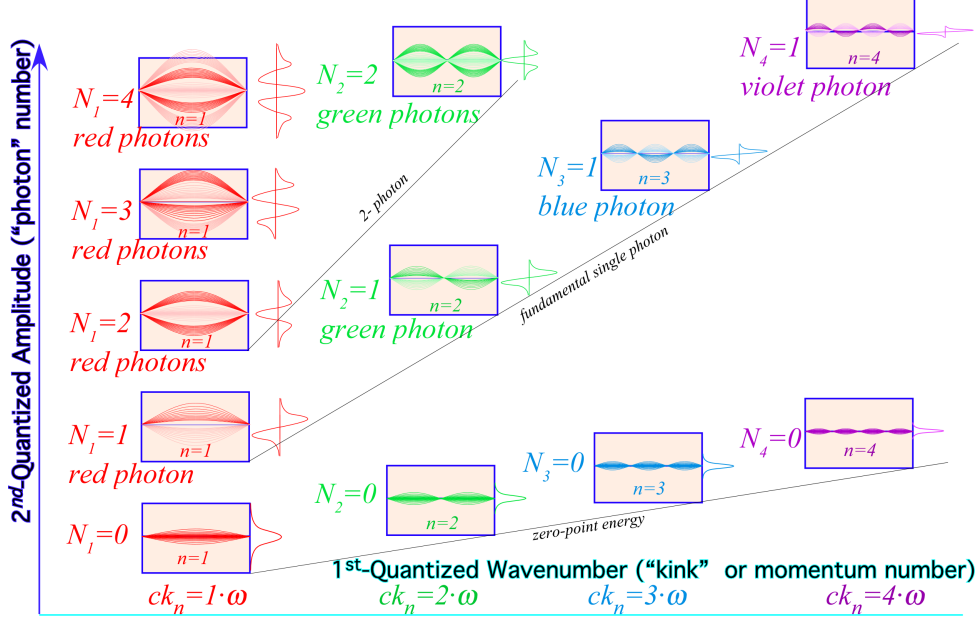


FIG. 24. 1st and 2nd quantized harmonic-oscillator cavity waves

A sketch of the first few quantum cavity wave states is given in Fig. 24. It is companion to Fig. 23 showing a stack of $N_{\mathbf{k}}$ -labeled energy-level hyperbolas for each cavity mode $k_n=\mathbf{k}$. The quantum numbers N (Number of photons) and n (number of ‘kinks’ or anti-nodes per cavity dimension ℓ) are invariant to observer rapidity ρ while wave energy (frequency) and momentum (wave number) vary with observer rapidity as $\cosh \rho$ and $\sinh \rho$, respectively.

Newton might be consoled that number N of photons in a box is invariant to speed $\rho \simeq \frac{u}{c}$ so they act like self-respecting corpuscles without ‘fits’ that he saw waves suffer. However, photon number N is a wave-based property, a wave kink-count in amplitude (A_x, A_y) space, just as mode number n of wavenumber k_n counts wave kinks in real (x, y, z) space.

2. Quantum wave normalization

Classical variables such as momentum, energy, or fields become operators whose eigenvalues are observed. This is discussed in a following section devoted to Hamiltonian and Lagrangian mechanics. Here the focus is upon field oscillators whose classical energy (63) has a form of 2nd-power amplitude-frequency product $E=kA^2\omega^2$, while quantum eigenvalues have the Planck form (66) that is only 1st-power in a frequency-quantum-number product $E_N=\hbar N\omega$. Planck may have had some anxious doubts about this.

This and other issues are resolved by re-examining quantum $|\mathbf{E}|$ -amplitude in (61). It shows that product $N\omega$ is proportional to $\omega^2|\mathbf{A}|^2$ in the expression for energy density U .

$$\langle U \rangle = \frac{\hbar N\omega}{V} = \frac{\varepsilon_0}{2}|\mathbf{E}|^2 = \frac{\varepsilon_0}{2}\omega^2|\mathbf{A}|^2 \quad \Rightarrow \quad |\mathbf{E}| = \omega|\mathbf{A}| = \sqrt{\frac{2\hbar N\omega}{\varepsilon_0 V}} \quad (67)$$

Scaling \mathbf{E} by $s = \sqrt{\frac{V\varepsilon_0}{2\hbar\omega}}$ gives an N -photon wave Ψ amplitude whose norm is N .

$$\vec{\Psi} = \begin{pmatrix} \Psi_x \\ \Psi_y \end{pmatrix} = s\mathbf{E} = \sqrt{\frac{\varepsilon_0 V}{2\hbar\omega}}\mathbf{E} \quad \Rightarrow \quad \vec{\Psi}^*\vec{\Psi} = |\Psi_x|^2 + |\Psi_y|^2 = N \quad (68)$$

Having the absolute-square $\Psi^*\Psi = |\Psi|^2$ or norm of a Ψ -wave function equal to the number N of quanta is a familiar axiom of modern quantum theory. If the wave is a variable wave-function $\Psi(x, y, z)$ then a volume integral is required to sum up energy density U .

$$\iiint d(xyz)\vec{\Psi}^*\vec{\Psi} = N \quad (69)$$

Elementary quantum theory of a single particle requires unit normalization $\int d(xyz)\Psi^*\Psi = 1$.

Poynting flux $\mathbf{S} = \mathbf{E} \times \mathbf{B}$ or “photon current” of a plane moving wave (1-CW ψ) also has a classical 2nd-power expression that reduces to a Planck 1st-power form. Flux \mathbf{S} has direction along \mathbf{k} and magnitude $S = cU$. The quantum number n for S is flux rate: $n = cN/V$ ($m^{-2}s^{-1}$).

$$S = cU = c\varepsilon_0|\mathbf{E}|^2 = \hbar n\omega \quad \text{where:} \quad n = cN/V \text{ (per } m^2s) \quad (70)$$

The 1-CW flux rate of photons n per square-meter per second is not invariant to observer rapidity ρ as is the cavity count of N/V photons per cubic meter of cavity in (61). Instead n transforms like frequency ω and suffers the same Doppler factor e^ρ for an observer approaching the source or else $e^{-\rho}$ when fleeing the source.

This amounts to a double-whammy for an approaching observer experiencing a Doppler increase in both *quality* (color or frequency $\omega = 2\pi\nu$) and *quantity* (of photon hits) and raises flux impact to 2nd-power $(e^\rho)^2$. This matches the 2nd-power $|\mathbf{E}|^2$ of the \mathbf{E} -field and implies that the \mathbf{E} -field *amplitude* shifts by e^ρ just like 1-CW wave vector \mathbf{k} and frequency $\omega = c|\mathbf{k}|$. Perhaps, this is a lesson from Planck quantum axiom reminding us that the relativistic wave amplitude is a *frequency*, too, just like energy and momentum.

C. Geometry of Hamiltonian and Lagrangian relativity

A 2-CW matter-wave has a rest frame with origin $x'=0$ and $k'=0=k_{phase}$ where the invariant phase function $\Phi=kx-\omega t=k'x'-\omega't'$ reduces to $\Phi=0-\varpi\tau$, a product of its proper or base frequency $B=\varpi=Mc^2/\hbar$ defined by (48) with proper time $t'=\tau$ defined by (28). The (x, t) -differential of phase is reduced as well to a similar negative mass-frequency ϖ -term.

$$d\Phi = k dx - \omega dt = 0 \cdot 0 - \frac{Mc^2}{\hbar} d\tau \equiv -\varpi d\tau \quad (71)$$

By (28) proper-time interval $d\tau$ dilates to ρ -moving frame time interval dt as follows.

$$dt = \frac{d\tau}{\sqrt{1 - \frac{u^2}{c^2}}} = d\tau \cosh \rho \quad \Leftrightarrow \quad d\tau = dt \sqrt{1 - \frac{u^2}{c^2}} = dt \operatorname{sech} \rho \quad (72)$$

One of the more interesting tales of modern physics is the first meeting between Dirac and the younger Richard Feynman. Both had been working on aspects of quantum phase and classical Lagrangian mechanics. Dirac mused about some formulas in one of his papers that showed similarities between a Lagrangian function and quantum phase. Feynman said abruptly, "That's because the Lagrangian *is* quantum phase!" At the time that was a fairly radical bit of insight. Below is a geometrical clarification of underlying phase relations.

1. Phase, action, and Lagrangian Hamiltonian functions

Feynman's observation needs some adjustment for units since Lagrangian L has units of energy (*Joules*) while phase Φ is a dimensionless invariant. A quantity S called *Action* is quantum phase Φ scaled by Planck's $\hbar = \frac{h}{2\pi} = 1.05 \cdot 10^{-34} Js$ and is a time integral of L .

$$S \equiv \hbar \Phi \equiv \int L dt \quad \text{where:} \quad \hbar \equiv \frac{h}{2\pi} = 1.05 \cdot 10^{-34} \text{Joule} \cdot \text{Second} \quad (73)$$

Differentials of action (74), phase (71) and time (72) combine to give expressions for Ldt .

$$dS \equiv Ldt = \hbar d\Phi = -Mc^2 d\tau = -Mc^2 \sqrt{1 - \frac{u^2}{c^2}} \cdot dt = -Mc^2 dt \operatorname{sech} \rho \quad (74)$$

Clearing ρ -frame time differential dt gives that frame's Lagrangian by itself.

$$L = -Mc^2 \sqrt{1 - \frac{u^2}{c^2}} = -Mc^2 \operatorname{sech} \rho = -Mc^2 \cos \sigma \quad (75)$$

Table II supplies identity $\text{sech}\rho=\cos\sigma$ for L in (75) and $\tanh\rho=\sin\sigma$ for group velocity u .

$$u \equiv V_{group} = c \tanh \rho = c \sin \sigma \quad (76)$$

It is conventional that Lagrangian L is explicit function of velocity. This is consistent with the low- $(\rho \cong \frac{u}{c})$ approximate Lagrangian that has the Newtonian $KE=\frac{1}{2}Mu^2$ term.

$$L = -Mc^2 \sqrt{1 - \frac{u^2}{c^2}} \xrightarrow{u \ll c} -Mc^2 + \frac{1}{2}Mu^2 + \dots \quad (77)$$

2. Hamiltonian functions, Poincare invariants, and Legendre contact transformation

The invariant phase differential (71) with an \hbar -factor as in (74) is a key relation.

$$dS \equiv Ldt \equiv \hbar d\Phi = \hbar k dx - \hbar \omega dt \quad (78)$$

Energy $E=\hbar\nu_{phase}=\hbar\omega=H$ and momentum $p=\hbar\kappa_{phase}=\hbar k$ from (49) for $N=1$ are used.

$$dS \equiv Ldt \equiv \hbar d\Phi = p dx - H dt \quad \Rightarrow \quad L = p \frac{dx}{dt} - H = p \cdot \dot{x} - H \quad (79)$$

Here energy E is identified with Hamiltonian function H . Results include the classical differential *Poincare invariant* $Ldt=pdx-Hdt$ and the *Legendre transform* $L=pu-H$ between Lagrangian L and Hamiltonian H . Remarkably, $\frac{L}{Mc^2}$ is the negative reciprocal of $\frac{H}{Mc^2}$.

$$\begin{aligned} H &= \hbar\omega = Mc^2 \cosh \rho & L &= \hbar\dot{\Phi} = -Mc^2 \text{sech}\rho \\ &= Mc^2 \sec \sigma & &= -Mc^2 \cos \sigma \\ &= \frac{Mc^2}{\sqrt{1 - \frac{u^2}{c^2}}} & &= -Mc^2 \sqrt{1 - \frac{u^2}{c^2}} \end{aligned} \quad (80)$$

Except for a (-)sign, H and L use the same co-inverse (cos,sec)-cousin functions (mid-columns of Table II) as Einstein t -dilation and Lorentz x -contraction, respectively. H (or L) are explicit functions of momentum p (or velocity u), the 1st cousin (sin,tan) pair in Table II.

$$\begin{aligned} cp &= \hbar ck = Mc^2 \sinh \rho & u &= V_{group} = c \tanh \rho \\ &= Mc^2 \tan \sigma = \frac{Mc u}{\sqrt{1 - \frac{u^2}{c^2}}} & &= c \sin \sigma \end{aligned} \quad (81)$$

Legendre contact transformation $H(cp)=up-L=\frac{u}{c}cp-L$ uses slope $\frac{u}{c}$ and intercept $-L$ of tangent line **LR** contacting H -hyperbola in Fig.25a to locate point $L(u)$ of Lagrangian plot.

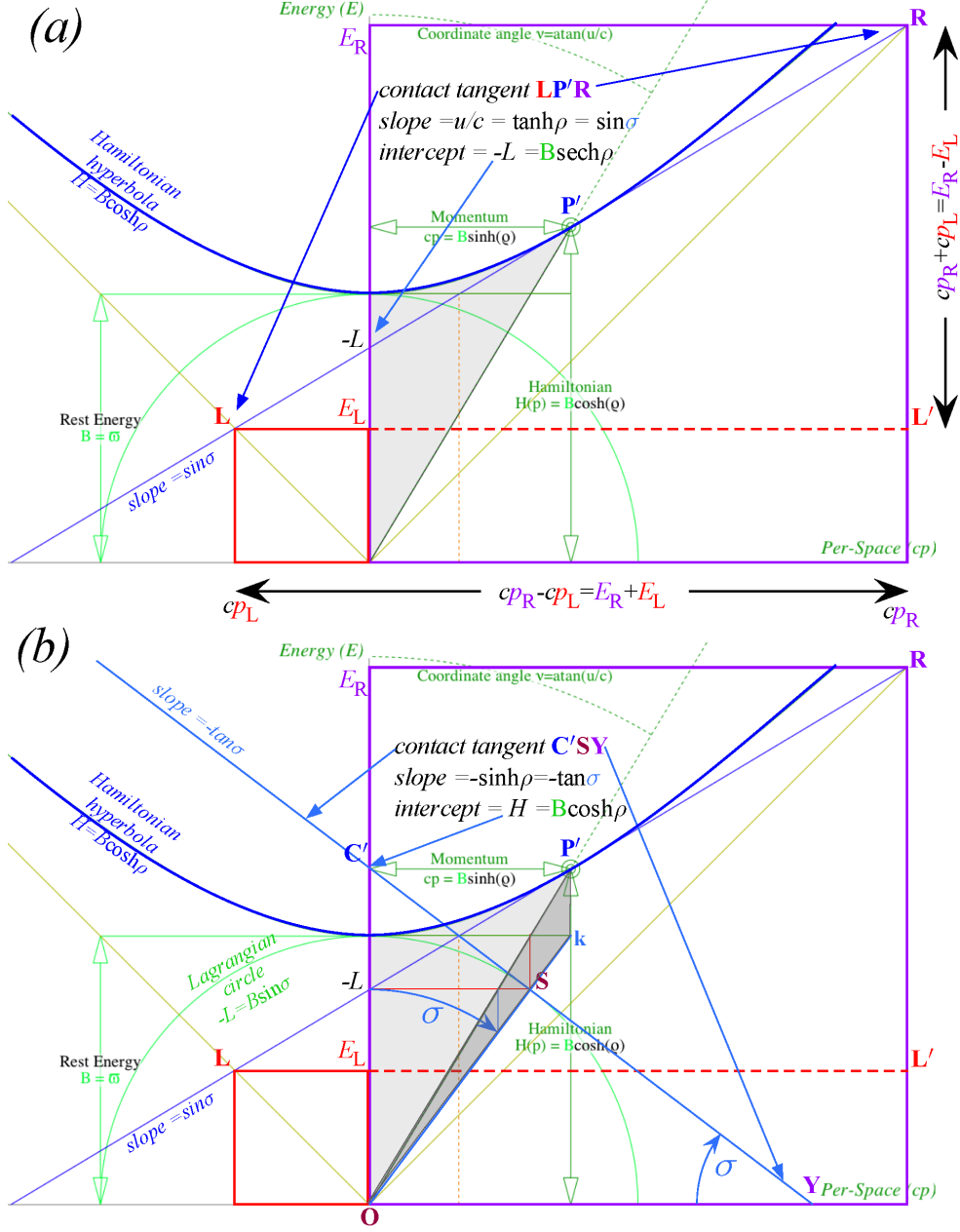


FIG. 25. (a) Slope $\frac{u}{c}$ and intercept $-L$ of $H(p)$ -tangent $-LP'$ give (u, L) point S on $L(u)$ -circle.

(b) Slope cp and intercept H of $L(u)$ -tangent $C'S$ give (p, H) point P' on $H(p)$ -hyperbola.

Inverse Legendre contact transformation $L(u) = pu - H$ uses slope p and intercept H of stellar tangent line $C'SY$ contacting L -circle in Fig. 25b to locate point $H(p)$ of Hamiltonian plot. This construction is clarified by separate plots of $H(p)$ in Fig. 26a and $L(u)$ in Fig. 26b.

Tangent contact transformation is a concept based upon wave properties and goes back to the Huygens and Hamilton principles discussed below. The basics of this lie in construction

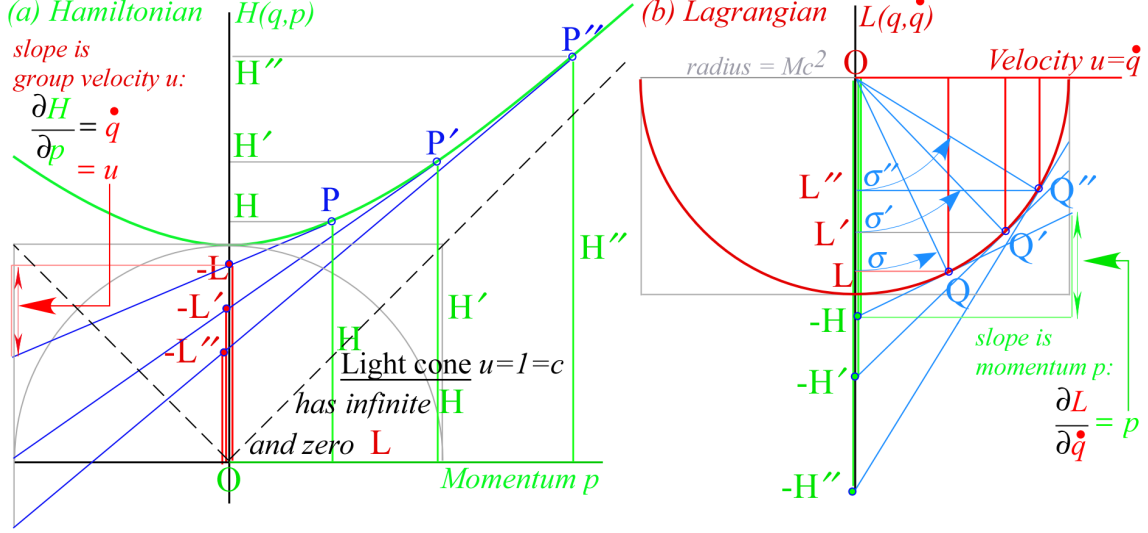


FIG. 26. Legendre contact transformation between (a)Hamiltonian $H(p)$ (b) Lagrangian $L(u)$

of space-time (x, ct) wave-grids given frequency- \mathbf{k} -vectors $(\nu, c\kappa)$ like \mathbf{P}' and \mathbf{G}' in Fig.7 and Fig.8. Each \mathbf{P}' or \mathbf{G}' coordinate pair $(\nu, c\kappa)$ determines lines with speed $\frac{\nu}{\kappa}$ and t -intercept spacing $\tau = \frac{1}{\nu}$ on ct -axis while x -intercept spacing is $\lambda = \frac{1}{\kappa}$ on x -axis. Together these phase and group grid lines make Minkowski crest-line coordinates. Now this geometry applies as well to energy-momentum $(E, cp) = h(\nu, c\kappa) = \hbar(\omega, ck)$ spaces. Functional dependence of wave grid spacing and slopes determines classical variables and equations of motion and so does functional *non*-dependence. For example, the Lagrangian L is an explicit function of velocity u but *not* momentum p , that is $\frac{\partial L}{\partial p} = 0$. The Hamiltonian H is an explicit function of momentum p but *not* velocity u , that is $\frac{\partial H}{\partial u} = 0$. These 0^{th} -equations and identity $L = pu - H$ give 1^{st} -Hamilton and 1^{st} -Lagrange equations.

$$\begin{aligned}
 0 &= \frac{\partial L}{\partial p} = \frac{\partial}{\partial p}(pu - H) & 0 &= \frac{\partial H}{\partial u} = \frac{\partial}{\partial u}(pu - L) \\
 u &= \frac{\partial H}{\partial p} \quad \left(\text{Hamilton's } 1^{st} \text{ equation} \right) & p &= \frac{\partial L}{\partial u} \quad \left(\text{Lagrange's } 1^{st} \text{ equation} \right)
 \end{aligned} \tag{82}$$

In Fig.25a slope of $H(p)$ -hyperbola at tangent point \mathbf{P}' is group velocity $\frac{u}{c} = \tanh \rho = \sin \sigma = \frac{3}{5}$. In Fig.25b slope of $-L(u)$ -circle at tangent point \mathbf{S} is momentum $cp = B \sinh \rho = B \tan \sigma = \frac{3}{4} Mc^2$ with minus (-) sign. A minus sign in (80) for Lagrangian ($L = -Mc^2 \cos \sigma$, for example) is a result of (-) in phase $(kx - \omega t)$ and phasor (They turn clockwise. $= \curvearrowright$) conventions.

For a low- $(\rho \cong \frac{u}{c})$ approximate Lagrangian (77), one may drop the $-Mc^2$ term and just keep the Newtonian kinetic energy term $\frac{1}{2} Mu^2$ that is equal to the corresponding kinetic

term $\frac{p^2}{2M}$ in the approximate Hamiltonian. Of course $\frac{p^2}{2M}$ reduces to $\frac{1}{2}Mu^2$ upon substituting approximate momentum $p=Mu$. Then students may ask, “Why be so fussy about having only momentum or p -dependence of H and only velocity or u -dependence of L ?”

Hamiltonian $H(p)$ hyperbola minimum in Fig.25 and Fig.26a is nearly identical to the Lagrangian $L(u)$ circle minimum in Fig.26b that lies below Fig.25b. There both curves are nearly parabolic. But, at higher speeds the Lagrangian $L(u)$ approaches zero as stellar angle σ approaches $\pm\frac{\pi}{2}$ and velocity u approaches c . Then Hamiltonian $H(p)=B\cosh\rho$ and its momentum $p=B\sinh\rho$ each approach $B\frac{e^\rho}{2}$ as rapidity ρ grows apparently without bound.

Clearly hyperbolic “Country cousin” functions involving rapidity ρ and momentum p fit a Hamiltonian infinite horizon, while circular “City cousin” functions of the restricted stellar angle $-\pi<\sigma<\pi$ and velocity $-c<u<c$ fit localized Lagrangian, the keeper of quantum phase.

The third (csc,cot)-cousin pair $\lambda_{phase}=B\csc\rho=B\cot\sigma$ and $V_{phase}=c\coth\rho=c\csc\sigma$ from Table II do not appear in the preceding discussions of classical correspondence. These describe the phase part or “quantum guts” of a 2-CW internal structure, and as such were not known by 19-century classicists and still difficult to observe. Now we see that phase is the heartbeat of quantum physics. Fig.27 shows DeBroglie wavelength λ_{phase} and V_{phase} at the edges of the geometric construction just inside the Doppler blue shift $b=e^\rho$.

3. Hamilton-Jacobi quantization

Integration of invariant phase differential (78) and (79) requires certain forms.

$$dS \equiv Ldt \equiv \hbar d\Phi = pdx - Hdt = \hbar kdx - \hbar\omega dt \quad (83)$$

Each coefficient of differential term dq in dS should be partial derivative $\frac{\partial S}{\partial q}$.

$$\frac{\partial S}{\partial x} = p, \quad \frac{\partial S}{\partial t} = -H. \quad (84)$$

These are known as *Hamilton-Jacobi equations* for the phase action function S . Classical HJ-action theory was intended to analyze families of trajectories (PW or particle paths). Dirac and Feynman showed its relevance to matter-wave mechanics (CW phase paths) by proposing approximate semi-classical wavefunction based on Lagrangian action as phase.

$$\Psi \approx e^{i\Phi} = e^{iS/\hbar} = e^{i\int L dt/\hbar} \quad (85)$$

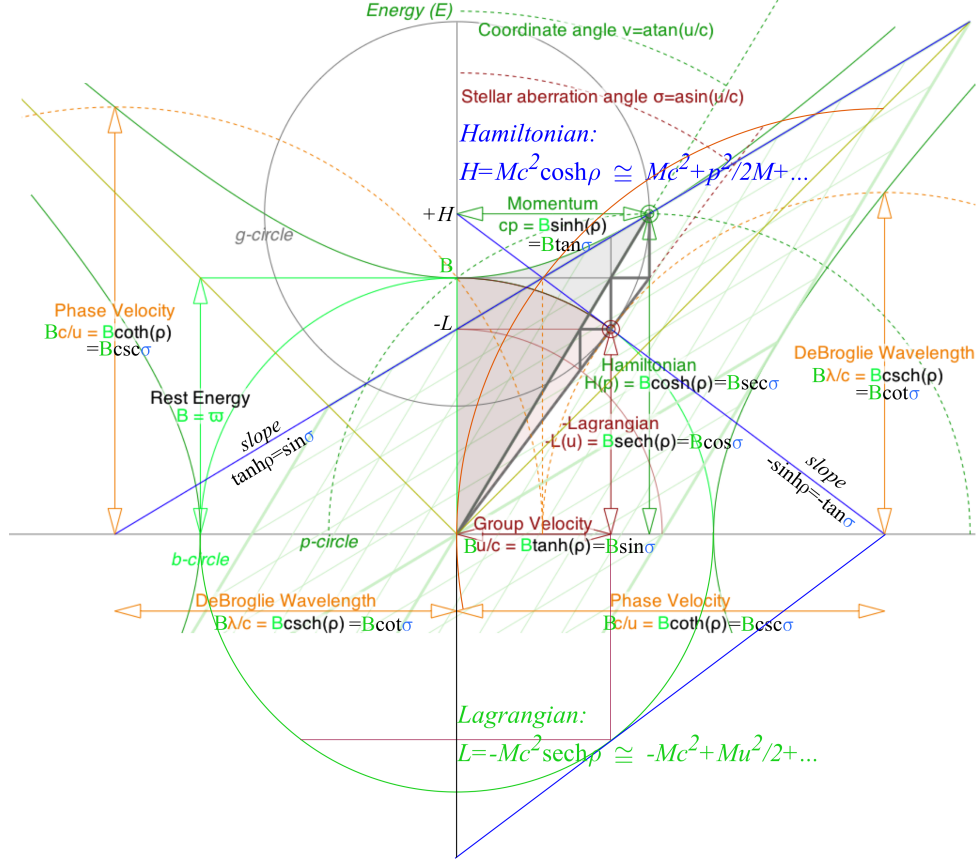


FIG. 27. Geometric elements of positive-energy relativistic quantum mechanics

Approximation symbol (\approx) indicates that phase but not amplitude is able to vary here. HJ form $\frac{\partial S}{\partial x} = p$ turns x -derivative of Ψ into standard quantum \mathbf{p} -operator form $\mathbf{p} = \frac{\hbar}{i} \frac{\partial}{\partial x}$.

$$\frac{\partial}{\partial x} \Psi \approx \frac{i}{\hbar} \frac{\partial S}{\partial x} e^{iS/\hbar} = \frac{i}{\hbar} p \Psi \quad \Rightarrow \quad \frac{\hbar}{i} \frac{\partial}{\partial x} \Psi = \mathbf{p} \Psi \quad (86)$$

The HJ form $\frac{\partial S}{\partial t} = -H$ turns t -derivative of Ψ similarly into Hamiltonian operator $\mathbf{H} = i\hbar \frac{\partial}{\partial t}$.

$$\frac{\partial}{\partial t} \Psi \approx \frac{i}{\hbar} \frac{\partial S}{\partial t} e^{iS/\hbar} = -\frac{i}{\hbar} H \Psi \quad \Rightarrow \quad i\hbar \frac{\partial}{\partial t} \Psi = \mathbf{H} \Psi \quad (87)$$

Action integral $S = \int L dt$ is to be minimized. Feynman's interpretation of this is depicted in Fig. 28. Any mass M appears to fly so that its phase proper time τ is maximized. The proper mass-energy frequency $\varpi = Mc^2/\hbar$ is constant for a mass M . Minimizing $-\varpi\tau$ is thus the same as maximizing $+\tau$. Clocks near light cone tick slowly compared ones near $\max\tau$.

One may explain how the flying mass finds and follows its $\max\tau$ path by imagining it is first a wave that could spread Huygen's wavelets out over all paths. But, an interference

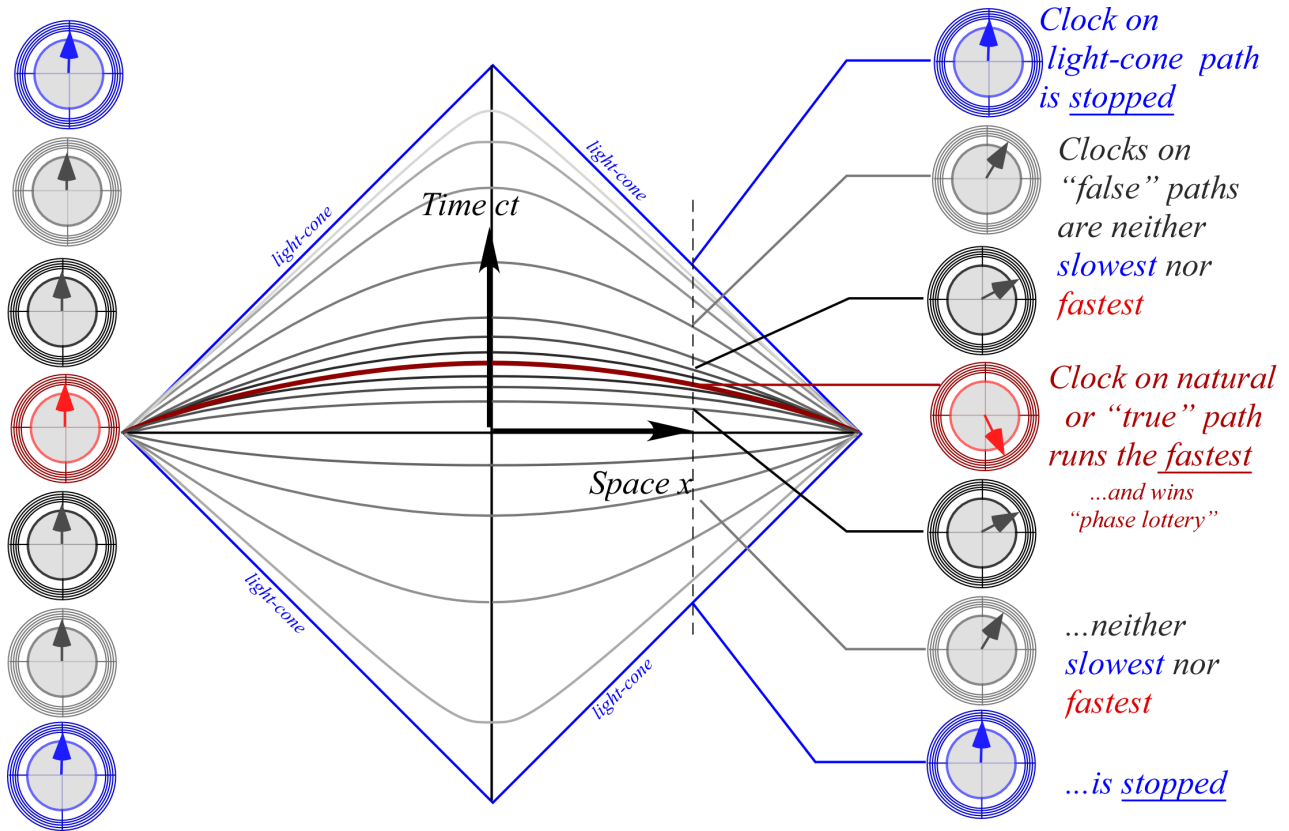


FIG. 28. Feynman’s flying clock contest winner has the greatest advance of time.

of Huygen wavelets favors stationary and extreme phase. This quickly builds constructive interference in the stationary phase regions where the the fastest possible clock path lies. Nearby paths contain a continuum of non-extreme or non-stationary wavelet phase that interfere *destructively* to crush wave amplitude off the beaten $\max\text{-}\tau$ path as sketched in Fig.29. The best are so-called stationary-phase rays that are extremes in phase and thereby satisfy Hamilton’s Least-Action Principle requiring that $S=\int Ldt$ is minimum for true classical trajectories. This in turn enforces Poincare invariance by eliminating, by de-phasing, any false or non-classical paths because they do not have an invariant (and thereby stationary) phase. So “bad” rays cancel each other in a cacophonous mish-mash of mismatched phases.

Each Huygen wavelet in Fig.29 is tangent to the next wavefront being produced. That contact point is precisely on a ray or true classical trajectory path of minimum action and on the resulting best wavefront. Time evolution from any wavefront to another is thus a contact transformation between two wavefronts described by geometry of Huygens Principle.

Thus a Newtonian clockwork-world appears to be the perennial cosmic gambling-house

winner in a kind of wave dynamical lottery on an underlying wave fabric. Einstein’s God may not play dice, but some persistently wavelike entities seem to be gaming at enormous $\frac{Mc^2}{\hbar}$ -rates down in the cellar! And in so doing, geometric order is created out of chaos.

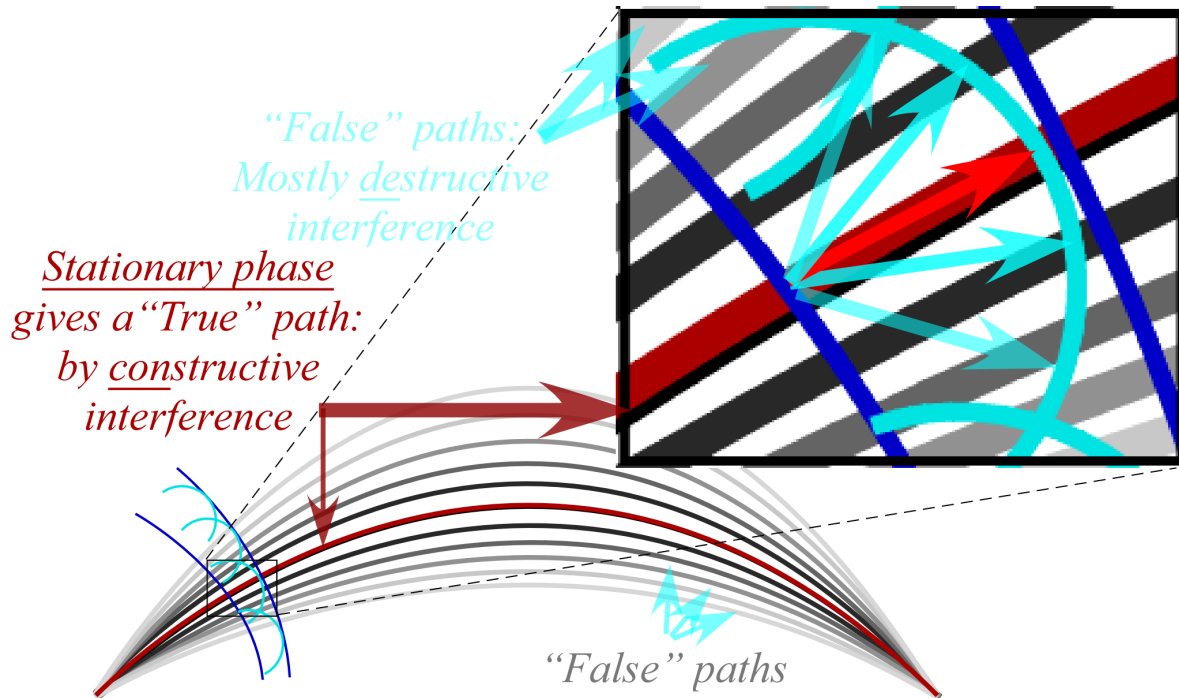


FIG. 29. Quantum waves interfere constructively on “True ” path but mostly cancel elsewhere.

It is ironic that Evenson and other metrologists have made the greatest advances of precision in human history, not with metal bars or ironclad classical mechanics, but by using the most ethereal and dicey stuff in the universe, light waves. This motivates a view of classical matter or particle mechanics that is more simply and elegantly done by its relation to light and its built-in relativity, resonance, and quantization that occurs when waves are subject to boundary conditions or otherwise confined. While Newton was complaining about fits of light, perhaps this crazy stuff was just trying to tell him something!

Derivation of quantum phenomena using a classical particle paradigm seems as silly now as deriving Newtonian results from an Aristotelian paradigm. It now seems much more likely that particles are made by waves, optical or otherwise, rather than vice versa as Newton believed. Also, CW trumps PW as CW symmetry axioms of Evenson (*All colors go c.*) and Doppler time-reversal ($r=\frac{1}{b}$) derive classical Lorentz-Einstein-Minkowski transformation algebra and geometry (14) through (25) summarized in Table II and give exact relations (49)

for relativity and quantum theory together. Such Occam economy is found lacking on any currently existing PW path from Newton to Einstein and Planck. Thus do basic CW half-sum-and-difference phase relations seem to underlie the physics of Poincare contact geometry and be based quite solidly upon ancient circular and hyperbolic geometry.

VI. GEOMETRY OF RELATIVISTIC QUANTUM TRANSITIONS

Preceding theory uses combinations of states $|N, \mathbf{k}_n, \omega\rangle$ or wavefunctions $\Psi_{N,\mathbf{k},\omega} = A_N e^{i(\mathbf{k}\cdot\mathbf{r} - \omega t)}$ of an ideal optical cavity that are quantized by quantum mode numbers n for phase and photon numbers N for amplitude. This leads to geometry of elementary quantum transitions that involve change or transition of one such state into another. Such a discussion begins with symmetry and related conservation rules that restrict such transitions.

A. Symmetry and conservation principles

In Newtonian mechanics the first law or axiom is one of momentum conservation. Such physical axioms, by definition, have only experimental proof or justification. Logical proof or disproof is possible only if an older theory like classical mechanics becomes undermined by a more general theory like relativity or quantum mechanics having finer axioms. Then an older axiom might be proved using newer and more basic axioms, or else it might be disproved or reduced to an approximate or conditional result.

Good teachers respect critically thinking students having doubt about the classical momentum conservation law. Indeed, How *does* Nature avoid losing even the tiniest bit of a momentum current however large it may be? This seems miraculous as does conservation of energy, though the latter is a provable result of the former given time reversal symmetry.

So it provides pedagogical relief to unite momentum and energy conservation rules using quantum wave nature of light that appears to be shared by all matter. Undermining Newton axiom-1 (momentum conservation) by Occam-shaved CW axioms gives Einsein-Planck-DeBroglie scaling results (49) matching momentum \mathbf{p} to wavenumber vector $\vec{\kappa}$ scaled in h or Nh units while doing the same to energy E and frequency ν . A rough statement of how CW axioms undermine or prove \mathbf{p} -or- E conservation axioms is that their conservation is required by wave coherence and so $\mathbf{p} = h\vec{\kappa}$ and $E = h\nu$ must be conserved, too. However, this

oversimplifies deeper concepts of symmetry logic, a kind of “grown-up” geometry.

A strength (and also, weakness) of CW axioms is that they are symmetry principles due to the Lorentz-Poincare isotropy of space-time that invokes invariance to translation $\mathbf{T}(\vec{\delta}, \tau)$ in the vacuum. Operator \mathbf{T} has plane wave eigenfunctions $\psi_{k,\omega}=Ae^{i(kx-\omega t)}$ and eigenstates $|\psi_{k,\omega}\rangle$ with roots-of-unity eigenvalues $e^{i(k\cdot\delta-\omega\cdot\tau)}$ as described by bra-ket relations below.

$$\mathbf{T}(\delta, \tau) |\psi_{k,\omega}\rangle = e^{i(k\cdot\delta-\omega\cdot\tau)} |\psi_{k,\omega}\rangle \quad (a) \qquad \langle\psi_{k,\omega}| \mathbf{T}^\dagger = \langle\psi_{k,\omega}| e^{-i(k\cdot\delta-\omega\cdot\tau)} \quad (b) \quad (88)$$

The relations apply also to N -part or N -particle states $\Psi_{K,\Omega} = \psi_{k_1,\omega_1} \psi_{k_2,\omega_2} \cdots \psi_{k_N,\omega_N}$ where exponents add (k_j, ω_j) -values of each constituent to a total \mathbf{K} -vector $K=k_1+k_2+\dots+k_N$ and total frequency $\Omega=\omega_1+\omega_2+\dots+\omega_N$ to give $\mathbf{T}(\vec{\delta}, \tau)$ -eigenvalue exponential form $e^{i(K\cdot\delta-\Omega\cdot\tau)}$.

Now \mathbf{T} -symmetry requires that quantum time evolution operator \mathbf{U} is unaffected by being moved by \mathbf{T} , that is $\mathbf{U}=\mathbf{T}\mathbf{U}\mathbf{T}^\dagger$ or that \mathbf{U} commutes with all \mathbf{T} , that is $\mathbf{U}\mathbf{T}=\mathbf{T}\mathbf{U}$ for all \mathbf{T} . So any transition matrix $\langle\Psi_{K',\Omega'}|\mathbf{U}|\Psi_{K,\Omega}\rangle$ can be replaced by $\langle\Psi_{K',\Omega'}|\mathbf{T}\mathbf{U}\mathbf{T}^\dagger|\Psi_{K,\Omega}\rangle$. Then eigenvalue relations (88) yield (K,Ω) conservation rules: $K'=K$ and $\Omega'=\Omega$.

$$\begin{aligned} \langle\Psi'_{K',\Omega'}|\mathbf{U}|\Psi_{K,\Omega}\rangle &= \langle\Psi'_{K',\Omega'}|\mathbf{T}^\dagger(\delta, \tau)\mathbf{U}\mathbf{T}(\delta, \tau)|\Psi_{K,\Omega}\rangle \quad (\text{if } \mathbf{U}\mathbf{T} = \mathbf{T}\mathbf{U} \text{ for all } \delta \text{ and } \tau) \\ &= e^{-i(K'\cdot\delta-\Omega'\cdot\tau)} e^{i(K\cdot\delta-\Omega\cdot\tau)} \langle\Psi'_{K',\Omega'}|\mathbf{U}|\Psi_{K,\Omega}\rangle = 0 \text{ unless: } K' = K \text{ and: } \Omega' = \Omega \end{aligned} \quad (89)$$

\mathbf{T} -symmetry requires that both total energy $E=\hbar\Omega$ and total momentum $\mathbf{P}=\hbar\mathbf{K}$ be conserved for ideal CW states.

However, laboratory CW have momentum uncertainty $\Delta k=1/\Delta x$ due to finite beam size Δx and energy uncertainty $\Delta E=\hbar\Delta\omega=\hbar/\Delta\tau$ due to finite lifetime $\Delta\tau$. Newton’s 1st law is verified but becomes precise only to the extent that lifetime or beam-width is large enough to accommodate great numbers of wavelengths or wave periods.

1. Single-photon transitions and Feynman diagram geometry

The geometric analysis of photon-affiliated transitions begins with the simple Doppler shifted or Lorentz transformed “baseball-diamond” geometry shown in Fig.30. Most figures showing this geometry so far, including Fig.15, Fig.10 and the original Fig.6, are drawn for velocity $\frac{u}{c}=\frac{3}{5}$ or Doppler shift $b=2$. Here, Fig.30 uses odd values $b=\frac{3}{2}$ or $\frac{u}{c}=\frac{5}{13}$ to avoid distracting crossings found in Fig.21. The Planck-Einstein-DeBroglie relation (49) is labeled by *energy* $E=\hbar\omega$ versus *comentum* $cp=\hbar ck$ so that both have the same dimensions of energy.

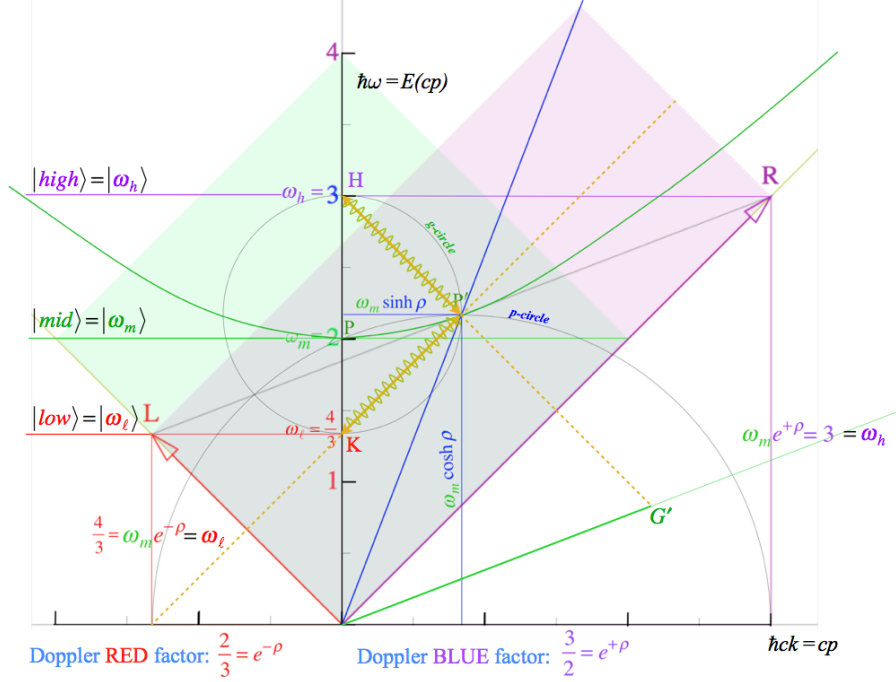


FIG. 30. Energy-comentum diagram for 1-photon transition H-to-P' having recoil $\frac{u}{c} = \frac{5}{13}$.

(Tiny photon momentum $p = \hbar k$ needs the c -factor to show up in plots.) Also, Fig.30 is bisected by a wavy right-angle $HP'K$ inscribed in the g -circle that represents photon (ω, ck) -vectors connecting levels of high-state $|\omega_h\rangle$ of rest frequency $\omega_h = 3$, middle-state $|\omega_m\rangle$ of rest frequency $\omega_m = 2$, and low-state $|\omega_l\rangle$ of rest frequency $\omega_l = \frac{4}{3}$.

Each frequency relates to one above it (or below it) by blue-shift factor $e^\rho = \frac{3}{2}$ (or red-shift factor $e^{-\rho} = \frac{2}{3}$) so middle frequency ω_m is the geometric mean $\omega_m = \sqrt{\omega_h \omega_l}$ of the other two.

$$3 = \omega_h = e^{+\rho} \omega_m \quad 2 = \omega_m = e^{+\rho} \omega_l \quad \frac{4}{3} = \omega_l = e^{-\rho} \omega_m = e^{-2\rho} \omega_h \quad (90)$$

Wavy segment HP' represents a photon of energy $\hbar\Omega_{HP'} = \hbar\omega_m \sinh \rho$ that would be emitted in a transition from a stationary mass $M_H = \hbar\omega_h/c^2$ at point H to a moving mass $M_P = \hbar\omega_m/c^2$ with rapidity ρ at point P'. Implicit in Fig.30 is the choice of right-to-left direction for the outgoing photon comentum $cp = -\hbar\omega_m \sinh \rho$ so that mass M_H recoils left-to-right by just enough to conserve comentum as (89) requires. Mass M_H loses energy (frequency) equal to comentum (wavevector) of outgoing photon. Since M_H is initially stationary, it must lose energy by reducing rest-mass from M_H to M_P by Doppler shift ratio $\frac{\omega_h}{\omega_m} = e^\rho$.

$$\frac{M_H}{M_P} = \frac{\omega_h}{\omega_m} = e^\rho \quad (91)$$

A rest mass formula results for recoil rapidity ρ with a simple low- $\rho \cong \frac{u}{c}$ approximation.

$$\rho = \ln \frac{M_H}{M_P} \xrightarrow{\rho \rightarrow \frac{u}{c}} u = c \ln \frac{M_H}{M_P} \quad (92)$$

Interestingly, this quantum recoil formula is reminiscent of a famous rocket formula.

$$V_{burnout} = c_{exhaust} \ln \frac{M_{initial}}{M_{final}} \quad (93)$$

One might recall a popular expression, “This isn’t rocket science!” Usual notions are that quantum transitions are infinite discrete “jumps” or that emitted (or absorbed) photons act like bullets. These appear wrong-headed in light of a more complete relativistic picture of an atom or nucleus in (92) gradually exhaling its mass with an optical exhaust velocity of c .

One may recall classical Lorentz resonance models of atomic transitions. (It is Lorentz of ELT but these are non-relativistic models.) They show atoms undergo over 10^5 “heartbeats” during their ring-down decay lifetime of roughly 10^{-8} seconds, hardly instant-death jumps. Here this beat frequency is not the enormous mass-energy phase velocity $\omega_h = \frac{M_H c^2}{\hbar}$ mentioned previously, but rather difference beats $\Delta_{hm} = \omega_h - \omega_m - \delta$ where δ is a tiny recoil downshift due to atom borrowing recoil kinetic energy. (Lorentz did not consider a δ .) The exact δ in Fig.30 is the height of point P’ above ω_m -baseline, and $\hbar\delta$ is KE acquired by mid-mass M_P .

$$\delta = \omega_m \cosh \rho - \omega_m \simeq \frac{\omega_m}{2} \rho^2 \quad \Rightarrow \quad KE_{recoil} \simeq \frac{\hbar\omega_m}{2} \rho^2 \simeq \frac{M_P}{2} u^2 \quad (94)$$

Recoil momentum p of the deflated M_P is exactly $p = M_P c \sinh \rho$ with $\hbar\omega_m = M_P c^2$.

The H-to-P’ transition just discussed could be followed by a P’-to-K transition with forward emission of a photon with the same energy and further reduction of mass from M_P to a stationary mass M_K . Lowest energy level $\hbar\omega_\ell = M_K c^2$ in Fig.31 has frequency $\omega_\ell = \frac{4}{3}$ and zero momentum due to its leftward recoil from rightward emitted photon. Feynman diagrams in right-hand inset panels are scale models of photon energy-momentum \mathbf{k}_{ab} -vectors emitted from head of initial mass- M_A \mathbf{K}_A -vector on the tail point of recoiling mass- M_B \mathbf{K}_B -vector. One may imagine these per-space-time (ω, k) diagrams as actual space-time (x, ct) mass and photon tracks because of the Fourier reciprocity demonstrated in Fig.7 and Fig.8. One may rearrange \mathbf{K} -vectors into head-to-tail zero-sum triangles representing energy-momentum conservation demanded by (89) and “relativity” geometry of optical wave interference.

Level sequence $\{\dots\omega_\ell, \omega_m, \omega_h, \dots\}$ in (90) is part of an infinite geometric series having blue-shift ratio $b = e^\rho = \frac{3}{2}$ or red-shift ratio $r = e^{-\rho} = \frac{2}{3}$ ranging from 0 to ∞ . The energy

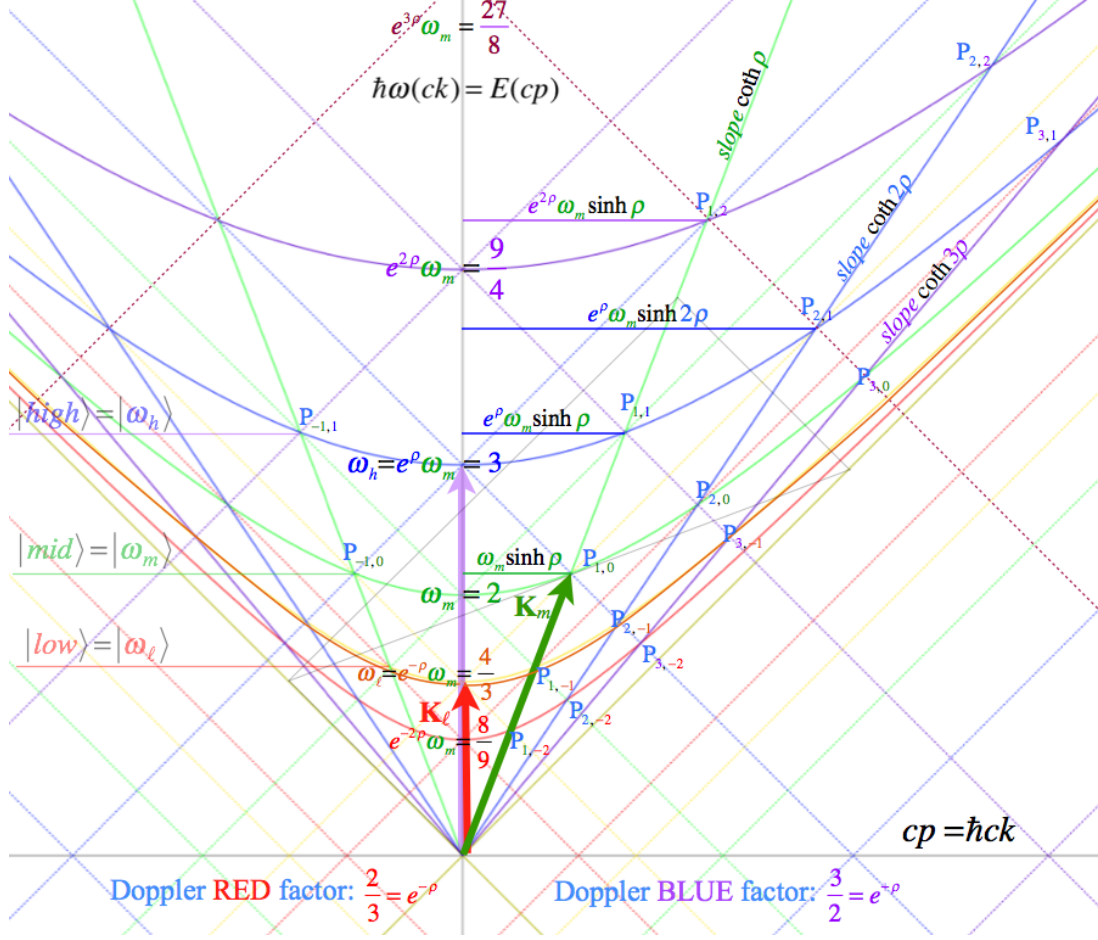


FIG. 32. Rapidity- $\rho_p = p\rho$ and rest-frequency- $\omega_m e^{q\rho}$ $P_{p,q}$ -lattice based on integer powers of $b = e^\rho = \frac{3}{2}$

may be viewed at $\pm 45^\circ$ as a Cartesian grid of lines. Each line is positioned according to rest-frequency power $\omega_m e^{q\rho}$ at its meeting point on the vertical ω -axis (or 2nd-base of a Doppler baseball diamond) as shown in Fig. 33. The $+45^\circ$ - R -axis (1st-baseline) is marked-off by sequence $\omega_R = \omega_m e^{R\rho}$ ($R = -2, -1, 0, 1, 2, \dots$) and the -45° - L -axis (3rd-baseline) is marked-off by sequence $\omega_L = \omega_m e^{L\rho}$ ($L = -2, -1, 0, 1, 2, \dots$). (Here base constants $e^\rho = \frac{3}{2}$ and $\omega_m = 1$ are fixed.) At the intersections of R and L grid-lines are discrete transition (p, q) -points $P_{p,q}$.

$$P_{p,q} = (ck_{p,q}, \omega_{p,q}) = \omega_m e^{q\rho} (\sinh p\rho, \cosh p\rho) \quad (95)$$

Each coordinate point is related by half-sum and difference coordinate transformations.

$$p = \frac{R - L}{2}, \quad q = \frac{R + L}{2} \quad \Leftrightarrow \quad R = p + q, \quad L = q - p \quad (96)$$

These are integer versions of the phase and group relations (14) and (15) to right and left laser \mathbf{K} -vectors, yet another result of factoring optical wave coordinate functions. The geometric

structure represented here might become a useful basis for a kind of lattice-gauge theory to explore cavity quantum electro-dynamics (CQED) or pseudo-relativistic theories of graphene gauge dynamics. Such a structure offers a possible solution to the flaw that made Feynman path integration so difficult due its uncountable universe of possible paths. The structure in Fig.33 offers a labeling of every discrete path by an operation in a discrete subgroup of the continuous Poincare-Lorentz group (PLG) that has a discrete Poincare-Lorentz algebra (PLA). The discrete paths are easily made as fine as desired so that each PLA becomes a larger and better approximation to the parent PLG. Each PLA has a discrete spectral decomposition that derives a range of Hamiltonians with their eigensolutions and transition amplitudes parametrized by discrete paths.

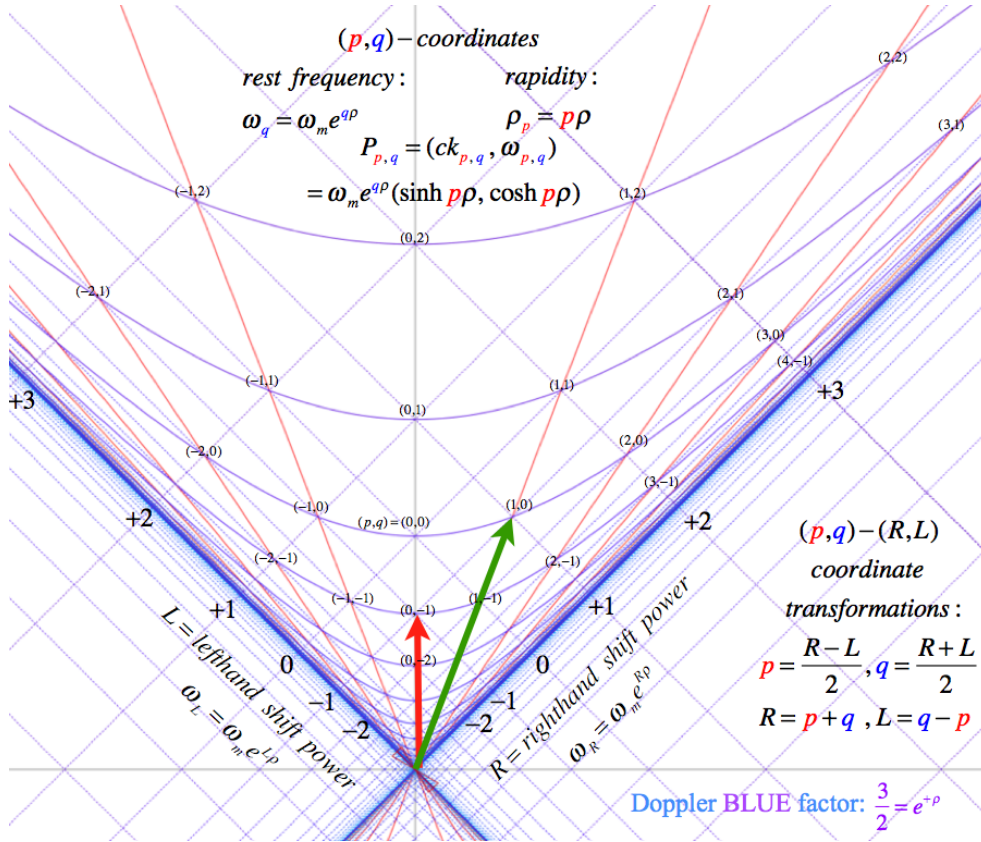


FIG. 33. Hyperbolic lattice of (p,q) -transition points for base $b=e^\rho=\frac{3}{2}$ and coordinate relations.

B. Accelerated frames and optical Einstein-elevator

Fig.5c and Fig.6c show Lorentz-Minkowski space-time frames made by a 2-CW pair of lasers. Fig.5c shows a Cartesian (x,ct) -grid made as Alice's and Carla's lasers collide 600THz beams. Fig.6c shows Bob's view of Alice coming in at $u=\frac{3}{5}c$ with her laser beam Doppler blue-shifted by $(B|A)=2=e^{+\rho}$ to 1200THz and Carla going away at $u=\frac{3}{5}c$ with her beam Doppler red-shifted by $(B|C)=\frac{1}{2}=e^{-\rho}$ to 300THz. If Bob attenuates Alice's beam \mathbf{E} -field amplitude by $\frac{1}{2}$ so its amplitude matches Carla's then he may see the Alice-Carla (x,ct) -grid in Fig.5c form the Minkowski (x',ct') -grid shown in Fig.6c. Alice and Carla can provide Bob with the same $\rho=\ln 2=0.69$ grid without expending the energy needed to move their lasers to enormous speeds of $u=\frac{3}{5}c$ relative to him. Instead they may be at rest in his frame and gradually tune up or up-chirp Alice's laser from $\nu_A=600\text{THz}$ to $e^{+\rho}\nu_A=1200\text{THz}$ while Carla is down-chirping from ν_A to $\nu_A e^{-\rho}=300\text{THz}$. This opens the possibility of projecting accelerating frames for optical "Einstein elevators" with curving space-time coordinates that span a finite region between the lasers for a finite time interval. Imagine Bob has a space ship that accelerates to a velocity $u=c \tanh \rho$ that Doppler shifts the Alice and Carla beams back to their initial green frequency $\nu_A=600\text{THz}$. (Or else, an excited atom b could be imagined to be trapped in a single group-wave anti-node space-time cell so b accelerates with that cell while staying in resonance with the cell's constant phase frequency ν_A .) The instantaneous velocity u of Bob (or the atom b) relative to Alice and Carla depends on their chirp factors $e^{\pm\rho}$ that vary with rapidity ρ . Bob can find his ρ relative to Alice if she broadcasts a fixed frequency ν_a that he sees at $\nu_b=\nu_a e^{-\rho}$. This rapidity is a function $\rho=\rho(\tau)$ of proper time τ for Bob (or atom) and τ is related by (72) to time t for Alice or Carla.

$$u = \frac{dx}{dt} = c \tanh \rho \quad \text{where:} \quad \frac{dt}{d\tau} = \cosh \rho \quad \text{and:} \quad \frac{dx}{d\tau} = \frac{dx}{dt} \frac{dt}{d\tau} = c \tanh \rho \cosh \rho = c \sinh \rho \quad (97)$$

Integrating the (97) relations gives Bob's time-space path (ct,x) as seen by Alice or Carla.

$$ct = c \int \cosh \rho(\tau) d\tau \quad \text{and:} \quad x = c \int \sinh \rho(\tau) d\tau \quad (98)$$

The simple case with constant rapidity $\rho=\text{const.}$ gives a Minkowski τ -axis of slope $\frac{x}{ct} = \frac{\sinh \rho}{\cosh \rho}$.

$$ct = c\tau(\cosh \rho) \quad \text{and:} \quad x = c\tau(\sinh \rho) \quad (99)$$

This case is sketched in Fig.34a as a tiny CW Minkowski frame at the intersection of paths of PW light waves from Alice and Carla. This repeats the situation described for Fig. 6.

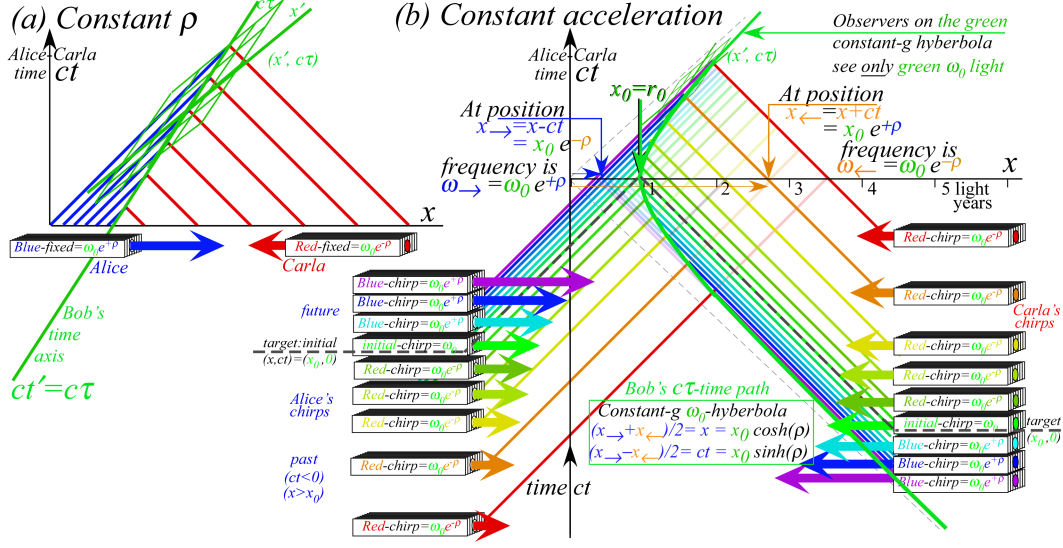


FIG. 34. Space-time laser-formed paths of constant g -acceleration (a) $g=0$, (b) $g=9.8 \frac{m}{s^2}$

Fig. 34b has a path of acceleration $g=9.8 \frac{m}{s^2}$. Rapidity is linear in Bob's proper time ($c\rho=g\tau$).

$$ct = c \int \cosh \rho d\tau = \frac{c^2}{g} \sinh \left(\frac{g\tau}{c} \right) \quad (\text{for: } u \sim \rho c = g\tau) \quad x = c \int \sinh \rho d\tau = \frac{c^2}{g} \cosh \left(\frac{g\tau}{c} \right) \quad (100)$$

Recall that low rapidity ($\rho \ll 1$) is approximated by $\frac{u}{c}$, and so setting $c\rho$ equal to $g\tau$ is approximated by the classical uniform acceleration equation ($u=g\tau$). The resulting space-time path shown in Fig. 34b is a hyperbola of radius $a = \frac{c^2}{g}$ that is enormous unless “gravity” g is also enormous. For terrestrial $1g$ acceleration ($g=9.8 \frac{m}{s^2}$) the radius is $a=0.97 \text{ Light Year}$. Even this small $1g$ acceleration can, over several years, rack up considerable light-year mileage. After the first year ($\tau_1=3.15 \cdot 10^7 \text{ sec.}$) the rapidity is $\rho_1 = \frac{g\tau_1}{c} = 1.03$ giving an x -coordinate of $x = a \cosh \frac{g\tau_1}{c} = 1.53 \text{ Light Yr}$ with a total mileage of $x-a = 0.56 \text{ Light Yr}$. But, after 21 years (the age of legality) it balloons to $x = a \cosh \frac{21g\tau_1}{c} = 1.22 \cdot 10^9 \text{ Light Yr}$! Now hyperbolic radius a is an insignificant part of a billion light-year journey. After 25 years (about the age of Einstein when he developed relativity theory) the mileage is 76 billion light-years, well beyond age-of-universe estimates in the frame of Alice (who has long since passed away). The geometric and exponential behavior of relativistic Doppler components dominates this example of space-time inflation and takes the Alice-Bob saga beyond the realm of possibility. Still it is instructive to explore such surprising thought experiments as far as possible and note the asymptotic extremes of scaling and curvature. Rapidity ρ is defined in Fig. 13b as twice the area subtended by a unit hyperbola, its radius vector, and the horizontal axis. The

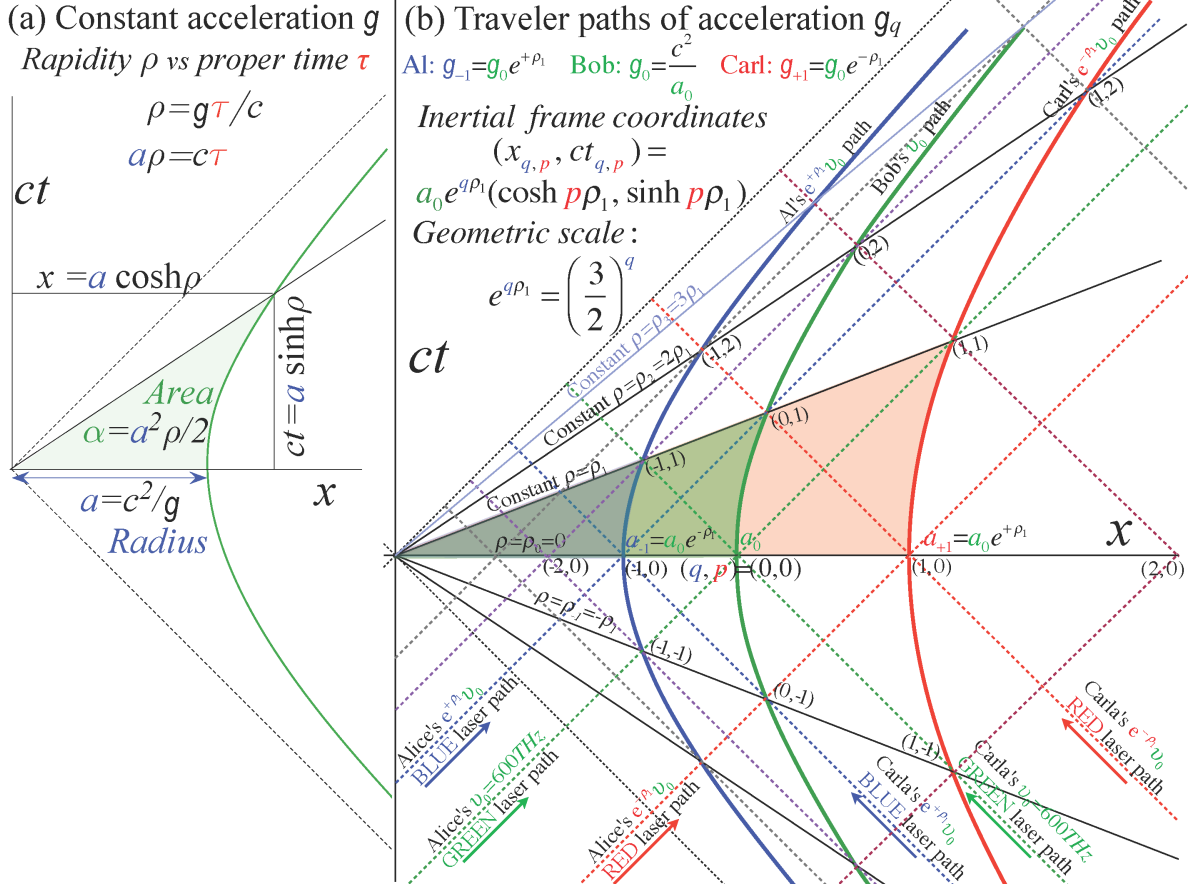


FIG. 35. Constant- $g_q = \frac{c^2}{a_q}$ paths ($q_{Al}=-1$, $q_{Bob}=0$, $q_{Carl}=1$) vary $\rho_p = p\rho_1 = p \ln \frac{3}{2}$ from $p=-1$ to 3.

independent rapidity variable $\rho = \frac{g\tau}{c}$ in (100) is proportional to the space-time area α swept in time τ by hyperbolic path radius as it grows from initial radius $r_0 = a = \frac{c^2}{g}$ shown in Fig. 35a.

$$\alpha(\text{Area}) = \frac{x \cdot ct}{2} - \int_0^{x_1} ct \cdot dx = \frac{x \cdot ct}{2} - \int_0^{\rho_1} ct \cdot \frac{dx}{d\rho} d\rho \quad (101)$$

Substituting $x = a \cosh \rho$ and $ct = a \sinh \rho$ from (100) gives swept area $\alpha(\rho_1)$.

$$\alpha(\rho_1) = a^2 \frac{\cosh \rho_1 \cdot \sinh \rho_1}{2} - \int_0^{\rho_1} (a \sinh \rho)^2 d\rho = \frac{a^2}{2} \rho_1 = \frac{a^2}{2} \frac{g\tau_1}{c} \quad (102)$$

Hyperbolic radius $a = \frac{c^2}{g}$ then gives proper time $c\tau_1$ as a radius-rapidity product $a\rho_1$.

$$a\rho_1 = c\tau_1 \quad (103)$$

Details of Fig. 34b optical geometry are revealed in Fig. 35b using three pairs of colliding Alice-versus-Carla laser beams. The central GREEN (lab frequency $\nu_0 = 600\text{THz}$) beam-pair meet at $t_0 = 0$ on the x -axis at $x_0 = a_0$ where Bob is instantaneously stationary but

accelerating to the right with $g_0 = \frac{c^2}{a_0}$. The righthand RED (lab frequency $\nu_1 = \nu_0 e^{-\rho_1}$) beam-pair meet at $t_0=0$ on the x -axis at $a_1 = a_0 e^{\rho_1}$ where Bob's companion Carl is also stationary but accelerating right with $g_1 = \frac{c^2}{a_1}$. The lefthand BLUE (lab frequency $\nu_{-1} = \nu_0 e^{+\rho_1}$) beam-pair meet at $t_0=0$ on the x -axis at $a_{-1} = a_0 e^{-\rho_1}$ where Bob's companion Al is also stationary but accelerating right with $g_{-1} = c^2/a_{-1}$. Bob and his companions share a line of rising slope $\frac{x}{ct} = \coth \rho$ as they travel up their respective hyperbolic paths in Fig. 35b as given by (100). All points on such a line share the same rapidity ρ and the same tangent slope $\frac{dx}{dct} = \tanh \rho$ or lab velocity $\frac{u}{c}$, and so Al, Bob, and Carl on the ρ_1 -line in Fig. 35b apply the same Doppler blue-shift factor $b_1 = e^{+\rho_1}$ to light they meet head-on and the same red-shift factor $r_1 = e^{-\rho_1}$ to light that catches them from behind. Thus Bob down-shifts Carla's blue beam from its lab BLUE frequency $\nu_{BLUE} = \nu_0 e^{\rho_1}$ to his observed GREEN $\nu_0 = 600\text{THz}$ and up-shifts Carla's red beam from its lab RED frequency $\nu_{RED} = \nu_0 e^{-\rho_1}$ to the same base frequency $\nu_0 = 600\text{THz}$. This is consistent with Alice and Carla's original plan for Bob on an optically accelerated "Einstein elevator" but now it includes two companions Al and Carl that travel in spatial lock-step beside Bob in Fig. 35b with Al maintaining a fixed distance $\Delta a_0 = a_0 - a_{-1}$ below Bob as Carl maintains a larger fixed distance $\Delta a_1 = a_1 - a_0 = e^{\rho_1} \Delta a_0$ above Bob (As plotted in their frames of equal rapidity ρ_1 .) Meanwhile, the lab x -view in Fig. 35b clearly shows their relative spatial separations suffering Lorentz contraction. Each hyperbolic path is invariant so a boost in rapidity by $\Delta \rho$ moves any of its points of rapidity ρ_p to $\rho_p + \Delta \rho$ on the same hyperbola. While Al, Bob, and Carl maintain initial spatial separations tallied by Alice and Carla at zero rapidity or velocity ($\rho_0 = 0 = \frac{u_0}{c}$), they do not maintain equal proper time- τ readings. According to (103) proper time $c\tau_{p,q}$ on hyperbola- q is a product of its radius $a_q = e^{q\rho_1} a_0$ with rapidity $\rho_p = p\rho_1$ for a given p -line shared by travelers $q = -1, 0$, and $+1$.

$$c\tau_{q,p} = a_q \rho_p = a_0 e^{q\rho_1} p\rho_1 \quad \text{where: } q = -1(\text{Al}), 0(\text{Bob}), \text{ and } 1(\text{Carl}). \quad (104)$$

Hyperbolas of smaller radius a_q have proportionally slower local or proper time evolution and proportionally greater acceleration $g_q = \frac{c^2}{a_q}$ hence more curvature of hyperbolas closer to origin in Fig. 35. Indeed, each (q, p) -cell has the same number of wavelengths and wave-periods packed into a tighter space-time as the radius a_q is reduced. The hyperbolic acceleration geometry of space-time in Fig. 35b has similar geometry (rotated by 90°) to that of Compton scattering in per-space-time of Fig. 33, but the physics is inverted. A boost of Bob ($q=0$) from ρ_0 to ρ_1 ($p=0 \rightarrow 1$) in Fig. 35b corresponds to a Compton transition of a rest-mass $q=0$

from ρ_0 to ρ_1 in Fig.33. Increased energy $E=h\nu$ and momentum $p=h\kappa$ on reciprocal (E,p) lattice Fig.33 is decreased wave length $\lambda=\frac{1}{\kappa}$ and wave period $\tau=\frac{1}{\nu}$ for space-time (x,ct) in Fig.35. And vice-versa, a low-hyper-radius $a_q=\frac{c^2}{g_q}$ or high acceleration $g_q=\frac{c^2}{a_q}$ in Fig.35 has high energy E (or frequency ν) and momentum p (or wavenumber κ) in Fig.33.

This mythical odyssey of intrepid accelerating voyagers (Al, Bob, and Carl) depends on optical metrology provided by a pair of laser-chirping Sirens (Alice and Carla) stationed at the left and right edges of Fig.34b and Fig.35b. While Carla leisurely de-tunes her right-to-left beam, Alice tries to meet an impossible up-tuning schedule of her left-to-right beam, planned to end with an exponential chirp and explosion of infinite frequency at $ct=0$. Her $ct_0=-a_0$ emission of frequency $\nu_0=600\text{THz}$ hits Bob at $x=a_0$, one of a geometric sequence of frequencies $\frac{\nu_q}{\nu_0}=e^{\rho_1}, e^{2\rho_1}, e^{3\rho_1}, \dots, e^{q\rho_1}$ emitted at times $\frac{ct_q}{a_0}=-e^{-\rho_1}, -e^{-2\rho_1}, -e^{-3\rho_1}, \dots, -e^{-q\rho_1} \rightarrow 0$, to hit a point $x_q=a_0e^{-q\rho_1}$ at $ct=0$. (The geometric ratio in Fig.35b is $e^{\rho_1}=\frac{3}{2}$.) No light emitted by Alice after $t=0$ can reach Al, Bob, Carl or any fellow traveler- q maintaining enough acceleration to stay under hyperbolic asymptote or “event-horizon” $x=ct$ in Fig.35b. Carla, the right-to-left half of this 2-CW metrology, hits the same q -points $x_q=a_0e^{q\rho_1}$ on the $(ct=0)$ -line (x -axis) with the same frequencies $\nu_q=\nu e^{q\rho_1}$ that Alice sent to each traveler- q . She can continue hitting Carl (traveler $q=1$) at (q,p) -points (1,1) and (1,2) with beams that later on hit Bob (traveler $q=0$) at (q,p) -points (0,1), (0,2) and (0,3) and Al (traveler $q=-1$) at (q,p) -points (-1,2), (-1,3) and (-1,4). However, Carl passes Carla soon thereafter (upper right hand corner of Fig.35b) and so also will Bob followed by Al. Thus laser coordination by either Siren, Alice or Carla, has a finite limit in its coverage.

C. Metrology in accelerated frames

Accelerated frame metrology of space, time, and relative velocity is quite counter-intuitive and easily misinterpreted. The space-time grid of CW and PW paths provided by Alice and Carla in Fig.34b (and with greater detail in Fig.35b) help to analyze what Al, Bob, and Carl might be able to observe at each (q,p) -intersection of light beams sent by Alice and Carla. Let us assume each intersection marks colliding pulse waves (PW) that are separated by the same number N of CW wavelengths in space and N wave periods in time. In Fig.36 the CW paths for $N=4$ are drawn as the finer CW grid for the sake of clarity, but it should be

evident that increasing integer scale N sharpens the space-time fine-grid precision. Meanwhile, the course-grid defined by integer coordinates (q, p) mark equally spaced proper time p -instants $c\tau_{q,p}=a_q\rho_p$ along the q -path hyperbola of traveler q according to Eq.(104). Bob ($q=0$), starting from his origin ($p=0$) at rest in Fig.36, accelerates past his proper time points $c\tau_{0p}=a_0\rho_1(0, 1, 2, 3, 4)$ before exiting at the very top of the plot. Bob sees the same proper time interval $c\tau_{01}=a_0\rho_1$ between each of his p -instants wherein he gains the same unit $\rho_1=\ln(\frac{3}{2})=0.405$ of rapidity per interval. (That is velocity $\frac{u}{c}=\tanh(\rho_1)=0.385$.) Meanwhile, distance x traveled in inertial frame (x, ct) of Fig.36 grows only quadratically at first but soon explodes exponentially due to hyperbolic cosine $x=a_0 \cosh \rho$ in Eq.(100). Meanwhile, Bob's companions, Al ($q=-1$) and Carl ($q=1$), also see equal proper time intervals between p -points, but each $c\tau_{q,p}$ is proportional to q^{th} hyperbolic radial constant $a_q=a_0e^{q\rho_1}$. So Al's proper time interval $c\tau_{-1,1}=a_0e^{-\rho_1}=\frac{2}{3}a_0$ is $(\frac{2}{3})$ -times less than Bob's interval while Carl's time interval $c\tau_{1,1}=a_0e^{\rho_1}=\frac{3}{2}a_0$ is $(\frac{3}{2})$ -times greater. Nevertheless, all three travelers gain exactly the same amount of rapidity $\rho_1=\ln(\frac{3}{2})$ during each of their intervals.

Having uniform proper $\Delta\tau_q$ -intervals allows spatial intervals between each pair of accelerating neighbors to be easily measured by radar echo ranging. A dash-line rectangle connecting (q, p) -points $[0,0]$, $[1,1]$, $[0,2]$, and $[-1,1]$ outlines paths of Bob's radar pulses he might send rightward (That is "up" in his perceived "gravity" field.) from $[0,0]$ to reflect from Carl at $[1,1]$ and leftward (that is down-field) to reflect from Al at $[-1,1]$. Both pulses return to Bob simultaneously at $[2,2]$ at precisely $c\tau_{0,2}=2a_0\rho_1$ or two "ticks" of his proper time given in distance units. (Recall that $a_0=0.97lt\text{-}yr$ was derived from Eq.(100) for $g=9.8\frac{m}{s^2}$.) Thus Bob finds a radar-range coordinate $x_{[-1,1]}=-a_0\rho_1=-0.39lt\text{-}yr$ for Al below him and a coordinate $x_{[1,1]}=a_0\rho_1=0.39lt\text{-}yr$ of equal distance for Carl above him. Bob gets the same $\pm a_0\rho_1$ coordinates if he sends out radar pulses one "tick" earlier from the $[0,-1]$ point (below $[0,0]$ and not visible in Fig.36) that return to him two "ticks" later at point $[0,1]$.

If Bob's radar pulses could echo off next-nearest neighbor's paths having radius $a_{\pm 2}=a_0e^{\pm 2\rho_1}$ or $a_{\pm 3}=a_0e^{\pm 3\rho_1}$ they would return four "ticks" later at $[0,4]$ (as shown in Fig.36) or six "ticks" later at $[0,6]$ (not shown in Fig.36). Such echo range values would indicate uniformly spaced neighbors at constant positions $\pm a_0\rho_1$, $\pm 2a_0\rho_1$, and $\pm 3a_0\rho_1$ above and below Bob.

Such uniformity of spacing seems paradoxical in light of a decidedly non-uniform spacing of neighbor- q positions $x_q(0)=a_q=a_0e^{q\rho_1}$ on the x -axis of Alice and Carla's inertial frame at

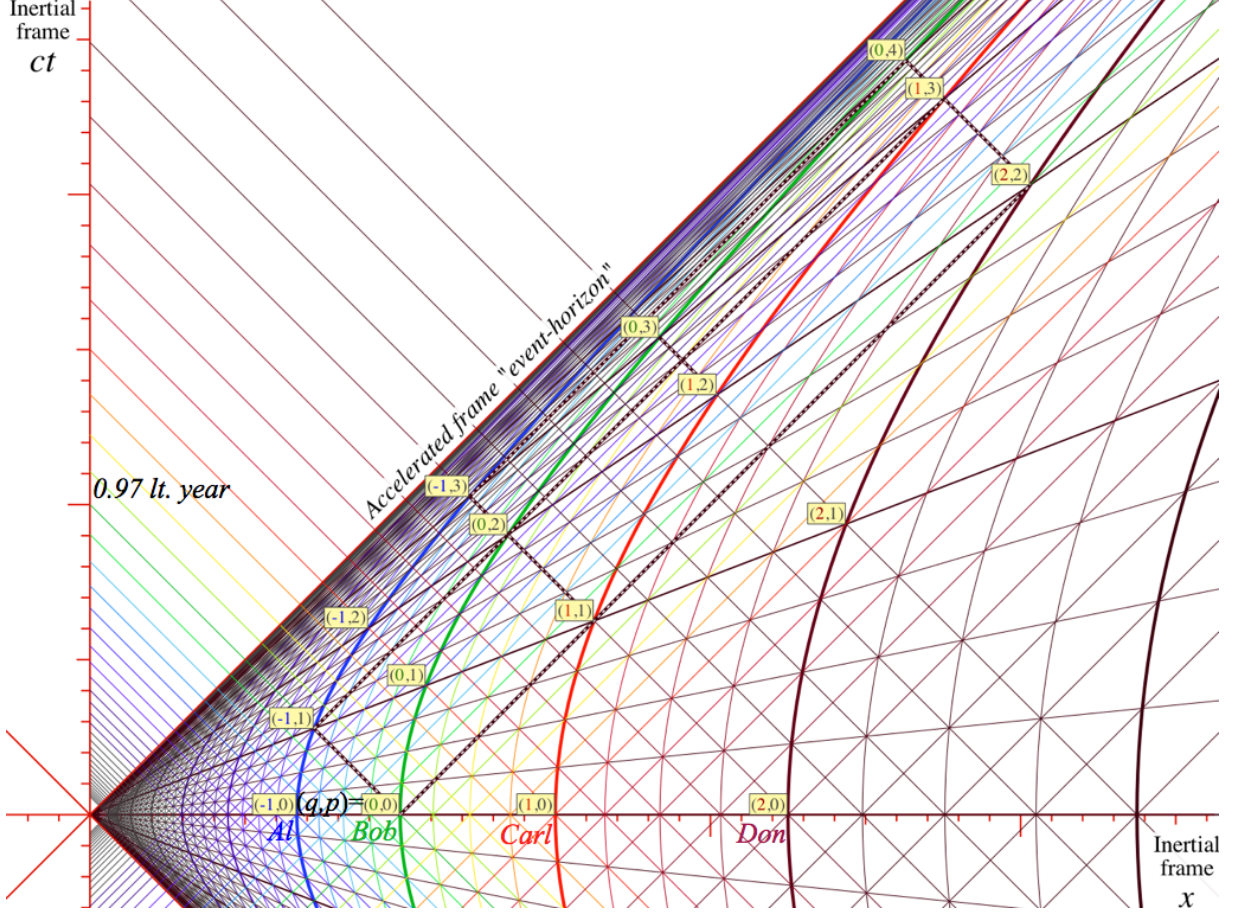


FIG. 36. CW Doppler and PW radar metrology for frame of constant acceleration $g=9.8 \frac{m}{s^2}$.

time $ct=0$ (and $\rho=0$). These make a geometric series $a_q = a_0 \{ \dots, e^{-2\rho_1}, e^{-\rho_1}, 1, e^{+\rho_1}, e^{+2\rho_1}, \dots \}$ of hyperbolic radii that includes Bob's radius a_0 at origin $[q, p]=[0,0]$.

However, the initial ($ct=0$) spacing of travelers, that is $\Delta a_q = a_0 (e^{q\rho_1} - e^{(q-1)\rho_1})$ in Alice's inertial frame, is to 1st-order in ρ_1 , a uniform $\Delta a_q = a_0 \rho_1$ that agrees with Bob's radar-range values. Later, as traveler- q gains speed according to its respective acceleration $g_q = \frac{c^2}{a_q}$, Alice will see neighbor intervals Lorentz contract non-uniformly by $\Delta a_q \text{sech} \rho_p$ factors.

When a neighbor- q of Bob sends his own inquiring radar-echo ranging pulses he will get results that differ by the same exponential factor $e^{q\rho_1}$ relating his proper time value $\tau_{q,p}$ to the corresponding value $\tau_{0,p}$ for Bob intercepting echo-return- p . Bob's radar-range intervals are all seen by up-stairs neighbor- q , to be uniformly expanded by $e^{q\rho_1}$, while down-stairs neighbor- $(-|q|)$, sees them uniformly contracted by $e^{-|q|\rho_1}$.

Consider Doppler blue-shifts $e^{+q\rho_1}$ seen by Bob ($q=0$) of CW light sent by an up-stairs

neighbor-($+|q|$) or a red-shift $e^{-\rho_1}$ of a down-stairs neighbor-($-|q|$) source. Each light beam on $\pm 45^\circ$ -paths in Fig.35b is a copy of laser light sent by Alice ($+45^\circ$) or Carla (-45°) and Doppler-shifted by Bob's velocity so he always sees a fixed green from either direction.

Al and Carl are similarly seeing fixed colors as long as they can maintain their respective accelerations g_{-1} and g_1 through a field of up-chirped frequency sent by Alice and down-chirped frequency sent by Carla. Thus each traveler only sends or receives its unique frequency: blue for Al, green for Bob, and red for Carl. So Bob always receives a green from Al down-stairs that is Doppler red-shifted by $e^{-\rho_1}$ from Al's blue or else a green from Carl up-stairs that is blue-shifted by $e^{+\rho_1}$ from Carl's red.

It might seem travelers sharing a line of equal ρ and fixed radar-range separation should see no Doppler shift between them, that is $(R|S)=1$. However, each $\pm 45^\circ$ -path connects a (q,p) -point to the nearest up-stairs $(q+1,p\pm 1)$ -points of traveler($q+1$) who deals in re-

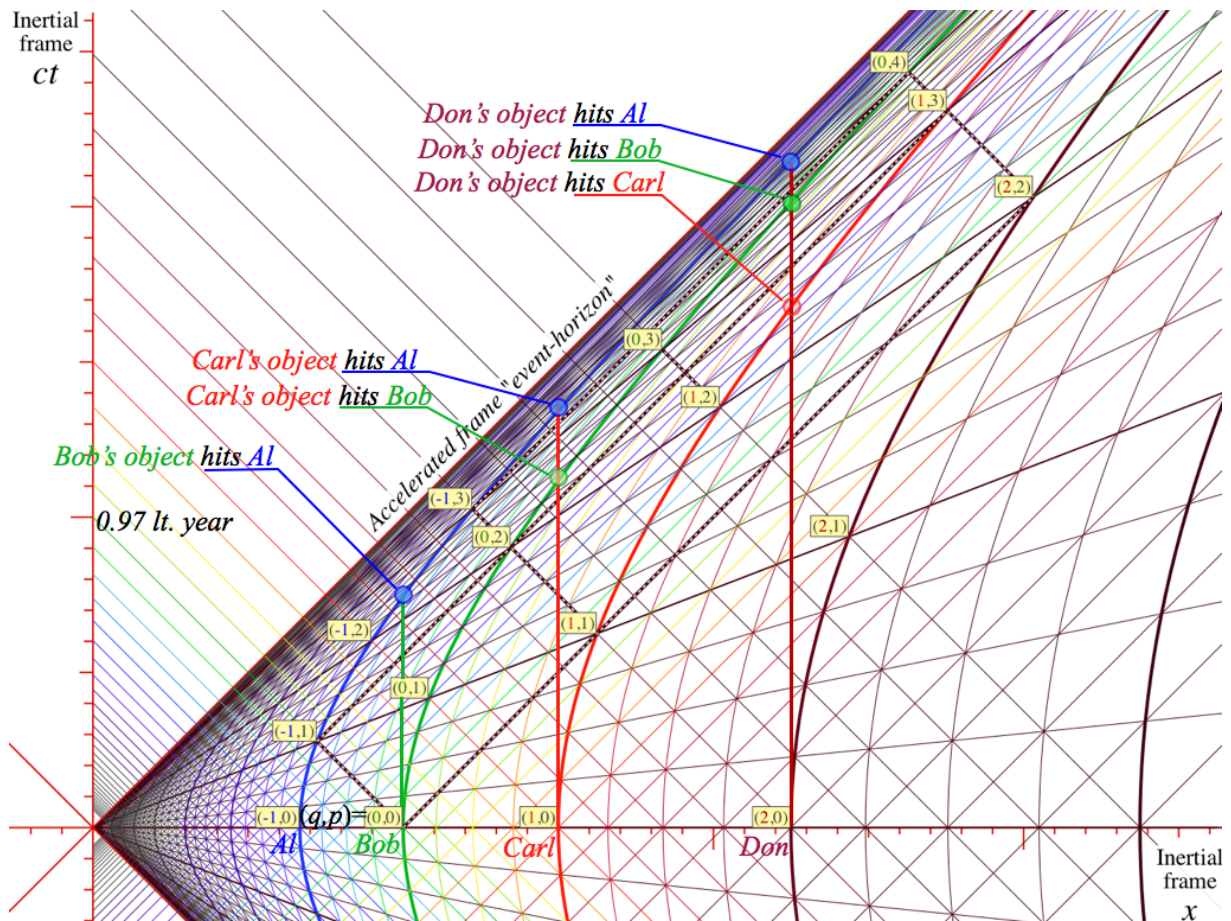


FIG. 37. Space-time paths of dropped objects hitting accelerating travelers

duced frequency and to the nearest down-stairs $(q-1, p \mp 1)$ -points of traveler $(q-1)$ who deals in higher frequency. In each case rapidity differs by one ρ_1 -unit implying a Doppler blue-shift factor $e^{+\rho_1}$ if light is falling down-stairs or a Doppler red-shift factor $e^{-\rho_1}$ if light is rising up-stairs. Travelers must have identical and *constant* rapidity for their shifts to go away.

D. Mechanics in accelerated frames

The curved space-time in Fig.36 facilitates tracking light waves going back-and-forth between the co-accelerating travelers Al($q=-1$), Bob($q=0$), Carl($q=1$) and Don($q=2$) and reconciling them to Alice and Carla with their inertial frame laser sources. The same may be done for freely flying massive objects that travelers might drop or throw at each other. A simple example involves travelers dropping objects on downstairs companions at just the moment they all have zero velocity in the inertial (x, ct) frame. Alice and Carla would see such objects to be stationary and represented by vertical lines parallel to their inertial ct -axis as shown in Fig.37. Each object dropped by traveler- $(q=Q)$ will hit (or pass closely by) traveler- $(q=Q-1)$ then traveler- $(q=Q-2)$ and so forth as seen by examples in Fig.37. The first example has Don($q=2$) drop something onto Carl($q=1$), Bob($q=0$), and Al($q=-1$) as is indicated at the top of the figure. Don's object hits Carl (or as witnessed by Alice and Carla: Carl hits Don's stationary object.) when Carl's x -coordinate equals a_2 of Don's object.

$$x_{2\text{HIT}1} = a_2 = a_0 e^{2\rho_1} = x_{\text{Carl}} = a_1 \cosh \rho_{2\text{HIT}1} = a_0 e^{\rho_1} \cosh \rho_{2\text{HIT}1} \quad (105)$$

This is solved for the relative rapidity $\rho_{2\text{HIT}1}$ between Carl and Don's "falling" object.

$$\rho_{2\text{HIT}1} = \cosh^{-1} e^{\rho_1} = \cosh^{-1} \frac{3}{2} = 0.962 \Rightarrow u_{2\text{HIT}1} = 0.745c \quad (106)$$

Course-grid scale factor $e^{\rho_1} = \frac{3}{2}$ yields high relative velocity. So, one hopes Don's object misses Carl. But, then it falls toward Bob($q=0$) and Al($q=-1$) with an ever increasing velocity.

$$\rho_{2\text{HIT}0} = \cosh^{-1} e^{2\rho_1} = 1.451 \Rightarrow u_{2\text{HIT}0} = 0.896c \quad (107)$$

$$\rho_{2\text{HIT}-1} = \cosh^{-1} e^{3\rho_1} = 1.887 \Rightarrow u_{2\text{HIT}-1} = 0.955c \quad (108)$$

From Fig.37 it is seen that Don's object hits (or passes) Carl with the same relative speed that Carl's object hits Bob or that Bob's object hits Al. These hits (or passings) lie on a single line of rapidity $\rho_{2\text{HIT}1} = \rho_{1\text{HIT}0} = \rho_{0\text{HIT}-1}$ as seen by generalizing Eq.(105).

$$x_{Q\text{HIT}q} = a_Q = a_0 e^{Q\rho_1} = a_q \cosh \rho_{Q\text{HIT}q} = a_0 e^{q\rho_1} \cosh \rho_{Q\text{HIT}q} \quad (109)$$

Thus rapidity $\rho_{Q\text{HIT}_q}$ and its hyper-cosine vary with the q -index difference $(Q-q)$.

$$e^{(Q-q)\rho_1} = \cosh \rho_{Q\text{HIT}_q} \quad (110)$$

The (q,p) points in Fig.36 or Fig.37 mark intersections of light rays or massive objects with members of a fleet of co-accelerating ships ($q=\dots-2,-1,0,1,2,\dots$) located at each moment ($p=\dots-2,-1,0,1,2,\dots$) on a line of equal rapidity $\rho_p=p\rho_1$ or velocity $u_p=c \tanh \rho_p$ with low- q ships accelerating more in the (x,ct) frame to have the same velocity u_p as their neighbors by gaining it sooner in local time τ or inertial time t than their high- q “upstairs” neighbors. Light acquires Doppler shift e^{ρ_1} in “falling” from a traveler to one below. A mass shifts its phase frequency (or Hamiltonian $H=Mc^2 \cosh \rho=hv_{\text{phase}}$ in(49)) by e^{ρ_1} according to (110).

VII. SYMMETRY ANALYSIS OF DOPPLER SHIFTS

Doppler blue-shift factor b for approach or arrival of a traveling source becomes the inverse $1/b=r$ (red-shift) if that source is receding or departing at the same speed. This was related to \mathcal{T} -symmetry with respect to time-reversal ($t\leftrightarrow-t$), a more general symmetry axiom that is usually assumed for fundamental processes.

\mathcal{T} -symmetry makes us unable to tell if a movie of action is being played forwards or backwards. Hollywood movies (especially Road-Runner cartoons) *never* have \mathcal{T} -symmetry. But fundamental processes at low to medium energies *are* supposed to have precise \mathcal{T} -symmetry as long as they remain undisturbed (and unobserved). This renders meaningless classical notions of cause and effect at the fundamental level and is the source of protracted arguments about the conservation of quantum information in extreme environments.

Inversion or parity \mathcal{P} -symmetry of space-reversal ($\mathbf{r}\leftrightarrow-\mathbf{r}$) is assumed for optical physics *en-vacuo* as are σ_μ -reflection symmetries for each spatial dimension $x_\mu = \{x, y, z\}$. So far \mathcal{P} -symmetry axioms engender fewer arguments. \mathcal{T} and \mathcal{P} together in a product is known as *charge conjugation* $\mathcal{PT}=\mathcal{C}=\mathcal{TP}$. \mathcal{C} -analysis factors a wave-sum (11) of plane waves $\Psi=e^{iR}+e^{iL}$ into a product $\psi_{\text{phase}}\psi_{\text{group}}$ of phase factor $\psi_{\text{phase}}=e^{i\frac{R+L}{2}}$ and group factor $\psi_{\text{group}}=e^{i\frac{R-L}{2}}+e^{-i\frac{R-L}{2}}=2\cos\frac{R-L}{2}$. The latter envelopes the former and together they define time axes or ct -grid lines and space axes or x -grid lines. (Recall Fig.5c and Fig.6c.) They also define the frequency axes or $(\omega=2\pi\nu)$ -grid lines and wave-number $(ck=2\pi c\kappa)$ -gridlines in per-space-time of Fourier space.

Each reflection operator $\sigma_x, \sigma_y, \sigma_z$, or σ_t , has a unit square ($\sigma_\mu^2=1$) and minimal equations.

$$\sigma_\mu^2 - 1 = 0 = (\sigma_\mu - 1)(\sigma_\mu + 1) \quad (111)$$

These yield spectral projectors \mathbf{P}^+ and \mathbf{P}^- for eigenvector and operator decomposition.

$$1=\mathbf{P}^++\mathbf{P}^- \quad \text{and} \quad \sigma_\mu=\mathbf{P}^+-\mathbf{P}^- \quad \text{where} \quad : \mathbf{P}^+=\frac{1+\sigma_\mu}{2} \quad \text{and} \quad \mathbf{P}^-=\frac{1-\sigma_\mu}{2} \quad (112)$$

These projectors produce half-sum and half-difference combinations in the exponents of the ψ_{phase} and ψ_{group} factors used in the wave factorization (11).

Appendix: CW-pairing vs. Newton's corpuscles: CW and PW space-time grids

It helps to see wave coordinate grids generated by general CW pairs. A CW sum with four parameters $\{\omega_1, k_1, \omega_2, k_2\} = \{4.5, 3.0, 0.5, -1.0\}$ chosen in Fig.38 will factor wave Ψ as shown in the upper half of the figure and trace a non-square or *affine* space-time grid shown in the lower half. A left-hand *source-1* emits a wave with a right-moving phase velocity equal to $\omega_1/k_1 = 4.5/3.0 = 1.5$ to collide head-on with *source-2* left-moving wave going at $\omega_2/k_2 = -0.5$. Here wave speed is not c , so Fig.38 waves are not light waves, rather each is a Schrodinger non-relativistic approximation to a matter wave that (as shown later) has a quadratic dispersion function $\omega = k^2/2$. This shows ways to analyze CW-pairs for any set of parameters $\{\omega_1, k_1, \omega_2, k_2\}$ including Evenson's linearly dispersive ($\omega_a = ck_a$) CW-light.

Dispersion (ω, k) -plot in per-space-time helps to sort complicated wave dynamics in space-time (x, ct) -plots such as Fig.38. One simply draws four parameters judiciously as a pair of vectors $\mathbf{K}_1 = (\omega_1, k_1)$ and $\mathbf{K}_2 = (\omega_2, k_2)$ in a per-space-time (ω, k) -plot in Fig.39. Then half-sum $\mathbf{K}_{phase} = (\mathbf{K}_1 + \mathbf{K}_2)/2$ and half-difference $\mathbf{K}_{group} = (\mathbf{K}_1 - \mathbf{K}_2)/2$ vectors are found. Fig.39a is a standard $\omega(k)$ dispersion plot. Fig.39b is a complementary plot of $k(\omega)$.

Fig.?? compares a square laser CW zero path lattice to diamond shaped laser PW path lattice. Henceforward short notation lets \mathbf{G} be \mathbf{K}_{group} , \mathbf{P} be \mathbf{K}_{phase} , \mathbf{R} be \mathbf{K}_1 , and \mathbf{L} be \mathbf{K}_2 . (\mathbf{L} and \mathbf{R} refer to single CW laser beams going left and right, respectively.) The PW simulation in Fig.39b was made using a tapered sum of several CW harmonics that pile up pulses moving diagonally at light speed $\pm c$ through the crest regions (light square areas in Fig.39a) and reduce trough regions (dark squares) to nearly zero. Thus the pulse pile-ups move more or less rigidly on diamond shaped PW tracks parallel to \mathbf{L} or \mathbf{R} in Fig.39b as

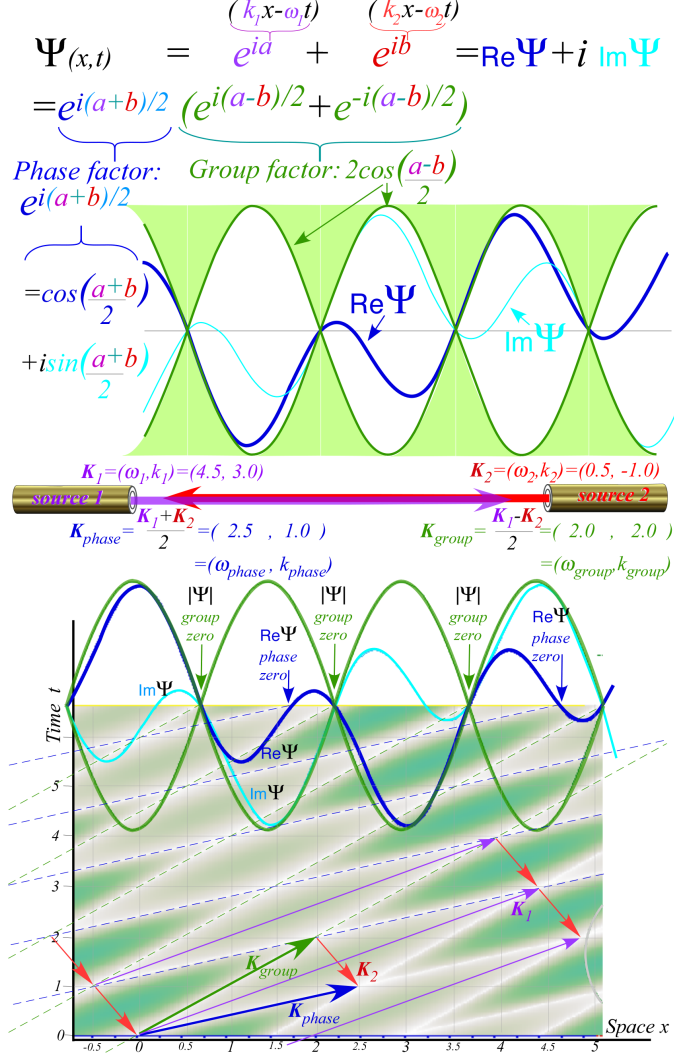


FIG. 38. General non-optical 2-CW factorization and resulting space-time grid.

though they were Newtonian “corpuscles.” Meanwhile, CW wave zeros stand still along \mathbf{G} paths or dart with velocity $\pm\infty$ along \mathbf{P} paths in the Minkowski plot of Fig. 39a. Note that \mathbf{P} paths (horizontal white lines in Fig. 39a) are separated in time by a half period ($\tau/2 = 5/6fs$) while the \mathbf{G} paths (vertical white lines) are separated by half wavelength ($\lambda/2 = 1/4\mu m$). The \mathbf{L} to \mathbf{R} pulse paths in Fig. 39b, having eliminated troughs, are separated from neighbors by a full period ($\tau = 5/3fs$) and a full wavelength ($\lambda = 1/2\mu m$). The size and shape of each pulse in a PW train made of harmonics $\{a_1 \cos \phi, a_2 \cos 2\phi, \dots, a_N \cos N\phi\}$ depends inversely on the number N of harmonics and is sensitive to how the amplitudes a_k converge. One can imagine that primitive source vectors $\mathbf{K}_1 = (\omega_1, k_1)$ and $\mathbf{K}_2 = (\omega_2, k_2)$ define paths for Newtonian “corpuscles” if the waves they represent were corpuscular bursts that did

many ways surpass the fictional characters in cinematic thrillers like *Raiders of the Lost Arc*. Indeed, there were some exciting real life moments shared by his wife Vera, one together with Ken in a canoe literally inches from the hundred-foot drop-off of Brazils largest water-fall. But, such outdoor exploits, of which Ken had many, pale in the light of an in-the-lab brilliance and courage that profoundly enriched the world. Ken is one of few researchers and perhaps sole physicist to be twice listed in the *Guinness Book of Records*. The listings are not for jungle exploits but for his labs highest frequency measurement and for a speed of light determination that made c many times more precise due to his labs pioneering work with John Hall in laser resonance and metrology. The meter-kilogram-second (mks) system of units underwent a redefinition largely because of these efforts. Thereafter, the speed of light c was set to $299,792,458\text{ms}^{-1}$. The meter was defined in terms of c , instead of the other way around since his time precision had so far trumped that for distance. Without

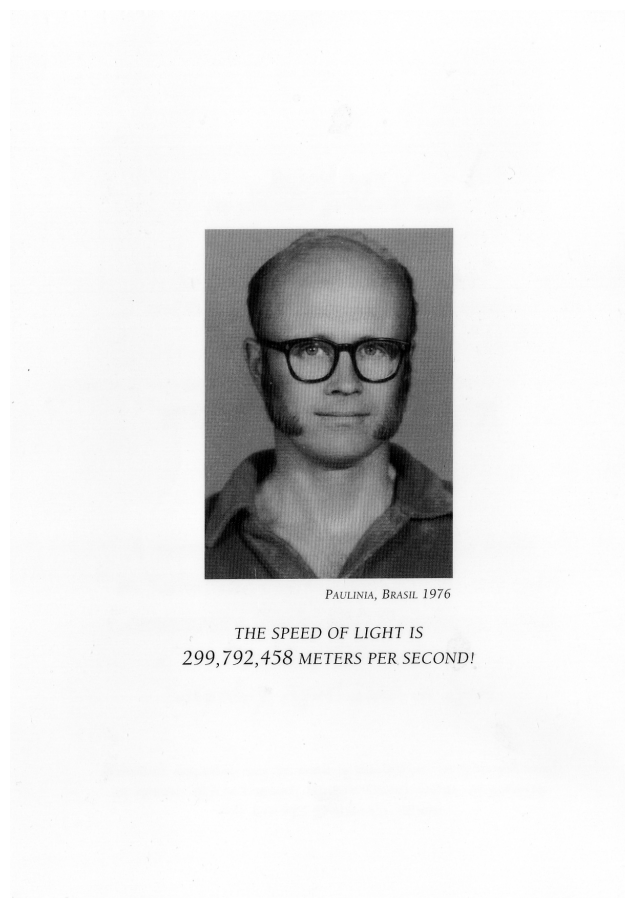


FIG. 40. Ken Evenson

such resonance precision, the Global Positioning System (GPS), the first large-scale wave space-time coordinate system, would not be practical. Ken's courage and persistence at the Time and Frequency Division of the Boulder Laboratories in the National Bureau of Standards (now the National Institute of Standards and Technology or NIST) are legendary as are his railings against boneheaded administrators who seemed bent on thwarting his best efforts. Undaunted, Ken's lab painstakingly exploited the resonance properties of metal-insulator diodes, and succeeded in literally counting the waves of near-infrared radiation and eventually visible light itself. Those who knew Ken miss him terribly. But, his indelible legacy resonates today as ultra-precise atomic and molecular wave and pulse quantum optics continue to advance and provide heretofore unimaginable capability. Our quality of life depends on their metrology through the Quality and Finesse of the resonant oscillators that are the heartbeats of our technology. Before being taken by Lou Gehrig's disease (ALS), Ken began ultra-precise laser spectroscopy of unusual molecules such as HO₂, the radical cousin of the more common H₂O. Like Ken, such radical molecules affect us as much or more than better known ones. But also like Ken, they toil in obscurity, illuminated only by the purest light in the universe. The 2005 Nobel Physics Prize was awarded to Glauber, Hall, and Hensch for laser optics and metrology.

K. M. Evenson, J.S. Wells, F.R. Peterson, B.L. Danielson, G.W. Day, R.L. Barger and J.L. Hall, Phys. Rev. Letters 29, 1346(1972)

ACKNOWLEDGMENTS

Thanking any granting agencies.

* Also at HarterSoft, 918 N Tanglebriar Ln, Fayetteville AR 72701

† wharter@uark.edu

¹ Max Planck. Zur theorie des gesetzes der energieverteilung im normalspectrum. *Deutsche Physikalische Gesellschaft*, 2(237–245), 1900.

² A. Einstein. Über einen die erzeugung und verwandlung des liches betreffenden heuris-

- tischen Gesichtspunkt. *Annalen der Physik*, 322(6):132–148, 1905. ISSN 1521-3889. doi: 10.1002/andp.19053220607. URL <http://dx.doi.org/10.1002/andp.19053220607>.
- ³ A. Einstein. Ist die Trägheit eines Körpers von seinem Energieinhalt abhängig?. (German) [Does the inertia of a body depend on its energy content?]. *Annalen der Physik*, 323:639–641, 1905.
 - ⁴ Michael Fowler. Special relativity: What time is it? URL <http://galileoandeinstein.physics.virginia.edu/lectures/srelwhat.html>.
 - ⁵ Fabrizio Logiurato. Relativistic derivations of de Broglie and Planck-Einstein equations. *Journal of Modern Physics*, 5:1–7, 2014. URL <http://dx.doi.org/10.4236/jmp.2014.51001>.
 - ⁶ H. A. Lorentz, A. Einstein, H. Minkowski, Hermann Weyl, and Arnold Sommerfeld. *The principle of relativity : a collection of original memoirs on the special and general theory of relativity*. Dover, [New York], 1952. ISBN 0486600815 9780486600819.
 - ⁷ William G. Harter. Wave node dynamics and revival symmetry in quantum rotors. *Journal of Molecular Spectroscopy*, 210(2):166–182, 12 2001.
 - ⁸ William G. Harter, John Evans, Roberto Vega, and Sanford Wilson. Galloping waves and their relativistic properties. *American Journal of Physics*, 53(7):671–679, 1985.
 - ⁹ W.G. Harter and T. C. Reimer. Poincaré invariant action, 2005. URL http://www.uark.edu/ua/pirelli/php/poincare_inv_2.php. ”http://www.uark.edu/ua/pirelli/php/poincare_inv_2.php”.
 - ¹⁰ D. E. Herschbach. 2005.
 - ¹¹ H. Minkowski. Die Grundgleichungen für die elektromagnetischen Vorgänge in bewegten Körpern. *Mathematisch-Physikalische Klasse*, 1:53, 1908.
 - ¹² H. A. Lorentz. Electromagnetic phenomena in a system moving with any velocity smaller than that of light. *Koninklijke Akademie van Wetenschappen te Amsterdam*, 6:809–831, 1904. URL <http://www.dwc.knaw.nl/DL/publications/PU00014148.pdf>.
 - ¹³ A. Einstein. Zur Elektrodynamik bewegter Körper. *Annalen der Physik*, 322(10):891–921, 1905. ISSN 1521-3889.
 - ¹⁴ Louis de Broglie. Waves and quanta. *Nature*, 112:540, October 1923.
 - ¹⁵ P. A. M. Dirac. Forms of relativistic dynamics. *Reviews of Modern Physics*, 21:392–399, Jul 1949.
 - ¹⁶ A. B. Arons and M. B. Peppard. Einstein’s proposal of the photon concept—a translation

- of the annalen der physik paper of 1905. *American Journal of Physics*, 33(5):367–374, 1965. doi:<http://dx.doi.org/10.1119/1.1971542>. URL <http://scitation.aip.org/content/aapt/journal/ajp/33/5/10.1119/1.1971542>.
- ¹⁷ Erwin Schrödinger. Quantisierung als Eigenwertproblem (Dritte Mitteilung: Störungstheorie, mit Anwendung auf den Starkeffekt der Balmerlinien). (German) [Quantization as an eigenvalue problem (Third report: perturbation theory, with application to the Stark effect of the Balmer lines)]. *Annalen der Physik*, 385(13):437–490, 1926. ISSN 1521-3889. doi:<http://dx.doi.org/10.1002/andp.19263851302>.
- ¹⁸ E Schrödinger. Quantisierung als eigenwertproblem. *Annalen der Physik*, 385(13):437–490, 1926. ISSN 1521-3889.
- ¹⁹ Erwin Schrödinger. Quantisierung als Eigenwertproblem (Zweite Mitteilung). (German) [Quantization as an eigenvalue problem (Second report)]. *Annalen der Physik*, 384(6):489–527, 1926. ISSN 1521-3889. doi:<http://dx.doi.org/10.1002/andp.19263840602>.
- ²⁰ Erwin Schrödinger. Vom radium. (German) [On Radium]. *Neue Zürcher Zeitung*, March 1923.
- ²¹ Erwin Schrödinger. Ton und Farbe. (German) [Sound and color]. *Neue Zürcher Zeitung*, February 1923.
- ²² Erwin Schrödinger. Über eine bemerkenswerte Eigenschaft der Quantenbahnen eines einzelnen Electrons. (German) [On a remarkable property of the quantum trajectory of a single electron]. *Zeitschrift für Physik*, 12(1):13–23, December 1923. doi:<http://dx.doi.org/10.1007/BF01328077>. URL <http://www.springerlink.com/content/j7117422717018jh/fulltext.pdf>.
- ²³ E Schrödinger. Schrodinger’s protests about prevailing quantum mechanical interpretations are widely circulated, 1910–1961. ”See smart groups in Schrodinger-Erwin Works.bib”.
- ³²]Einstein:1942os Albert Einstein. Quantum theory completeness, 1942 [1926]. URL <https://sec2.einstein.caltech.edu/archives/scans/015/15294.pdf>. ”I shall never believe that god plays dice with the universe” - Albert Einstein Archives, The Jewish National University Library, The Hebrew University of Jerusalem (www.albert-einstein.org), Letter to Cornelius Lanczos, March 21, 1942”.
- ²⁵ Lewis C. Epstein. *Relativity visualized*. Insight Press, San Francisco, CA, 1985. ISBN 093521805X 9780935218053. URL <http://www.allbookstores.com/book/compare/093521805X>.
- ²⁶ Niels Bohr. Der bau der atome und die physikalischen und chemischen eigenschaften der

- elemente. *Zeitschrift für Physik*, 9(1):1–67, 1922. doi:10.1007/BF01326955. URL <http://dx.doi.org/10.1007/BF01326955>.
- ³²]Heisenberg:2013zt Werner Heisenberg. *The Physical Principles of the Quantum Theory*. Courier Dover Publications, 2013 [1930].
- ²⁸ P. A. M. Dirac. *Lectures on quantum mechanics*. Belfer Graduate School of Science, Yeshiva University, New York, 1964. "Dirac's first text in 1931 used \langle and \rangle to denote bra-ket duality."
- ²⁹ Robbins Jeffrey. Feynman, Richard P. *The pleasure of finding things out : the best short works of Richard P. Feynman*. Perseus Books, Cambridge, Mass., 1999. ISBN 0738201081 9780738201085.
- ³⁰ William G Harter. A huge energy shift is used for sake of geometric clarity. Atoms usually lose less than one part in 10^9 or 10^{10} of their rest mass in optical emission. The atom in the example loses rest mass $1/2 M_0 c^2$ emitting a $3/8 M_0 c^2$ photon., 2012.
- ³² Feynman, Leighton, and Sands]Feynman:2000gb Richard P. Feynman, Robert B. Leighton, and Matthew Sands. *The feynman lectures on physics : the new millennium edition.*, 2000–2013 [1964]. URL <http://www.feynmanlectures.info>. "Our development owes a lot to Feynman's treatment cavity wave dispersion in Vol. II Ch. 24 and Vol. III Ch. 7".
- ³²]Rindler:2000qq Wolfgang Rindler. *Essential Relativity: Special, General, and Cosmological*. Springer, 2000 [1977]. p. 18. See also ref. 8, p. 111.
- ³³ E F Taylor and J A Wheeler. *Spacetime Physics*. W. H. Freeman, 2nd edition, 1992.